

UC Berkeley

UC Berkeley Electronic Theses and Dissertations

Title

Carbon Dioxide Reduction at Organic-Metal Interfaces

Permalink

<https://escholarship.org/uc/item/51k089gr>

Author

Buckley, Aya Kate

Publication Date

2020

Peer reviewed|Thesis/dissertation

Carbon Dioxide Reduction at Organic-Metal Interfaces

By

Aya K. Buckley

A dissertation submitted in partial satisfaction of the

requirements for the degree of

Doctor of Philosophy

in

Chemistry

in the

Graduate Division

of the

University of California, Berkeley

Committee in charge:

Professor F. Dean Toste, Chair

Professor Kurt Vollhardt

Professor Michael Crommie

Fall 2019

Abstract

Carbon Dioxide Reduction at Organic-Metal Interfaces

by

Aya K. Buckley

Doctor of Philosophy in Chemistry

University of California, Berkeley

Professor F. Dean Toste, Chair

Chapter 1 – The rising levels of CO₂ in the atmosphere necessitate further investigation into methods of converting CO₂ into more valuable products. In this chapter, we introduce the chemistry of CO₂ conversion, particularly via electrocatalytic methods, and the strategies and considerations involved in selectively reducing CO₂ to desirable products.

Chapter 2 – We describe the effects of the CO₂ reduction device on the observed product selectivity and the method used herein to evaluate the performance of metallic catalysts.

Chapter 3 – We develop a predictive framework to understand how organic modifiers on a Cu surface influence the selectivity of the CO₂ reduction reaction at the metallic surface. This study of a series of polymeric and molecular modifiers indicates that protic species enhance selectivity for H₂, hydrophilic species enhance formic acid formation, and cationic hydrophobic species enhance CO selectivity. The relationship between these structural features of the modifiers and the changes in selectivity yields insights into how these modifiers influence catalytic behavior. We hypothesize that the hydrophilic/hydrophobic modifiers influence the binding strength of surface hydrides, which yield formic acid or H₂. This study demonstrates how the selectivity of a single metallic surface may be tuned to favor formic acid or CO simply by changing the properties of the added organic modifier and may aid in the future implementation of organic structures in CO₂ reduction devices.

Chapter 4 – The study of cationic ammonium salts on a Ag surface allows a closer investigation of how these salts influence CO formation. The trends observed with these ammonium salts indicate that the selectivity-determining factor is not the hydrophilicity/phobicity, but rather the length of the longest hydrocarbon substituent. This correlation suggests that the ordering of the ammonium salts at the Ag surface plays a key role in obtaining improved CO selectivity. We discuss possible mechanisms by which these ordered ammonium salts may influence the formation of CO. The emergence of the organization of these organic modifiers as an important parameter demonstrates that strategic design of these modifiers requires an understanding of not only the mechanism, but also of ancillary features of the organic species that impact their ability to influence surface processes.

Acknowledgments

Francesca Toma and Dean Toste – time and time again, you buoyed the work in this thesis, the progress of my degree, and, without exaggeration, my faith in science and the scientific community. Thank you both for seeing me through this process.

Francesca, your wide-ranging scientific curiosity is unmatched. Even now, I am taken aback and impressed as you draw ideas from some firsthand experience with carbon-based materials... peptoid chemistry... perovskites... AFM... a million synchrotron-based methods... just this past week, I learned about your long-standing interest in quantum computing. Your broad interests have not only enriched my experience doing research as a graduate student, but also provided a lot of inspiration to me on the roughest days. The trips to the synchrotron that you facilitated reminded me that science is fun! This truly interdisciplinary outlook as to how science can be conducted and your reminders to us to enjoy our work are two lessons that I hope to carry with me.

Dean, I am so grateful that you took me into your group and put me on this project. So many times, you have guided me through this degree, not only with incredible insights into the chemistry, but also with great perception about people and human nature. While I don't think that perceptiveness can be learned, I hope to remember that doing great science and being compassionate are not mutually exclusive. Thanks for fostering such a collaborative and supportive culture in your group.

I would also like to thank my committee, including Profs. Peter Vollhardt, Michael Crommie, Robert Bergman and Richard Andersen. Their keen advice helped me dig even deeper than I would have otherwise, and I truly appreciate their influence on this work and my time at Berkeley.

Prof. William Goddard and Dr. Tao Cheng were instrumental to developing an understanding of our catalytic interface. I always enjoyed our discussions and learned so much from your thought-provoking questions and intriguing results. Thank you so much for all of your hard work examining our system.

The northern branch of the Joint Center for Artificial Photosynthesis is housed in a giant glass building that, to a visitor, might look more cold and sterile than warm and welcoming. Nonetheless, in my mind, it feels like a second home, thanks to its inhabitants (and, of course, its unrivaled view of the Bay Area sunset, which certainly adds to the aura too). I would first like to thank my coworkers in the Toma group. There have been many, but in particular, I would like to extend my appreciation to the postdoc crew, including Roman Kazantsev, Guiji Liu, Johanna Eichhorn, Ashley Gaulding, Gideon Segev, and Guosong Zeng. Roman, I am so grateful that you were there with me at the beginning of this CO₂ reduction process. In the challenging first days, your upbeat attitude and willingness to try new things brought some light to 109. Guiji, thanks for always providing a smile in 305 when things were not going to plan in 307. I must also specifically thank Gideon for bringing inspiration to Friday morning group meetings in the form of Cheeseboard pastries and homemade hummus.

Speaking of food, I would also like to thank Michelle Lee, fellow grad student, who provided experimental support with the copper chapter, combed through my drafts with an eagle

eye, provided sound suggestions in many brainstorming sessions, produced baked goods and snacks at key moments, and never failed to remind me of the changing of the seasons- i.e. a new seasonal menu at Asha tea house.

David Larson, engineer extraordinaire, thank you so much for fabricating electrochemical cells, providing training and maintenance on a multitude of instruments, and generally holding the building together. You were always willing to drop your work to help me with something, and I am so grateful that you always did so with patience and cheer.

Sean Utan and Jenny Garrison, thank you for all of the great work you have done at JCAP. You've both had such thoughtful questions and spot-on experimental suggestions, and I've learned a lot from working with you. Best of luck to you in your scientific careers.

The work described herein would not have been possible without the incredible network of people at JCAP. Over the years, conversations with several of the staff scientists helped me understand CO₂ chemistry from different perspectives- I would like to extend an extra thank you to Jason Cooper, Dan Miller, Carolin Sutter-Fella and Walter Drisdell for patiently teaching me and fixing various instruments. Frances Houle provided insightful suggestions in our annual meetings and I really appreciate her support for this work. I would also like to thank Sherry Chan, Zhicheng Zhang, Martin Neitzel, Theresa Short, Deborah Reed, Kristin Camarena and Riyaz Mohammed for making research in Building 30 possible.

Graduate school does not always reward the time we take away from our own projects to help others, so I am especially grateful to the grad students, postdocs, and other researchers who stepped away from their benches to help me out. At JCAP, they include: Erin Creel, Elizabeth Corson, Sarah Dischinger, Blaine Carter, Matt Kuchta, Yanwei Lum, Ezra Clark, Jinkyu Lim, Chang-Ming Jiang, Kurt Van Allsburg, Hilda Buss, Drew Higgins, and Chris Hahn. Thank you for the instrument trainings, helpful discussions, friendship, and for bringing lots of pink to the workplace.

From campus, I would like to thank: Stephen von Kugelgen, Ryan Cloke, William Wolf, Mark Levin, Dave Kaphan, and Julia Oktawiec. Thank you for helping me survive classes and prep for quals, supplying chemistry expertise, and providing reassurance that it will all work out in the end. Many thanks to Cindy Hong and Tamara Sparks for taking in a stranger the first week of grad school and providing me with a happy home for the initial two years. Anna Wuttig, thank you so much for the food excursions and electrochemistry advice. Lynn Keithlin and Chona de Mesa helped me through many administrative pickles, and their kindness is much appreciated.

I also must try to express my deep gratitude for some friends from undergrad years, many of whom continued to help me throughout my Ph.D. Jon Owen, I cannot put into words how lucky I am that you stopped by one of my freshman classes to talk about how cool and colorful quantum dots are. You and your group taught me so much about how to conduct research, and your support over the years has meant the world to me. Nick Anderson, thanks teaching me, not just about the science part of research, but also about how to make figures, discuss data, collaborate with others, and the numerous other tools that are required as a graduate student. I fully realize now that you could have asked me to wash NMR tubes for three years, and I am so appreciative that you made the time and effort to make my undergraduate research experience so

much more fulfilling. Brandi Cossairt, thank you so much for encouraging me and for being an awesome role model. Mark Hendricks and Mike Campos, thanks for being the best labmates and visiting Wanda and me out here in the Bay. I would also like to thank Theo Agapie and Maddy Radlauer, who mentored me over a summer at Caltech and provide so much inspiration with their love of chemistry.

Finally, I would like to thank some family and friends for their support. My past teachers, including Marcia Renzetti, Yuka Yanagi, Suzanne Broffman and Johanna Urzedowski, are experts in different areas of study but are all incredible teachers who encouraged their students to think critically and draw connections. William Buckley, Mike and Penny Buckley, Katy and Allen Morris, and Patsy and Ted Buckley- thank you so much for being there when I needed it. Sean, your strong principles and stick-to-it-ness always impress me and I'm so excited about your unfolding new career in Seattle. To my parents, Tom and Midori Buckley- thank you so much for always being supportive, even as grad school brought me to the other side of the country. Daddy- I really appreciate that you encouraged us to think independently, not take things too seriously and use fewer commas. Okaasan- knowing that you are commuting 90 minutes each way, by train, bus and automobile, inspires me every day to try just a little bit harder. Thank you for being such an amazing role model and always reminding us to eat more vegetables. I love you!

Richard, there were so many days in which rough experiments got me down, and then your insightful chemistry suggestions, reassuring words, bright smile and unwavering confidence in my abilities enabled me to shake off the self-doubt and keep going. I cannot thank you enough for that. I love you and can't wait for our next adventure.

Dedicated to Kazue Nakamura and Mary Kate Baugh Buckley
who overcame so many obstacles with strength, grace, and a sense of humor.

Table of contents

Chapter 1. Introduction

1.1 Introduction	2
1.2 Electrocatalytic CO ₂ reduction: from starting materials to multi-electron products	2
1.3 Organic species in the tuning of electrocatalytic CO ₂ reduction selectivity	4
1.4 Summary and outlook	5
1.5 References	6

Chapter 2. Description of the Electrochemical Cells and Setup Used for the Described Experiments

2.1 Discussion	10
2.2 References	14

Chapter 3. Electrocatalysis at Organic-Metal Interfaces: Identification of Structure-Reactivity Relationships for CO₂ Reduction at Modified Cu Surfaces

3.1 Introduction	16
3.2 Results and discussion	17
3.2.1 Structurally diverse organic modifiers result in divergent catalytic behavior from Cu	17
3.2.2 Classification of modifiers by promoted products	19
3.2.3 Proposed mechanisms of influence of organic modifiers on CO ₂ R selectivity	21
3.3 Conclusions	25
3.4 References	26
3.5 Supplementary information	
3.5.1 Experimental methods	29
3.5.2 Experiments with Nafion	32
3.5.3 Chronoamperometry traces	35
3.5.4 Experiments with varying amounts of modifier	38
3.5.5 Product distribution at more negative potentials	40
3.5.6 Experiments under N ₂	41
3.5.7 NMR characterization of modifiers and electrolyte	42
3.5.8 Partial current densities	61
3.5.9 Contact angle and summarized product distribution data	62
3.5.10 Contact angle measurements, CO ₂ R partial current densities and total current for modified Cu surfaces	64
3.5.11 Relationship between Faradaic efficiency for CO, H ₂ and the contact angle	66
3.5.12 Relationship between formation of H ₂ , CO and formic acid	69
3.5.13 Tables of Faradaic efficiency data	71
3.5.14 References	74

Chapter 4. Effect of Quaternary Ammonium Salts on the Behavior of Ag in the CO₂ Reduction Reaction	75
4.1 Introduction	76
4.2 Results and discussion	76
4.3 Conclusions	79
4.4 References	80
4.5 Supplementary information	82
4.5.1 Experimental methods	82
4.5.2 Partial current densities	83
4.5.3 Contact angle of functionalized Ag surfaces	84
4.5.4 References for supplementary information	85

Chapter 1:

Introduction

1.1 Introduction

Since the Industrial Revolution, the amount of carbon dioxide in the atmosphere of our blue marble has increased from 300 to 400 ppm, resulting in wide-ranging effects on the climate and environment.^{1,2} An efficient method of converting this greenhouse gas into more desirable compounds would help address both rising atmospheric temperatures and the need for new sources for fuels and specialty chemicals (**Fig. 1**).

Existing catalysts for this process, however, demonstrate insufficient selectivity towards desirable species.^{3,4} When CO₂ is subjected to electrochemically reducing conditions, up to 16 different carbon-based products may be observed, in addition to H₂ from the competing reduction of protons.⁵ An improved understanding of how these reactions occur and novel methods of tuning the behavior of the catalyst are necessary to develop a more practically viable system.

This thesis describes the development and study of systems that catalyze this conversion of CO₂ into CO and formic acid. Specifically, the use of organic species to tune the selectivity of a heterogeneous metal catalyst was investigated. This chapter describes the chemistry of the CO₂ reduction process and the strategies and important considerations in working to improve the selectivity towards compounds of interest. Next, the role of organic species as a readily tunable additive to help address the limitations of existing single-metal catalysts is described.

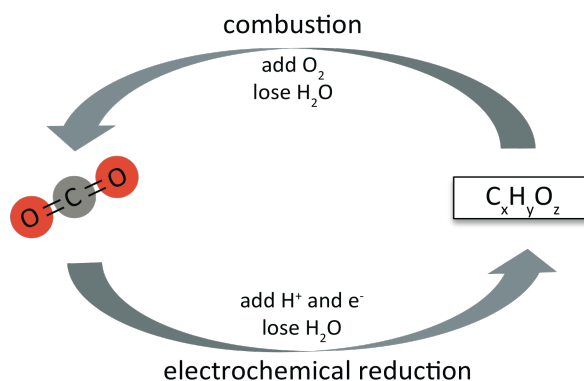


Figure 1. Electrochemical reduction of CO₂ may be used to close the cycle of carbon loss into the atmosphere.

1.2 Electrocatalytic CO₂ reduction: from starting materials to multi-electron products

In addition to the practical motivations for studying the CO₂ reduction reaction, the complexities and challenges of this process have inspired a vast array of creative studies, including fundamental and interdisciplinary approaches.⁶ The CO₂ molecule is small, linear, and nonpolar, as well as relatively stable and inert⁶; in the atmosphere, methane, for example, will decompose over a decade, but CO₂ persists for centuries.⁷ A number of strategies have been employed to transform this stable and persistent molecule, some of which will be discussed below.

Methods of converting CO₂ have included thermocatalytic,⁸ photocatalytic,⁹ biocatalytic,¹⁰ and electrocatalytic¹¹ means, as well as organic transformations¹². The most common mode of reactivity in these reactions is via bending of the CO₂ molecule from its thermodynamically favored linear geometry, in conjunction with nucleophilic attack at the carbon center.^{6,13} In the absence of stabilizing interactions, the energetic penalty for this rearrangement is high. From the lens of electrochemical reactivity, a highly negative potential is necessary to add an electron to CO₂ and form the bent radical species (with potential reported vs. the normal hydrogen electrode, (NHE)):⁶



Due to the reorganizational energy necessary to form this intermediate, many in the literature have called for catalytic strategies that draw inspiration from biological mechanisms, in which pendant nucleophilic and electrophilic groups stabilize the intermediates formed and facilitate transfer of additional electrons and protons.^{10,14}

The addition of two protons and two electrons yields either CO or formic acid.^{15,16} The formation of these two molecules thermodynamically requires relatively low potentials:⁶



However, due to the kinetic barriers, substantially higher potentials are often necessary to form these species, with this difference between the thermodynamic and kinetic barriers known as the overpotential.

Proposed mechanisms for the formation of CO and formic acid are often supported with the use of volcano plots.^{16,17} The Sabatier principle states that, if a catalyst binds an intermediate too strongly, it will fail to dissociate, whereas a catalyst that binds an intermediate too weakly will desorb the species too readily for the reaction to proceed. A plot of the binding energy of *COOH on various metal surfaces against the activity of these surfaces towards CO formation illustrates this volcano-type trend.¹⁶ Repeating this analysis with *COOH against the activity towards formic acid, on the other hand, does not result in this type of trend. A more pronounced volcano-type relationship is observed with *OCHO and formic acid.¹⁶

Based upon this analysis, as well as Tafel studies,¹⁸ computational work,¹⁶ and other studies, a number of reports in the literature have therefore proposed that the formation of a carbon-bound intermediate kinetically favors the generation of CO, whereas the formation of an oxygen-bound intermediate results in the formation of formic acid. As our work in chapter 3 suggests, other mechanisms may act as better descriptors in certain systems, and the details of these mechanisms are still under investigation and debate. Nonetheless, these descriptors provide a helpful framework with which we can describe observations to date in single-metal heterogeneous systems.

These analyses and experimental works have found that Au and Ag are fairly selective for CO over formic acid or H₂. Sn and other p-block metals primarily yield formic acid. Other metals, such as Pt and Ni, bind CO strongly and are poisoned by its formation, and H₂ evolution predominates.^{11,15}

The interesting outlier in this framework is Cu. With a Cu catalyst, up to 16 different carbon-based compounds have been observed, in addition to H₂ from the competing side reaction (**Fig. 2**).⁵ While traces of these further reduced products have been observed on other single-metal surfaces, Cu is the only metal to yield these species of interest in substantial amounts.¹¹

Experimental studies have indicated that formic acid cannot be further reduced electrochemically, whereas subjecting CO to a Cu catalyst yields a similar distribution of hydrocarbons

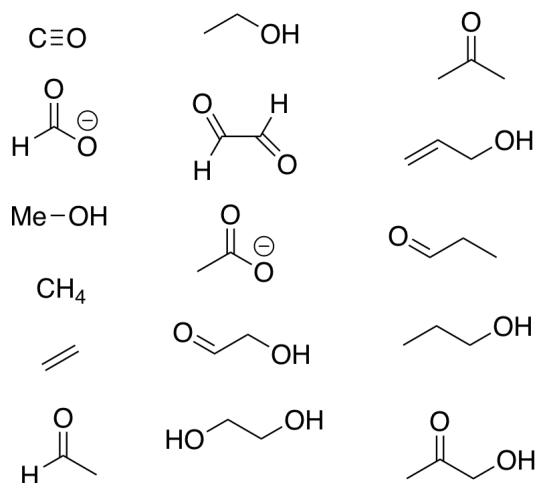


Figure 2. Products from CO₂ reduction on Cu characterized by Jaramillo, *et al.*⁵

to that found with CO₂. This suggests that CO is the intermediate through which the other hydrocarbons are formed.¹⁵ It is hypothesized that the unique ability of Cu to catalyze the formation of these molecules is due to its intermediate binding strength for this CO intermediate, facilitating the additional transfer of protons and electrons to form further downstream species.¹⁵

Significant effort has been dedicated to tuning the selectivity of Cu surfaces. Briefly, some of the parameters that have been examined include:

- 1) single crystalline surfaces^{19,20}
- 2) pronounced changes in morphology²¹
- 3) pH²²⁻²⁴
- 4) applied potential and electric field effects²⁵⁻²⁷
- 5) electrolytes^{11,25}
- 6) alloys with other metals²⁸
- 7) temperature and pressure²⁹
- 8) cell design³⁰

The eighth point, the device that is used to test the catalyst, can have a significant impact on the catalytic behavior, and so our group took additional steps to verify that the system employed in our experiments performed consistently with similar devices reported in the literature (see **Chapter 2**).

These studies build a picture of the complexity of this system and of the challenge of improving the selectivity. While these changes to the catalyst and catalytic environment influence the distribution of products generated, a mixture of species is still formed in almost all of the precedents discussed above.

One consideration is that it is difficult to attribute a change in the system to just one of the above parameters. A change in the surface morphology, for example, may not only influence the binding of species to the surface sites, but also the local pH gradients and other components of the electrochemical double layer.

Another consideration is that these dynamic interfaces also include variations in the local environment and catalyst structure that influence the catalytic environment over the surface area of the catalyst and over time.

In addition, the number of observed products complicates experimental and computational efforts to understand the relevant mechanisms, particularly as more than one mechanism may be operative for the formation of a given compound under different reaction conditions.³¹

Therefore, while many in the literature have delved into the effects of changing a single parameter, this strategy has often resulted in more questions than are answered. In our studies, we have taken a different approach, in which we impose a substantial change onto the catalytic system and use the resulting behavior to determine which parameters are the most sensitive and readily tunable.

1.3 Organic species in the tuning of electrocatalytic CO₂ reduction selectivity

Our research group has been interested in the application of organic modifiers to tune the selectivity of these heterogeneous, metallic electrodes. Theoretical work in CO₂ reduction suggested that changes in single-metal systems, such as in surface morphology, are not sufficient to introduce substantial differences in binding energies toward similar carbon-bound

intermediates and drastically improve the selectivity for one species over another. The Norskøv group suggested that additional ancillary interactions, such as hydrogen bonding with surface intermediates, may introduce more substantial changes in the product distribution.³²

Organic modifiers have been employed in a few different examples in the CO₂ reduction literature. The majority of these studies center around the use of ionic liquids as the electrolyte, particularly with imidazolium salts.^{33,34} In addition to electrolyte engineering, organic species including porphyrins³⁶ and carbenes³⁶ have been covalently bound to metallic surfaces to influence the catalytic behavior of the metal interface. In these precedents, however, we noticed that the structures tended to be both complex and diverse; the structural complexity of the organic modifiers renders it difficult to definitively determine which feature is responsible for the change in catalytic behavior, and the variety of structures studied makes it difficult to draw comparisons and general conclusions from existing precedents in the literature. In our study, we begin to address these gaps in our understanding by employing structurally simple modifiers, and we find that the mechanism by which these species influence catalysis is not what we expected.

1.4 Summary and Outlook

The challenge of improving the selectivity for the CO₂ reduction reaction remains a platform for a wealth of future studies. While a number of studies have documented how the selectivity will change with variations in certain parameters, such as the electrode morphology or the electrolyte, the mechanistic pathways by which these changes occur, in many cases, are still under debate. Because of these gaps in our understanding, it remains difficult to predict how further changes in a catalyst may affect catalytic behavior, or to understand how changes in a combination of parameters may be used to achieve improved selectivity.

The changing atmosphere and environment also motivate our efforts to improve the selectivity of these catalysts. Technoeconomic analyses have indicated that improvements in selectivity are a vital component towards an economically viable CO₂ reduction system.^{3,4} The most substantial cost in the system is the electricity input; therefore, the loss of current to less desirable products and high overpotentials has a significant impact on the profitability.³ Recent estimates have suggested that formic acid and CO may be industrially viable at their current selectivities, but such compounds as ethylene and ethanol require improved catalytic performance to be profitable.³ We hope that recent advancements in our understanding of this reaction will bring us closer to a method of recycling the CO₂ we have been generating for decades.

1.5 References

1. Hansen, J.; Johnson, D.; Lacis, A.; Lebedeff, S.; Lee, P.; Rind, D.; Russell, G. Climate Impact of Increasing Atmospheric Carbon Dioxide. *Science* **1981**, *213*, 957-966.
2. Brewer, P. G. A Changing Ocean Seen with Clarity. *Proc. Nat. Acad. Sci.* **2009**, *106*, 12213-12214.
3. Jouny, M.; Luc, W.; Jiao, F. General Techno-Economic Analysis of CO₂ Electrolysis Systems. *Ind. Eng. Chem. Res.* **2018**, *57*, 2165-2177.
4. Greenblatt, J. B.; Miller, D. J.; Ager, J. W.; Houle, F. A.; Sharp, I. D. The Technical and Energetic Challenges of Separating (Photo)Electrochemical Carbon Dioxide Reduction Products. *Joule* **2018**, *2*, 381-420.
5. Kuhl, K. P.; Cave, E. R.; Abram, D. N.; Jaramillo, T. F. New Insights into the Electrochemical Reduction of Carbon Dioxide on Metallic Copper Surfaces. *Energy Environ. Sci.* **2012**, *5*, 7050-7059.
6. Schneider, J.; Jia, H.; Muckerman, J. T.; Fujita, E. Thermodynamics and Kinetics of CO₂, CO, and H⁺ Binding to the Metal Centre of CO₂ Reduction Catalysts. *Chem. Soc. Rev.* **2012**, *41*, 2036-2051.
7. Khalil, M. A. K. Non-CO₂ Greenhouse Gases in the Atmosphere. *Annu. Rev. Energy Environ.* **1999**, *24*, 645-661.
8. Yang, H.; Zhang, C.; Gao, P.; Wang, H.; Li, X.; Zhong, L.; Wei, W.; Sun, Y. *Catal. Sci. Technol.* **2017**, *7*, 4580-4598.
9. Kumar, B.; Llorente, M.; Froehlich, J.; Dang, T.; Sathrum, A.; Kubiak, C. P. Photochemical and Photoelectrochemical Reduction of CO₂. *Annu. Rev. Phys. Chem.* **2012**, *63*, 541-569.
10. Appel, A. M.; Bercaw, J. E.; Bocarsly, A. B.; Dobbek, H.; DuBois, D. L.; Dupuis, M.; Ferry, J. G.; Fujita, E.; Hille, R.; Kenis, P. J. A.; Kerfeld, C. A.; Morris, R. H.; Peden, C. H. F.; Portis, A. R.; Ragsdale, S. W.; Rauchfuss, T. B.; Reek, J. N. H.; Seefeldt, L. C.; Thauer, R. K.; Waldrop, G. L. *Chem. Rev.* **2013**, *113*, 6621-6658.
11. Hori, Y. In *Modern Aspects of Electrochemistry*; Vayenas, C. G., White, R. E., Gamboa-Aldeco, M. E., Eds.; Springer: New York, **2008**; pp 89-189.
12. Sakakura, T.; Choi, J.-C.; Yasuda, H. Transformation of Carbon Dioxide. *Chem. Rev.* **2007**, *107*, 2365-2387.
13. Nakamura, S.; Hatakeyama, M.; Wang, Y.; Ogata, K.; Fujii, K. In *Advances in CO₂ Capture, Sequestration, and Conversion*; Jin, F.; He, L.-N.; Hu, Y. H., Eds.; Oxford University Press: Oxford, **2015**; pp 123-134.
14. Benson, E. E.; Kubiak, C. P.; Sathrum, A. J.; Smieja, J. M. Electrocatalytic and Homogeneous Approaches to Conversion of CO₂ to Liquid Fuels. *Chem. Soc. Rev.* **2009**, *38*, 89-99.
15. Kortlever, R.; Shen, J.; Schouten, K. J. P.; Calle-Vallejo, F.; Koper, M. T. M. Catalysts and Reaction Pathways for the Electrochemical Reduction of Carbon Dioxide. *J. Phys. Chem. Lett.* **2015**, *6*, 4073-4082.
16. Feaster, J. T.; Shi, C.; Cave, E. R.; Hatsukade, T.; Abram, D. N.; Kuhl, K. P.; Hahn, C.; Nørskov, J. K.; Jaramillo, T. F. Understanding Selectivity for the Electrochemical Reduction of Carbon Dioxide to Formic Acid and Carbon Monoxide on Metal Electrodes. *ACS Catal.* **2017**, *7*, 4822-4827.
17. Peterson, A. A.; Nørskov, J. K. Activity Descriptors for CO₂ Electroreduction to Methane on Transition-Metal Catalysts. *J. Phys. Chem. Lett.* **2012**, *3*, 251-258.

18. Dunwell, M.; Luc, W.; Yan, Y.; Jiao, F.; Xu, B. Understanding Surface-Mediated Electrochemical Reactions: CO₂ Reduction and Beyond. *ACS Catal.* **2018**, *8*, 8121-8129.
19. Hahn, C.; Hatsukade, T.; Kim, Y.-G.; Vailionis, A.; Baricuatro, J. H.; Higgins, D. C.; Nitopi, S. A.; Soriaga, M. P.; Jaramillo, T. F. Engineering Cu Surfaces for the Electrocatalytic Conversion of CO₂: Controlling Selectivity toward Oxygenates and Hydrocarbons. *Proc. Nat. Acad. Sci.* **2017**, *114* 5918-5923.
20. Huang, Y.; Handoko, A D.; Hirunsit, P.; Yeo, B. S. Electrochemical Reduction of CO₂ Using Copper Single-Crystal Surfaces: Effects of CO* Coverage on the Selective Formation of Ethylene. *ACS Catal.* **2017**, *7*, 1749-1756.
21. Li, C. W.; Ciston, J.; Kanan, M. W. Electroreduction of Carbon Monoxide to Liquid Fuel on Oxide-Derived Nanocrystalline Copper. *Nature* **2014**, *508*, 504-507
22. Hori, Y.; Takahashi, R.; Yoshinami, Y.; Murata, A. Electrochemical Reduction of CO at a Copper Electrode. *J. Phys. Chem. B* **1997**, *101*, 36, 7075-7081.
23. Schouten, K. J. P.; Gallent, E. P.; Koper, M. T. M. The Influence of pH on the Reduction of CO and CO₂ to Hydrocarbons on Copper Electrodes. *J. Electroanal. Chem.* **2014**, *716*, 53-57.
24. Liu, X.; Schlexer, P.; Xiao, J.; Ji, Y.; Wang, L.; Sandberg, R. B.; Tang, M.; Brown, K. S.; Peng, H.; Ringe, S.; Hahn, C.; Jaramillo, T. F.; Nørskov, J. K.; Chan, K. pH Effects on the Electrochemical Reduction of CO₍₂₎ towards C₂ Products on Stepped Copper. *Nat. Commun.* **2019**, *10*.1038.
25. Resasco, J.; Chen, L. D.; Clark, E.; Tsai, C.; Hahn, C.; Jaramillo, T. F.; Chan, K.; Bell, A. T. Promoter Effects of Alkali Metal Cations on the Electrochemical Reduction of Carbon Dioxide. *J. Am. Chem. Soc.* **2017**, *139*, 11277-11287.
26. Chen, L. D.; Urushihara, M.; Chan, K.; Nørskov, J. K. Electric Field Effects in Electrochemical CO₂ Reduction. *ACS Catal.* **2016**, *6*, 7133-7139.
27. Liu, M.; Pang, Y.; Zhang, B.; De Luna, P.; Voznyy, O.; Xu, J.; Zheng, X.; Dinh, C. T.; Fan, F.; Cao, C.; de Arquer, P. G.; Safaei, T. S.; Mepham, A.; Klinkova, A.; Kumacheva, E.; Filleter, T.; Sinton, D.; Kelley, S. O.; Sargent, E. H. Enhanced Electrocatalytic CO₂ Reduction via Field-Induced Reagent Concentration. *Nature* **2016**, *537*, 382-386.
28. Nitopi, S.; Bertheussen, E.; Scott, S. B.; Liu, X.; Engstfeld, A. K.; Horch, S.; Seger, B.; Stephens, I. E. L.; Chan, K.; Hahn, C.; Nørskov, J. K.; Jaramillo, T. F. J.; Chorkendorff, I. Progress and Perspectives of Electrochemical CO₂ Reduction on Copper in Aqueous Electrolyte. *Chem. Rev.* **2019**, *119*, 7610-7672.
29. Ramdin, M.; Morrison, A. R. T.; de Groen, M.; van Haperen, R.; de Kler, R.; van den Boroeke, L. J. P.; Trusler, J. P. M.; de Jong, W.; Vlugt, T. J. H. High Pressure Electrochemical Reduction of CO₂ to Formic Acid/Formate: A Comparison between Bipolar Membranes and Cation Exchange Membranes. *Ind. Eng. Chem. Res.* **2019**, *58*, 1834-1847.
30. Burdyny, T.; Smith, W. A. CO₂ Reduction on Gas-Diffusion Electrodes and Why Catalytic Performance Must be Assessed at Commercially-Relevant Conditions. *Energy Environ. Sci.* **2019**, *12*, 1442-1453.
31. Garza, A. J.; Bell, A. T.; Head-Gordon, M. Mechanism of CO₂ Reduction at Copper Surfaces: Pathways to C₂ Products. *ACS Catal.* **2018**, *8*, 1490-1499.
32. Peterson, A. A.; Nørskov, J. K. Activity Descriptors for CO₂ Electroreduction to Methane on Transition-Metal Catalysts. *J. Phys. Chem. Lett.* **2012**, *3*, 251-258.

33. Rosen, B. A.; Salehi-Khojin, A.; Thorson, M. R.; Zhu, W.; Whipple, D. T.; Kenis, P. J. A.; Masel, R. I. Ionic Liquid-Mediated Selective Conversion of CO₂ to CO at Low Overpotentials. *Science* **2011**, *334*, 643-644.
34. Lau, G. P. S.; Schreier, M.; Vasilyev, D.; Scopelliti, R.; Grätzel, M.; Dyson, P. J. New Insights into the Role of Imidazolium-Based Promoters for the Electroreduction of CO₂ on a Silver Electrode. *J. Am. Chem. Soc.* **2016**, *138*, 7820-7823.
35. Gong, M.; Cao, Z.; Liu, W.; Nichols, E. M.; Smith, P. T.; Derrick, J. S.; Liu, Y.-S.; Liu, J.; Wen, X.; Chang, C. J. Supramolecular Porphyrin Cages Assembled at Molecular–Materials Interfaces for Electrocatalytic CO Reduction. *ACS Cent. Sci.* **2017**, *3*, 032-1040.
36. Cao, Z.; Kim, D.; Hong, D.; Yu, Y.; Xu, J.; Lin, S.; Wen, X.; Nichols, E. M.; Jeong, K.; Reimer, J. A.; Yang, P.; Chang, C. J. A Molecular Surface Functionalization Approach to Tuning Nanoparticle Electrocatalysts for Carbon Dioxide Reduction. *J. Am. Chem. Soc.* **2016**, *138*, 8120-8125.

Chapter 2:

Description of the Electrochemical Cells and Setup Used for the Described Experiments

2.1 Discussion

The chemistry of CO₂ reduction is sensitive to a variety of factors, including mass transport of CO₂ to the surface, the local pH, the local electric field, the temperature and the solvent, as described in the introductory chapter. Hori suggests that even the stirring in the cell affects the product distribution, as “when the electrolyte is stirred, CO desorbs easily from the surface”.¹ Therefore, the chemistry observed with a given catalyst can be strongly dependent on various features of the electrochemical cell that is used to test its CO₂ reduction behavior.

In order to evaluate catalysts for their CO₂ reduction behavior, we needed an electrochemical cell setup that:

- 1) yielded results that were illustrative of the behavior of the catalyst in the given conditions (and not dependent upon a limitation of the cell, such as rapid depletion of CO₂ or the presence of impurities),
- 2) yielded data consistent with others in the literature and within our research center, JCAP, and
- 3) yielded consistent results over time and across trials.

We therefore assembled our electrochemical cells and product detection setup, and then conducted a series of experiments to verify that the above criteria were met.

We decided to use two different cell designs, both previously described in the literature by other groups within our research center.^{2,3} They are both flow cells, i.e. both cells have CO₂ flowing continuously through the system, allowing the electrolyte to remain saturated throughout the experiment. A static cell, in contrast, would allow buildup of products over time, but also would not demonstrate consistent catalytic behavior as the CO₂ is consumed. The two cells differ in geometry and certain other features- for example, the cell reported by the Ager group features a glass frit to generate smaller bubbles and help maintain saturation, while the Jaramillo cell features a larger electrolyte volume to maintain saturation.

Our copies of these electrochemical cells were fabricated out of polyether ether ketone (PEEK) or polychlorotrifluoroethylene (Kel-F), so that they could be soaked in 20% nitric acid (PEEK cell) or in aqua regia (Kel-F), then sonicated in water and isopropanol, to remove impurities before use. This was particularly important, as traces of metallic impurities can catalyze hydrogen evolution and substantially impact the observed catalytic behavior.⁴ All of the fittings for the cell that could come in contact with the electrolyte were also treated with nitric acid or aqua regia, and then rinsed with water, before use.

In line with the electrochemical cell, we collected gas chromatography data with a multiple gas analyzer #5 from SRI Instruments. The thermal conductivity detector (TCD) was not sufficiently sensitive to detect the hydrocarbon products being generated, and so the flame ionization detector (FID) of this instrument was used for these products (including CO, methane, ethylene and ethane), while hydrogen formation was detected with the TCD. Liquid products were analyzed with an aliquot collected after the experiment with an UltiMate 3000 High Performance Liquid Chromatograph from Thermo Fisher Scientific or an Ascend 500 MHz NMR from Bruker.

To test the cleanliness and overall performance of our electrochemical cell and product detection method, we performed a series of tests using polycrystalline Cu foil. We sanded and electropolished the Cu as described in the literature³ and then evaluated its catalytic performance in both cells. The graphs are expressed in terms of Faradaic efficiency, or the amount of each

product formed (expressed in terms of the number of electrons needed to form each product) divided by the number of electrons input into the system (in other words, the current):

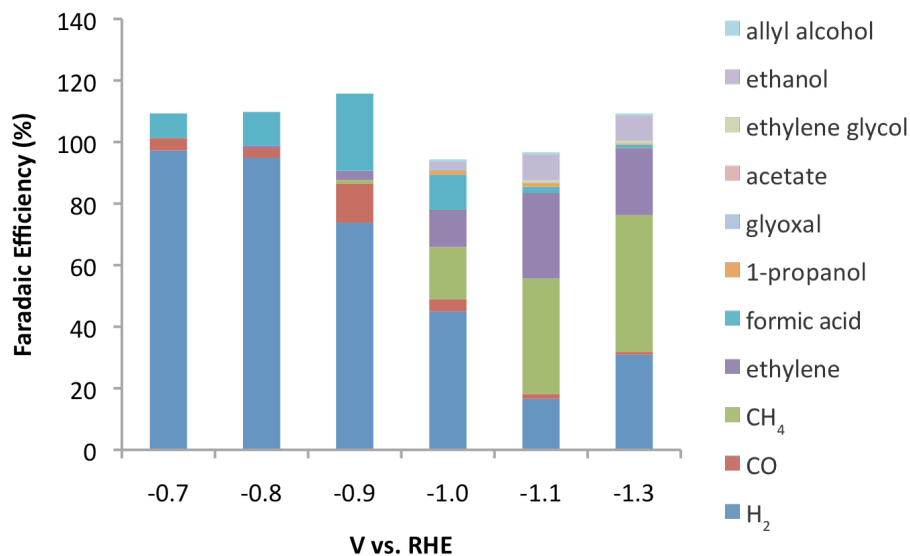


Figure 1. CO₂ reduction product selectivity obtained with polycrystalline Cu foil using a cell reported by Jaramillo, *et al.*³

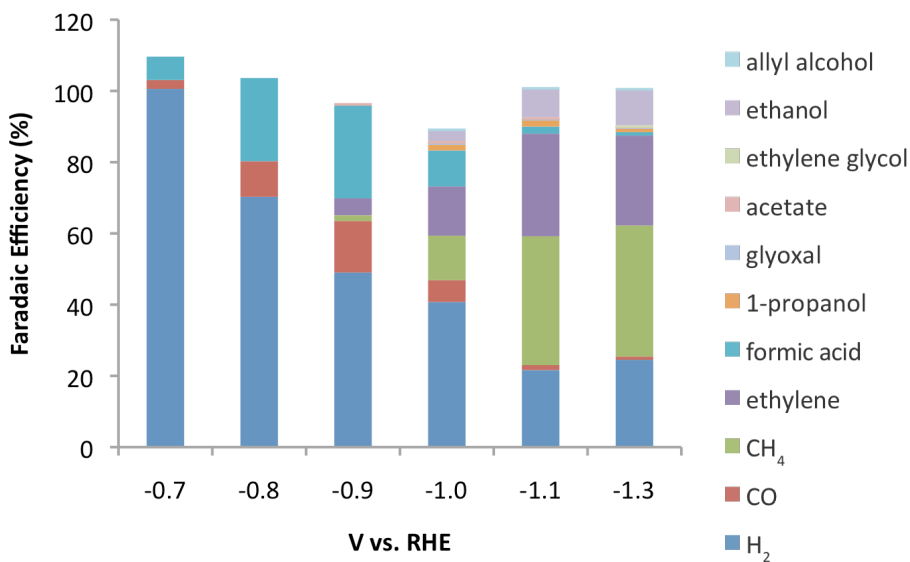


Figure 2. CO₂ reduction product selectivity obtained with polycrystalline Cu foil using a cell reported by Ager, *et al.*²

Examining the graphs individually, we observe that the total Faradaic efficiency adds up to approximately 100%. This suggests that we are accurately accounting for all of the products formed. We attribute the slight deviations, where some trials result in numbers slightly greater than or less than 100%, to such variables as imperfect mixing of the gaseous products,

fluctuations in the current and products formed, and other values that are averaged over time to obtain the total selectivity.

In comparing the data between the two graphs, we observe that the overall trends are consistent, with two-electron products such as CO and formic acid formed at lower potentials, and multi-electron, multi-carbon products formed at higher potentials. At lower potentials, we observe that the Ager cell demonstrates higher selectivity for formic acid, lower selectivity for H₂, relative to the Jaramillo cell. We hypothesize that this may be due to the improved CO₂ distribution in the electrolyte with the glass frit. Due to this difference and the ease of use of the smaller cell design, we decided to use the Ager cell for the experiments within the thesis.

We also compared our data to those in the literature:

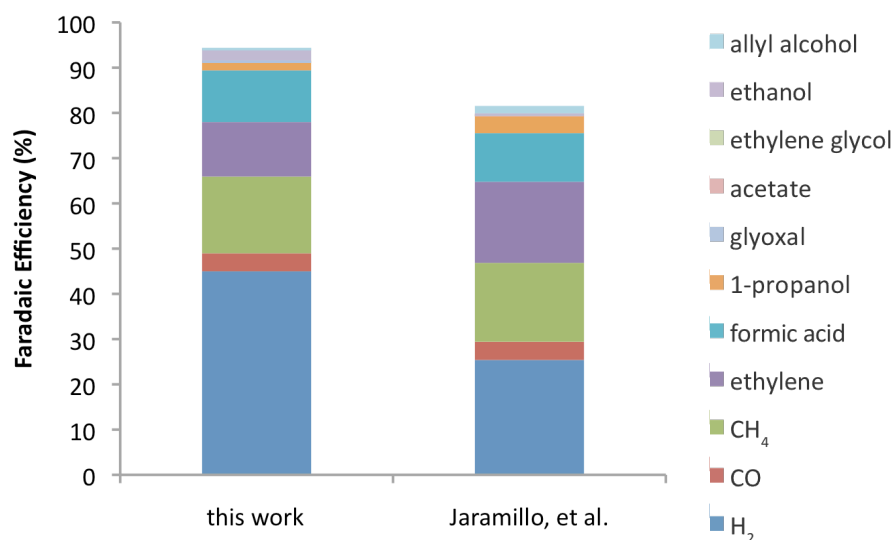


Figure 3. CO₂ reduction product selectivity obtained with polycrystalline Cu foil at -1.0 V vs. RHE in the Jaramillo cell, and data collected by Jaramillo, *et al.*³

We find that the distribution of products is quite similar to that found by Jaramillo, *et al.*, for the same cell design and applied potential. We were also able to verify with collaborators at Caltech and Stanford that our data obtained with the two cells were consistent with those collected at the other research sites.

To test the consistency of our setup, we examined Cu foil over multiple trials:

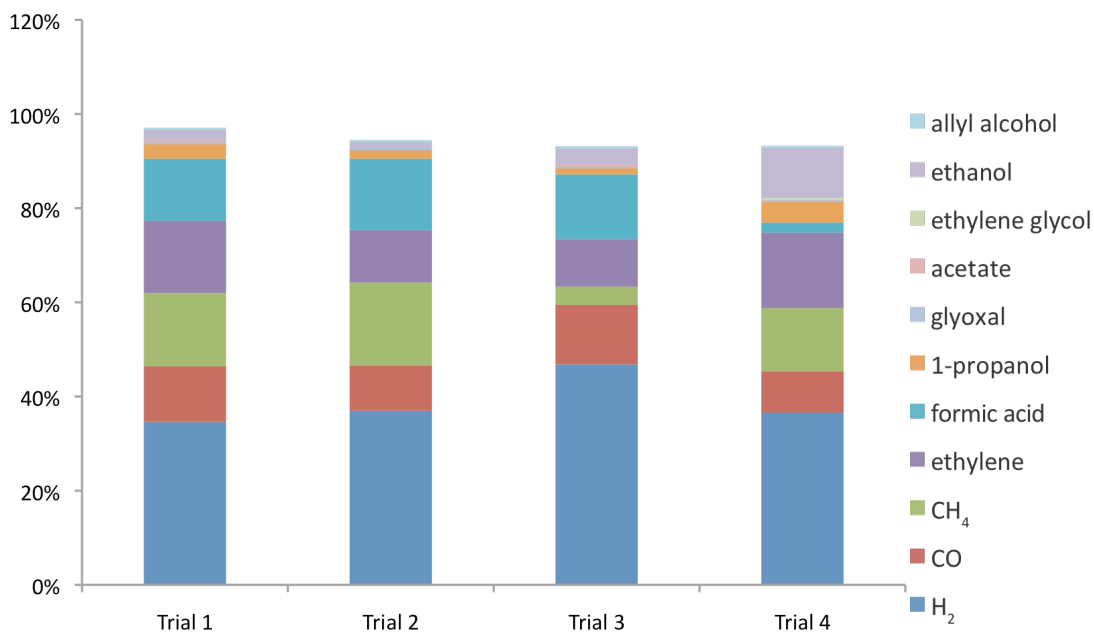


Figure 4. Polycrystalline Cu foil tested at -1.0 V vs. RHE. Trials were conducted using different samples of Cu foil and collected on different days, over the period of several weeks.

We find that the selectivity remains fairly consistent over multiple trials. In many of the experiments in the thesis, we report an average of multiple trials with error bars depicting the standard error of the mean, in order to illustrate the degree of variability we observe.

These data demonstrate that our electrochemical cells exhibit very similar behavior to that previously described in the literature. This similarity suggests that we are able to accurately characterize the CO₂ reduction behavior of Cu in an aqueous environment, with CO₂ transport and lack of impurities comparable to that reported by others. These comparisons with the literature and others in our research center also allow us to draw direct comparisons with catalysts developed in other research groups. The consistency of our system over multiple trials also speaks to the reliability of this method. With this data collected on a known catalyst, we were able to test novel catalysts with greater confidence in our analytical method.

2.2 References

1. Hori, Y. In *Modern Aspects of Electrochemistry*; Vayenas, C. G., White, R. E., Gamboa-Aldeco, M. E., Eds.; Springer: New York, **2008**; pp 89-189.
2. Lobaccaro, P.; Singh, M. R.; Clark, E. L.; Kwon, Y.; Bell, A. T.; Ager, J. W. Effects of Temperature and Gas-Liquid Mass Transfer on the Operation of Small Electrochemical Cells for the Quantitative Evaluation of CO₂ Reduction Electrocatalysts. *Phys. Chem. Chem. Phys.* **2016**, *18*, 26777-26785.
3. Kuhl, K. P.; Cave, E. R.; Abram, D. N.; Jaramillo, T. F. New Insights into the Electrochemical Reduction of Carbon Dioxide on Metallic Copper Surfaces. *Energy Environ. Sci.* **2012**, *5*, 7050-7059.
4. Clark, E. L.; Resasco, J.; Landers, A.; Lin, J.; Chung, L.-T.; Walton, A.; Hahn, C.; Jaramillo, T. F.; Bell, A. T. Standards and Protocols for Data Acquisition and Reporting for Studies of the Electrochemical Reduction of Carbon Dioxide. *ACS Catal.* **2018**, *8*, 6560-6570.

Chapter 3

Electrocatalysis at Organic-Metal Interfaces: Identification of Structure-Reactivity Relationships for CO₂ Reduction at Modified Cu Surfaces

This chapter has previously appeared in:

Buckley, A. K.; Lee, M.; Cheng, T.; Kazantsev, R. V.; Larson, D. M.; Goddard III, W. A.; Toste, F. D.; Toma, F. M. *J. Am. Chem. Soc.* **2019**, *141*, 18, 7355-7364.

3.1 Introduction

The electrocatalytic reduction of carbon dioxide (CO₂R) offers an efficient strategy to reduce the presence of greenhouse gases in the atmosphere while concurrently producing valuable carbon-based products.^{1,2} Existing electrocatalysts for this process, however, are insufficiently active or selective for attractive energy dense products, particularly in the face of the competing hydrogen evolution reaction (HER).^{3,4} Cu surfaces, for example, have drawn interest because they are the only single-metal electrodes that produce significant amounts of hydrocarbons. However, the inability to tune the selectivity among 16 observed products, particularly under mild, aqueous conditions, poses a challenge.³⁻⁶

In order to address this challenge, adjustable catalytic systems need to be identified to systematically evaluate how changes in structure affect catalyst selectivity. This strategy may reveal design principles that enable development of active and selective catalysts and provide further insights into the reaction mechanism. As an example, in electrocatalytic molecular systems for CO₂R, hydricity (i.e., the energy required to cleave a M-H bond to form a hydride) has been identified as a key selectivity-defining parameter.⁷⁻¹⁰ Specifically, the initial reduction of CO₂ with two protons and two electrons can produce either CO or formic acid, with HER as a competitive side reaction. While preferential interaction of the catalytic metal center with CO₂ over protons is thought to be key to selectivity for CO, moderate hydricity facilitates migratory insertion of CO₂ into M-H bonds to yield formic acid, and strong hydride donors catalyze H₂ formation.⁸⁻¹⁰

While heterogeneous metal catalysts provide a more recyclable alternative to homogeneous complexes, the selectivity of heterogeneous systems has proved difficult to predictably alter.⁷ Main group metals, such as In, Sn, Hg, and Pb, are selective for the synthesis of formic acid,¹¹ a fuel with practical applications in hydrogen storage^{12,13} and direct formic acid fuel cells.¹⁴ However, these metals often require high overpotentials.¹¹ In addition to formic acid, CO is also a product of interest because it serves as the intermediate towards all other observed products in electrochemical CO₂R, including ethylene and ethanol, and it is currently of use in the formation of hydrocarbons through Fischer-Tropsch chemistry. However, high selectivity for CO requires metals with weak CO binding energies, such as the precious metals Au or Ag.¹¹

The ability to tune the product selectivity between CO and formic acid with a non-precious metal would not only be of interest due to the practical applications of these products, but also because existing tools to control this initial bifurcation in the process of electrochemical CO₂R on Cu are limited.¹⁵⁻¹⁷ Several notable, recent studies have examined product selectivity by starting with CO₂ reduction intermediates, especially with CO.¹⁸⁻²⁰ The study of the initial two proton, two electron transfer to CO₂ may open doors to tandem catalytic processes, combining multiple steps of the CO₂R process, or yield insights that are applicable to further downstream processes.

In this chapter, organic modifiers are employed to alter the CO₂R selectivity of a single non-precious metal surface, modifying Cu surfaces to alter CO₂R selectivity between CO, formic acid and H₂. Towards this goal, we first examined polymeric and molecular modifiers that feature a wide variety of functional groups (aryl, amine, amide and ether groups, for example) as well as diverse structural features (e.g., neutral or cationic, protic or aprotic). We characterized their effect on the electrocatalytic behavior of Cu at -0.7 V vs. RHE, at which the unfunctionalized Cu surface generates CO, formic acid and H₂ in roughly equivalent proportions. In the presence of organic modifiers, we observed significant changes in CO₂R selectivity

between these three products, with selectivities of up to 76% CO or 62% formic acid, and tuning of H₂ selectivity from 97% down to 2%. These changes allowed classification of the modifiers by the products that they promote. Examination of these classes allowed identification of the common structural characteristics that are key in influencing product selectivity.

While experimental and computational studies have examined CO₂R catalysis at metal surfaces, the complexity of the catalyst/electrolyte interface makes it difficult to identify the mechanism by which a change in the catalyst affects the CO₂R selectivity. As a consequence, the most commonly adopted approach has been to select specific parameters and investigate their effect on the observed selectivity.²¹ In this study, in contrast, we allow a substantial degree of freedom for the surface chemistry to provide information on relevant parameters that may have an important role in determining CO₂R selectivity. Organic structures hold promise for various roles in CO₂R devices, including their use as membranes,²² electrolytes,²³⁻²⁵ coatings for the preparation of nanoparticulate or surface electrodes,²⁶ or supports to improve electrode stability;²⁷ therefore, we expect that the parameters highlighted in our study will help guide the further development of CO₂R catalysts and organic structures for CO₂R devices.

3.2 Results and Discussion

3.2.1 Structurally diverse organic modifiers result in divergent catalytic behavior from Cu: We tested a series of organic polymeric and molecular structures on Cu electrodes (**Fig. 1** and section **3.5.1** in Supplementary Information). Oxide-derived Cu surfaces were prepared as described in a reported procedure.²⁸ The organic modifier of interest was dissolved in a volatile organic solvent and dropcast onto the Cu surface (**Fig. 1a**). In order to focus on interactions at the electrode/electrolyte interface, we studied surface modifiers with relatively low water solubility, such as polymeric species and molecular species with long hydrocarbon chains. Once the Cu electrode with the organic modifier was prepared, a solution of Nafion was dropcast onto the electrode. Nafion was found to act as an effective binder for the modifier without influencing the CO₂R selectivity (see **3.5.2**). The electrode was placed in a two-chamber flow cell of a reported cell design,²⁹ and the CO₂R behavior was evaluated by conducting a chronoamperometry (CA) experiment at -0.7 V vs. RHE for 65 minutes. During the experiment, gaseous products were characterized via injections with an in-line gas chromatograph (GC), while liquid products were characterized via high performance liquid chromatography (HPLC) after the CA experiment.

In examining the effects of organic modifiers on the CO₂R behavior of Cu, we discovered that the relative formation of H₂, formic acid or CO could be altered by varying the modifier. **Fig. 1b** illustrates three representative modifiers that demonstrate enhanced selectivity or activity for these products. We chose these modifiers to discuss and analyze in detail due to their structural diversity. Polyvinylpyrrolidone (**1**) is a neutral polymer that is often used as a ligand in nanoparticle synthesis.³¹ Tetrahexadecylammonium bromide (**2**) is a cationic salt with low solubility in water, which aids in binding the modifier to the electrode. Polyallylamine (**3**) is a neutral polymer with primary amine groups, which can participate in hydrogen bonding interactions.

Compared to the unfunctionalized Cu electrode (**Ox Cu**), selectivity for formic acid (blue), CO (red), or H₂ (gray) improved in the presence of **1**, **2**, or **3**, respectively (**Fig. 1c** and **3.5.3**). The other observed products (yellow) were present in traces at this potential and largely consisted of ethylene and ethane. In the presence of **1**, the Faradaic efficiency (i.e. the percentage of electrons that were transferred to a given product) for formic acid increased to

45% \pm 2% from 34% \pm 3% in the **Ox Cu** case, accompanied by an increase in H₂ selectivity to 43% \pm 1% from 28% \pm 2%. In the presence of **2**, CO selectivity increased slightly from 28% \pm 2% in the **Ox Cu** case to 33.8% \pm 0.9%. H₂ selectivity drastically increased to 97% \pm 2% with the addition of **3**, as compared to 28% \pm 2% with **Ox Cu**.

Experiments with varying loadings of **1** and **2** demonstrate similar selectivities towards more formic acid or CO, and are described in more detail in the Supplementary Information (3.5.4). In addition, similar trends were observed in experiments at higher overpotentials, with higher selectivity for formic acid, CO and H₂ obtained with **1**, **2**, and **3**, respectively (3.5.5).

When CO₂ was replaced by N₂ under otherwise identical conditions, the absence of CO₂R products was observed, thus supporting that the detected products were formed via CO₂R rather than decomposition of the organic modifier (2.5.6). The organic modifiers were also analyzed by ¹H-NMR after the hour-long CA experiment to examine whether the organic modifiers maintained their chemical structure (3.5.7).

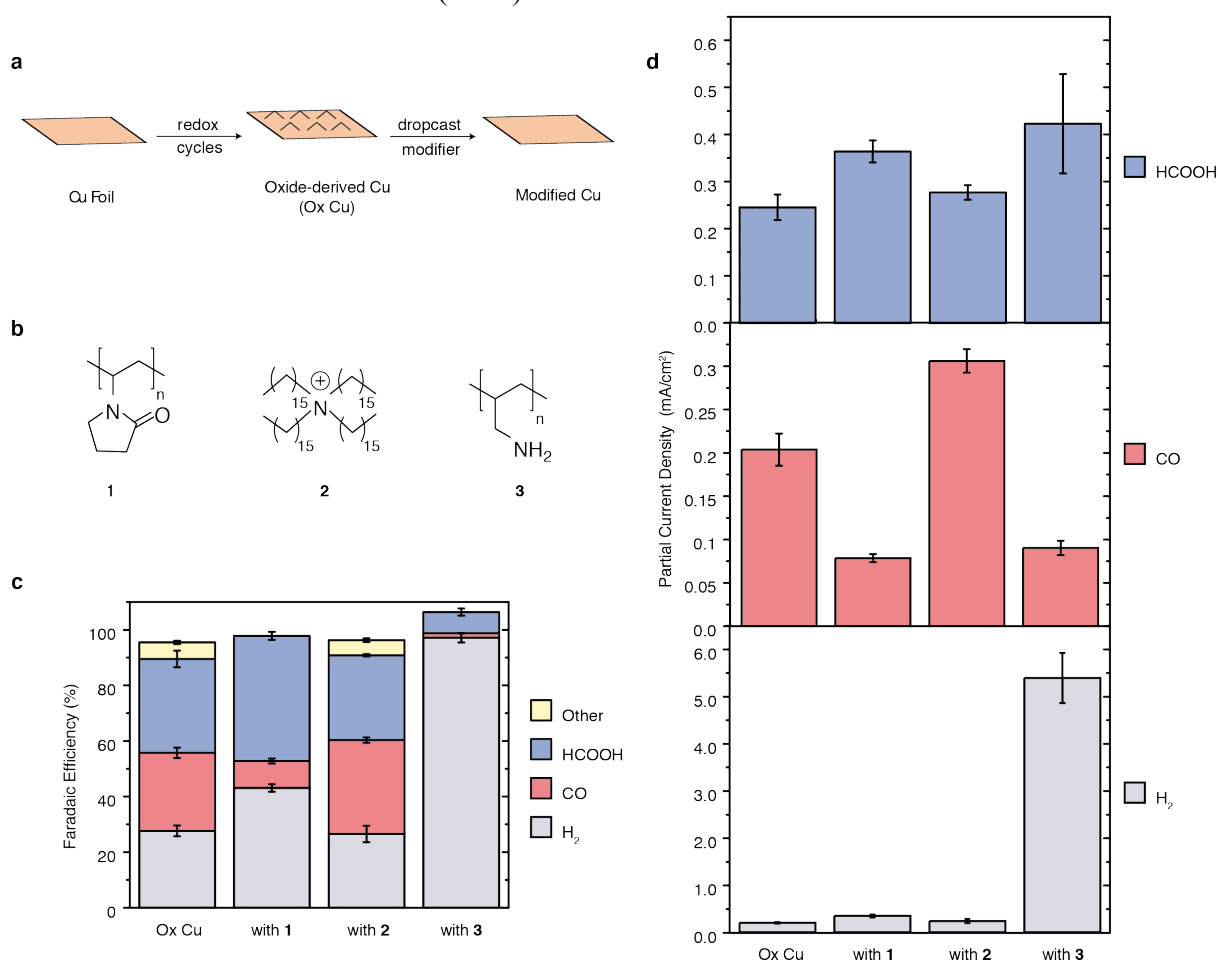


Figure 3. Modifiers to promote H₂, CO or formic acid formation. To readily prepare functionalized surfaces, oxide-derived Cu surfaces were generated, and the organic modifiers were then dropcast onto the surface (a). Three modifiers, namely polyvinylpyrrolidone (**1**), tetrahexadecylammonium (**2**) with bromide anion not shown, and polyallylamine (**3**), tested to promote H₂ (gray), CO (red), or formic acid (blue) formation on Cu at -0.7 V vs. RHE (b). Traces of other products (yellow) indicate the presence of ethylene and ethane. Plots of product selectivity in terms of the Faradaic efficiencies (c) or partial current densities (d) of unfunctionalized Cu (**Ox Cu**) and of **Ox Cu** with **1**, **2**, and **3** illustrate the change in selectivity and activity with each added modifier. Values and error bars are calculated from at least three trials. Error bars are reported as standard error of the mean.

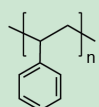
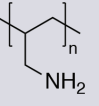
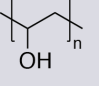
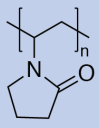
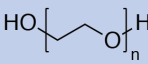
In addition to the Faradaic efficiencies, we also considered the partial current densities towards each product, which depict the amount of current transferred to generate a given product (**Fig. 1d**). These data provide more information regarding whether an increase in selectivity is due to a higher amount of product formed, or whether it is due to the selective suppression of other products caused by a decrease of the total current. **Fig. 1d** illustrates that the increase in Faradaic efficiency for H₂, CO and formic acid is accompanied by an increase in the partial current density as well. The partial current for formic acid, for example, increased from 0.25 mA/cm² ± 0.03 mA/cm² in the unfunctionalized case to 0.36 mA/cm² ± 0.02 mA/cm² with the addition of **1**, an increase of 44%. The partial current for CO increased from 0.20 mA/cm² ± 0.02 mA/cm² to 0.31 mA/cm² ± 0.01 mA/cm² with the addition of **2**, an increase of 55%. The partial current for H₂ increased 27 times from **Ox Cu** to the sample modified with **3**. These reported values are based upon geometric current densities; current densities normalized by electrochemically active surface area demonstrate similar trends (**3.5.8**). For many of the modifiers discussed in this text, increases in selectivity are accompanied by increases in partial current densities, thus demonstrating that these organic modifiers may be used to enhance the amount of product formed.

3.2.2 Classification of modifiers by promoted products: The changes in product distribution with the addition of the organic modifiers in **Fig. 1** raise the question of how these changes are effected. Previous works employing organic modifiers to tune CO₂R product selectivity have evoked different explanations, including interactions between modifiers with surface intermediates and effects on the local electrode environment.^{19,30-33} We decided to study a diversity of structures in order to identify which common characteristics play a key role in influencing the product distribution. While a number of factors may be at play, we believe that this strategy would help ascertain which structure-reactivity relationships are the most sensitive and readily tunable.

A series of neutral organic modifiers was dropcast onto Cu electrodes as previously described. The product distribution of these samples in the CO₂R reaction yielded insights into possible structure-reactivity relationships at work (**Table 1**). With the addition of polymers with protic functional groups (entries **c** and **d**, in gray), we observed a substantial increase in HER selectivity, whereas with the addition of polymers with aprotic groups (entries **e** and **f**, in blue), we observed an increase in the selectivity for formic acid. Addition of polystyrene (entry **b**, in green), a hydrocarbon, results in decreased selectivity for both CO and formic acid.

While primary amines such as **3** have been reported to form carbamates,³⁴ we hypothesize that the protic functionality is responsible for this observed catalytic behavior. The enhancement of HER with the addition of protic functional groups is consistent with precedents in both homogeneous and heterogeneous HER catalysis. In addition to molecular examples,³⁵ primary amines have also been used to promote HER on heterogeneous Pt catalysts and has recently also been reported with **3** on Cu.^{36,37} Our hypothesis is also supported by the enhancement in HER selectivity with **5**. It is possible that the protic groups act as proton shuttles, as previously suggested, or possibly that these groups have an electronic effect that promotes HER. These results suggest that protic functional groups should be avoided in the design of organic structures for CO₂R devices due to this observed tendency to promote HER.

Table 1. Neutral polymers and their effect on CO₂R selectivity at Cu. Faradaic efficiencies and total current for Cu surfaces modified with neutral polymers. Samples were prepared with the same loading of polymer by mass. CA experiments were conducted at -0.7 V vs. RHE for 65 minutes. Values represent averages of at least three trials.

Table Entry	Modifier	Modifier Number	H ₂	CO	Formic Acid	Other	Total FE	Total Current (mA/cm ²)
a	Ox Cu	-	28% ± 2%	28% ± 2%	34% ± 3%	6.0% ± 0.6%	96% ± 2%	0.73 ± 0.05
b		4	44.6% ± 0.6%	19% ± 2%	23.5% ± 0.8%	3.5% ± 0.7%	91% ± 2%	0.80 ± 0.13
c		3	97% ± 2%	1.63% ± 0.04%	8% ± 1%	0%	106.4% ± 0.4%	5.6 ± 0.6
d		5	71% ± 2%	15.1% ± 0.6%	17% ± 1%	0%	103% ± 1%	0.54 ± 0.06
e		1	43% ± 1%	10% ± 1%	45% ± 2%	0%	98% ± 1%	0.81 ± 0.05
f		6	44% ± 6%	16% ± 3%	38% ± 3%	0%	98% ± 2%	0.70 ± 0.08

We were intrigued by the enhanced selectivity for formic acid observed with aprotic species. Therefore, we increased the diversity of examined structures to better understand this phenomenon. In addition to the functional groups exemplified by these neutral polymers, we applied the strategy outlined in **Fig. 1a** to probe cationic species. In the literature, cationic species have been employed to influence CO₂R behavior at various metals.^{23-25,30} In these precedents, the cationic species employed are often *N*-containing heterocyclic compounds, which have been theorized to influence catalytic behavior via a number of possible molecular orientations at the electrode.²⁴ These heterocycles have also demonstrated ancillary reactivity or fragmented under electrochemically reducing conditions, adding to the uncertainty regarding which species is responsible for observed changes in catalytic behavior.²⁵ Therefore, we chose to test acyclic quaternary ammonium and phosphonium salts to provide structural simplicity, mitigate the potential for the modifier to be directly involved in electron transfer processes, and to readily allow for stepwise changes in structure.

In addition to the previously discussed tetrahexadecylammonium salt **2**, we tested a series of ammonium salts with varying hydrocarbon chain lengths (**Fig. 2a**) to ascertain how this structural change affects the influence of these modifiers. We had previously observed that the addition of **2**, which features four 16-carbon chains, slightly increased selectivity for CO. Changing these hydrocarbon substituents to feature three methyl groups and a C-16 chain, as in cetyltrimethylammonium bromide (**10**), yielded more formic acid (**Fig. 2b**).

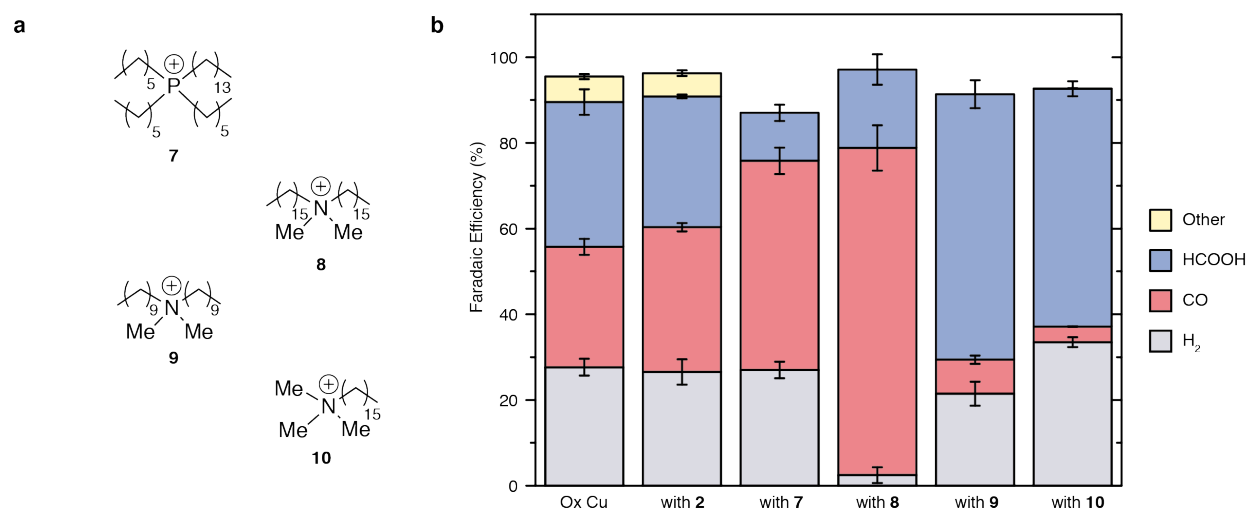


Figure 4. Study of cationic modifiers. Quaternary cationic modifiers, namely trihexyltetradecylphosphonium (7), dihexadecyldimethylammonium (8), didecyldimethylammonium (9), and cetyltrimethylammonium (10), were tested in CO₂R on Cu at -0.7 V vs. RHE (a). For all of these cases, the bromide of the salt was used. The Faradaic efficiencies of **Ox Cu** and the Cu surfaces modified with cationic species are compared (b). Data and error bars in bar graphs are calculated from at least three trials. Error bars are reported as standard error of the mean.

Unexpectedly, salts with intermediate hydrocarbon content also demonstrated a stark difference in selectivity. Didecyldimethylammonium bromide (9) increased formic acid selectivity, while dihexadecyldimethylammonium bromide (8) increased CO selectivity. The observed products for 2, 8, 9 and 10 appear to fit a trend in which salts with greater hydrocarbon content improve selectivity for CO, while those with less improve formic acid selectivity. To further probe this observation, a phosphonium salt with relatively high hydrocarbon content (trihexyltetradecylphosphonium bromide, 7) was also tested and found to enhance CO selectivity. Notably, the breaking point in the selectivity trend between two dimethyl substituted ammonium salts suggests that steric hindrance about the heteroatom center is not the sole root of the observed selectivity changes. In order to better understand this overall trend observed with these modifiers, we conducted additional experimental and theoretical studies to delve into the mechanism of this effect, particularly as observed with modifiers 8 and 9, as described below.

3.2.3 Proposed mechanisms of influence of organic modifiers on CO₂R selectivity: Faced with this unexpected relationship between the organic modifiers and the observed product distribution, we collaborated with Dr. Tao Cheng and Prof. William A. Goddard, who carried out multiscale ReaxFF reactive molecular dynamics (RMD) simulations to model the morphology of the two dimethyl substituted ammonium salts, 8 and 9, at the Cu electrode (Fig 3a-b). We chose these two cases because they led to dramatically different product distributions. For 9, the surfactant molecules are well solvated in the electrolyte and widely distributed on the Cu electrode, forming a dispersed network (Fig. 3a). For 8, the surfactant assembles into larger clusters on the Cu electrode with the ammoniums exposed to the solvent and hydrocarbon chains inside (Fig. 3b).

This difference in behavior was also probed experimentally by characterizing how Cu surfaces modified with 8 and 9 interact with water. We measured the contact angle of a 3 μ L

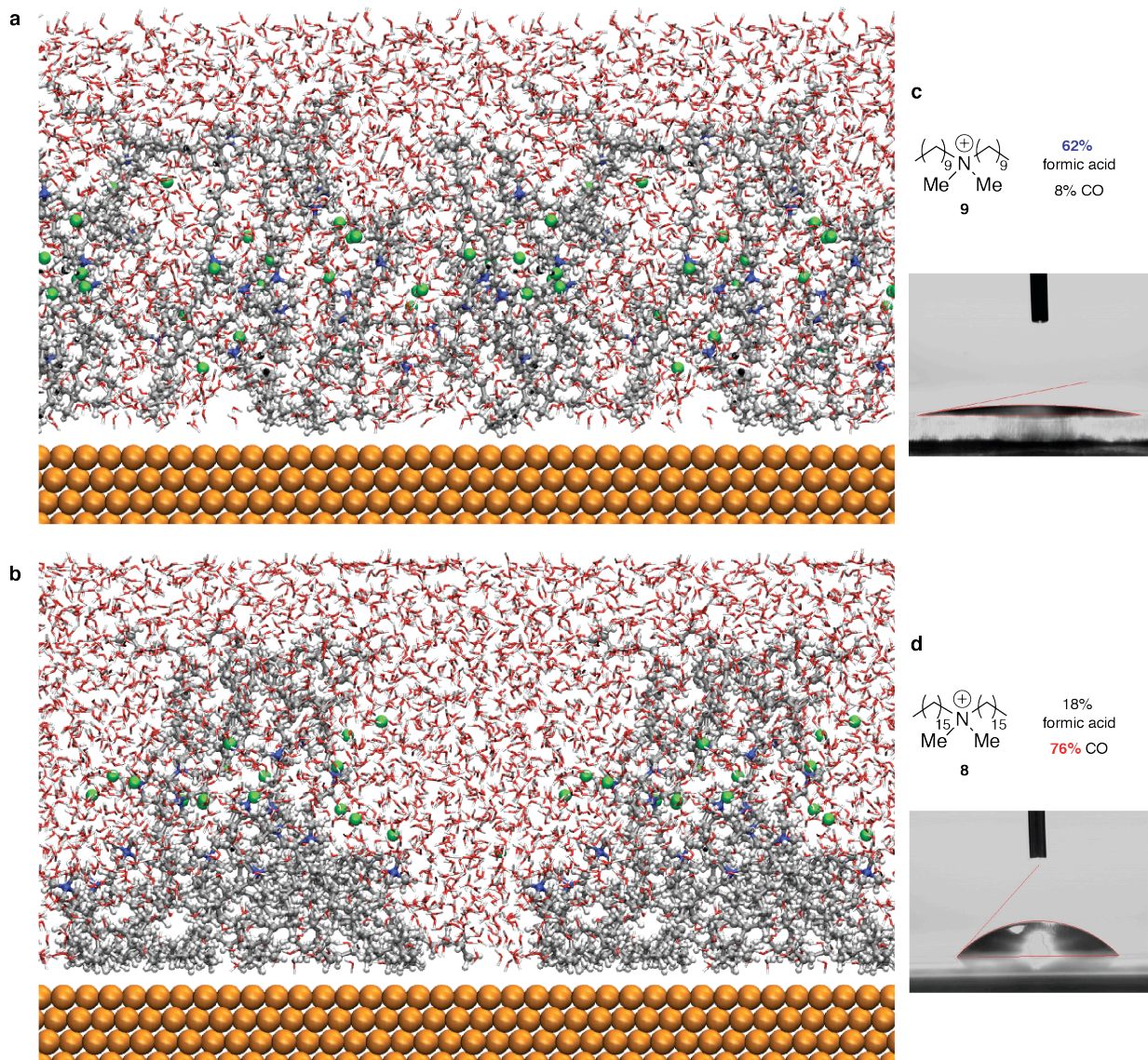


Figure 5. Study of Cu surfaces modified with 8 and 9. The last snapshot of the interface between Cu, water, and hydrophilic species **9** (a) and hydrophobic species **8** (b), extracted from 5 ns of RMD canonical ensemble (NVT) simulations at 298 K to equilibrate the interface. The colors are N in blue, C in gray, O in red, H in white, and Br in green. The contact angle between a 3 μ L drop of water and Cu surfaces modified with **9** (c) and **8** (d).

drop of water on the two modified surfaces (Fig. 3c-d and 3.5.9). We found that **9** yielded a smaller contact angle with water, indicating that the surface is relatively hydrophilic, while **8** yielded a larger contact angle, indicating that the surface is more hydrophobic. Intrigued by this effect, we expanded the contact angle measurements to include previously examined species (Fig. 4a and 3.5.9). In addition, we analyzed the increase in formic acid production as a function of increasing hydrophobicity (Fig. 4b). Modifiers that enhanced the formation of formic acid were more hydrophilic than the unmodified Cu surface, and those that enhanced the formation of CO were more hydrophobic. We also find that the maximum selectivity for CO was obtained with **8**, which is slightly more hydrophobic than **Ox Cu**, and that this selectivity for CO

decreased as the hydrophobicity further increased. In line with this observation, the most hydrophobic species studied here, polystyrene, did not yield more CO than **Ox Cu**; but, rather yielded slightly more H₂. Polystyrene and **2** are also outliers in **Fig 3a**. The observation that substantial increases in hydrophobicity resulted in decreased, or loss of, selectivity for CO and increased selectivity for formic acid and H₂, may further support the importance of complex surface interactions with water at the molecular scale in the CO₂R mechanism. Specifically, we hypothesize that the presence of the heteroatom in modifiers **7**, **8**, **9**, and **10** plays an important role in determining these interactions with water, which are reduced in the presence of hindered ammonium salts (**2**) and the hydrocarbon polystyrene, thus explaining why these latter modifiers yield a product distribution more similar to **Ox Cu**.

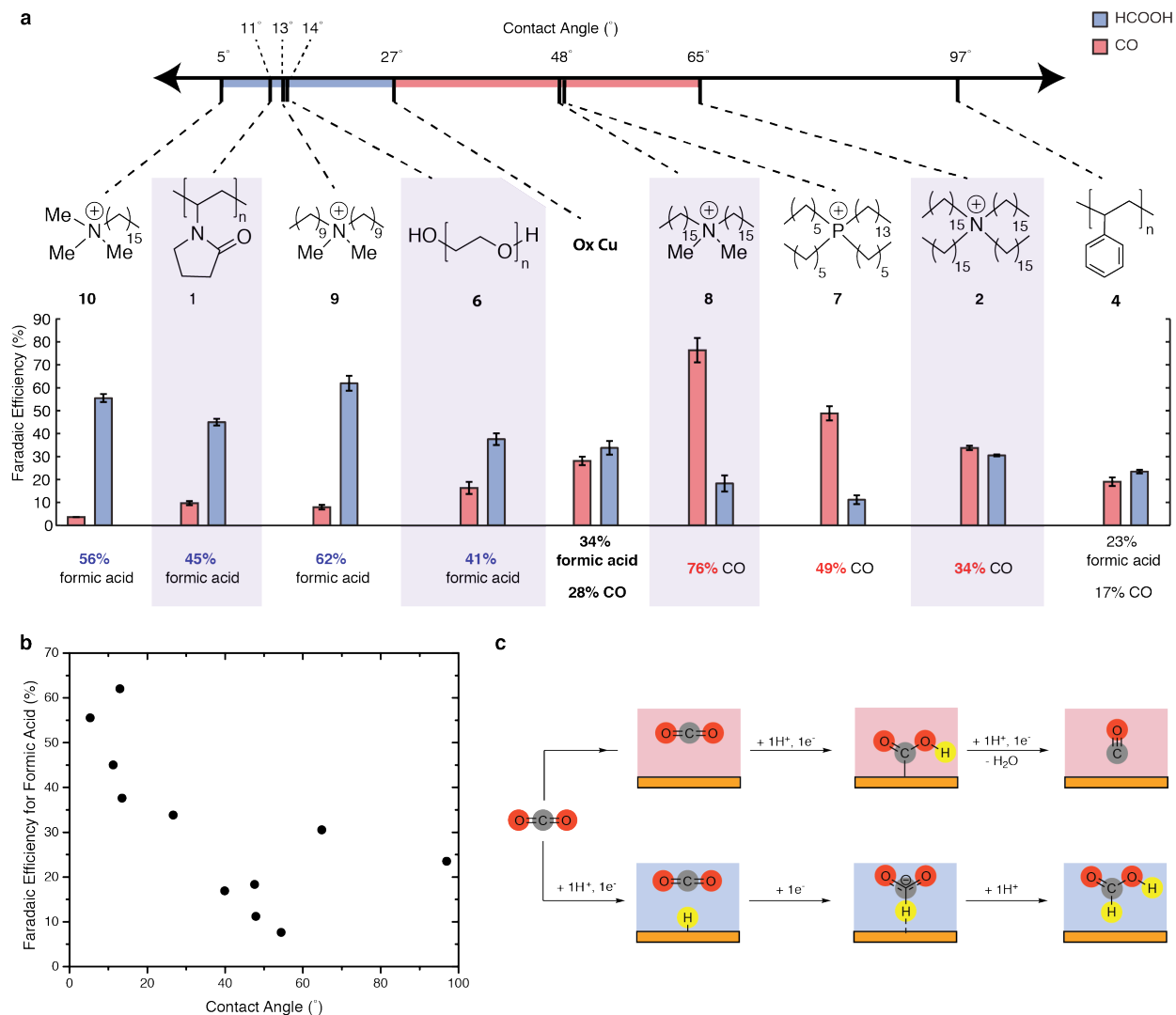


Fig. 4. Relationship between hydrophilicity/phobicity and product selectivity. The contact angle was determined for Cu surfaces modified with the organic species shown. Surfaces that are more hydrophilic than **Ox Cu** were more selective for formic acid (highlighted in blue), and those that are cationic and more hydrophobic were more selective for CO. The CO, formic acid product selectivity for the modifiers is also included. Boxes are included to guide the eye (a). Plotting the selectivity towards formic acid against the contact angle yields a marked relationship, with modifiers **2** and **4** as outliers at 65° and 97°, respectively (b). The mechanism for the formation of CO proceeds through a C-bound intermediate, while formic acid formation proceeds through addition to a surface hydride (c).

These observed relationships between the organic modifier and the CO₂R selectivity suggest that the effects of the modifiers involve properties that are structure non-specific (i.e. not related to the exact molecular structure). For example, the observation that two dimethyl substituted ammonium species can result in substantially different product distributions suggests that their bulk properties have a generalized effect on the local surface environment, consequently influencing chemical transformations at the Cu surface.

In order to better understand how these modifiers may influence the observed product distribution, we considered mechanisms for the formation of CO and formic acid developed from full solvent quantum mechanics (**Fig. 4c**).³⁸ The formation of CO proceeds via a bent CO₂ stabilized by water, which extracts an H from a H₂O molecule to form the bent carbon-bound *COOH intermediate. In turn, *COOH extracts an H from a second H₂O molecule to form aqueous H₂O and surface bound CO. In contrast, formation of formic acid occurs via direct addition of CO₂ to a surface M-H to yield formate, followed by extraction of H from a H₂O molecule to yield formic acid. Thus, changes in the bonding of H and the availability of H₂O at the surface have a strong influence on which products are formed.

The partial current densities of the modified Cu surfaces studied herein also support the intermediacy of a surface hydride species in the formation of both formic acid and H₂. The modifiers that promote formic acid formation also tend to yield more H₂, while those that generate less formic acid also tend to yield less H₂ (**3.5.10**). This type of relationship is not observed between CO and H₂ or CO and formic acid.

While the binding strength of this surface hydride species is generally considered to be intrinsic to the metal surface, previous work from the Goddard group has demonstrated that it is sensitive to the surrounding water environment.³⁹ Increasing the hydrophobicity of a Pt(100) surface decreased the adsorbed water (i.e., the local density of water), reorganized the water structure and changed the hydrogen bonding energies of this water. Studies of the Pt system also demonstrated that this decrease in water adsorption on a hydrophobic surface stabilized the binding of H to the metal surface.

With these precedents in mind, we sought to understand whether the addition of hydrophilic and hydrophobic modifiers to the Cu surface may similarly influence the water at the

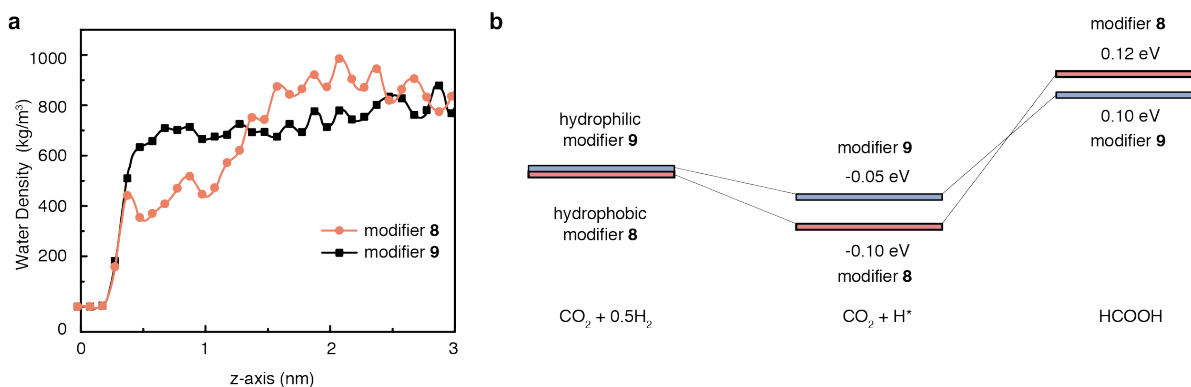


Figure 5. Role of hydrophobic modifier 8, hydrophilic modifier 9, and the surrounding water. Profile of density of water along the z axis, perpendicular to the Cu surface, on surfaces modified with 8 and 9 (a). Formation energies predicted from ReaxFF for the formation of formic acid at Cu surfaces modified with 8 and 9 (b).

Cu interface, and whether these changes in the local electrolyte environment may impact the formation of CO₂R products. In order to understand how **8** and **9** influence the local aqueous environment, the Goddard group examined the density of water at varying distances perpendicular to the copper electrode.

Consistent with the bulk measurement of the interaction of water with these modified electrodes (**Fig. 3c-d**), the availability of water at the nanometer scale is lower with **8**, the more hydrophobic molecule, than with **9**, the more hydrophilic molecule (**Fig. 5a**). From this density profile of water, we estimate that the electrode area covered by water with **9** is 1.55 times of that with **8** at a cut-off of 0.67 nm from the surface of the electrode, a distance that corresponds to about two monolayers of water.

With this understanding of how **8** and **9** influence the availability of water at the Cu interface, we examined how these changes at the electrode interface influence the binding energy of a M-H at the Cu surface, and, in turn, the formation of formic acid. As shown in **Fig. 5b**, ReaxFF calculations demonstrate that a surface hydride species is stabilized in the presence of hydrophobic species **8** compared to hydrophilic species **9**. This finding is consistent with previously described calculations conducted on Pt.³⁹ Addition of CO₂ to the stronger M-H bond to yield formic acid, as previously described (**Fig. 4c**), is more difficult than with the weaker M-H bond found on the hydrophilic surface. We therefore propose that the promotion of formic acid formation on the hydrophilic surface is due to this weakened M-H species, while hydrophobic species **8** results in stronger M-H bonds, suppressing formic acid formation and allowing CO formation to predominate.

3.3 Conclusions

With this study, we provide a strategy to identify important structure-reactivity relationships and tune selectivity in CO₂R. We tested organic modifiers featuring a wide variety of characteristics and found that protic modifiers enhanced HER selectivity, demonstrating that aprotic species are necessary to hone CO₂R selectivity. We identify structures that improve selectivity towards CO, formic acid, or H₂, reaching selectivities of up to 76% CO or 62% formic acid, and tuning the H₂ selectivity from 97% down to 2%. By comparison, Ag foil at the same potential yields less than 20% CO, only reaching 90% CO formation around -1.0 V vs. RHE,⁴⁰ while Sn foil yields around 30% formic acid at -0.7 V vs. RHE, reaching a maximum around 70% between -0.9 and -1.0 V vs. RHE.¹⁵ Among these aprotic species, cationic hydrophobic modifiers enhanced selectivity for CO, while hydrophilic modifiers enhanced selectivity for formic acid. In addition, we find that within the tested hydrophobic modifiers, small perturbations from the **Ox Cu** wettability resulted in improved selectivity for CO, while substantially more hydrophobic species resulted in lower selectivity for CO. This ability to alternately tune between CO and formic acid, and suppress H₂ production, is unprecedented for a non-precious metal catalyst for CO₂R. These structure-reactivity relationships illuminate important design principles for novel, selective CO₂R electrocatalysts.

This correlation of observed products with hydrophilicity/phobicity and study of surface hydride formation demonstrates that the role of water deserves careful consideration in designing organic modifiers for CO₂R. Previous works have delved into possibilities of using strategic hydrogen bonding and Lewis acidic interactions to stabilize specific intermediates and aid in tuning CO₂R selectivity. Our study suggests that these modified Cu systems are sensitive to the structure of the surrounding water, and therefore, that strategies in ligand design moving forward may find interesting new avenues in targeting how the surrounding water may be manipulated.

3.4 References

1. Artz, J.; Müller, T. E.; Thenert, K.; Kleinekorte, J.; Meys, R.; Sternberg, A.; Bardow, A.; Leitner, W. Sustainable Conversion of Carbon Dioxide: An Integrated Review of Catalysis and Life Cycle Assessment. *Chem. Rev.* **2018**, *118*, 434-504.
2. Seh, Z. W.; Kibsgaard, J.; Dickens, C. F.; Chorkendorff, I.; Nørskov, J. K.; Jaramillo, T. F. Combining Theory and Experiment in Electrocatalysis: Insights into Materials Design. *Science* **2017**, *355*, eaad4998.
3. Qiao, J.; Liu, Y.; Hong, F.; Zhang, J. A Review of Catalysts for the Electroreduction of Carbon Dioxide to Produce Low-Carbon Fuels. *Chem. Soc. Rev.* **2014**, *43*, 631-675.
4. Hori, Y. In *Modern Aspects of Electrochemistry*; Vayenas, C. G., White, R. E., Gamboa-Aldeco, M. E., Eds.; Springer: New York, **2008**; pp 89-189.
5. Kuhl, K. P.; Hatsukade, T.; Cave, E. R.; Abram, D. N.; Kibsgaard, J.; Jaramillo, T. F. Electrocatalytic Conversion of Carbon Dioxide to Methane and Methanol on Transition Metal Surfaces. *J. Am. Chem. Soc.* **2014**, *136*, 14107-14113.
6. Kuhl, K. P.; Cave, E. R.; Abram, D. N.; Jaramillo, T. F. New Insights into the Electrochemical Reduction of Carbon Dioxide on Metallic Copper Surfaces. *Energy Environ. Sci.* **2012**, *5*, 7050-7059.
7. Francke, R.; Schille, B.; Roemelt, M. Homogeneously Catalyzed Electroreduction of Carbon Dioxide—Methods, Mechanisms, and Catalysts. *Chem. Rev.* **2018**, *118*, 4631-4701.
8. Dubois, M. R.; Dubois, D. L. Development of Molecular Electrocatalysts for CO₂ Reduction and H₂ Production/Oxidation. *Acc. Chem. Res.* **2009**, *42*, 1974-1982.
9. Taheri, A.; Berben, L. A. Tailoring Electrocatalysts for Selective CO₂ or H⁺ reduction: Iron Carbonyl Clusters as a Case Study. *Inorg. Chem.* **2016**, *55*, 378-385.
10. Waldie, K. M.; Ostericher, A. L.; Reineke, M. H.; Sasayama, A. F.; Kubiak, C. P. Hydricity of Transition-Metal Hydrides: Thermodynamic Considerations for CO₂ Reduction. *ACS Catal.* **2018**, *8*, 1313-1324.
11. Kortlever, R.; Shen, J.; Schouten, K. J. P.; Calle-Vallejo, F.; Koper, M. T. M. Catalysts and Reaction Pathways for the Electrochemical Reduction of Carbon Dioxide. *J. Phys. Chem. Lett.* **2015**, *6*, 4073-4082.
12. Mellmann, D.; Sponholz, P.; Junge, H.; Beller, M. Formic Acid as a Hydrogen Storage Material—Development of Homogeneous Catalysts for Selective Hydrogen Release. *Chem. Soc. Rev.* **2016**, *45*, 3954-3988.
13. Sordakis, K.; Tang, C.; Vogt, L. K.; Junge, H.; Dyson, P. J.; Beller, M.; Laurenczy, G. Homogeneous Catalysis for Sustainable Hydrogen Storage in Formic Acid and Alcohols. *Chem. Rev.* **2018**, *118*, 372-433.
14. Yu, X.; Pickup, P. G. Recent Advances in Direct Formic Acid Fuel Cells (DFAFC). *J. Power Sources* **2008**, *182*, 124-132.
15. Feaster, J. T.; Shi, C.; Cave, E. R.; Hatsukade, T.; Abram, D. N.; Kuhl, K. P.; Hahn, C.; Nørskov, J. K.; Jaramillo, T. F. Understanding Selectivity for the Electrochemical Reduction of Carbon Dioxide to Formic Acid and Carbon Monoxide on Metal Electrodes. *ACS Catal.* **2017**, *7*, 4822-4827.
16. Shinagawa, T.; Larrazábal, G. O.; Martín, A. J.; Krumeich, F.; Pérez-Ramírez, J. Sulfur-Modified Copper Catalysts for the Electrochemical Reduction of Carbon Dioxide to Formate. *ACS Catal.* **2018**, *8*, 837-844.

17. Huan, T. N.; Simon, P.; Rouse, G.; Génois, I.; Artero, V.; Fontecave, M. Porous Dendritic Copper: An Electrocatalyst for Highly Selective CO₂ Reduction to Formate in Water/Ionic Liquid Electrolyte. *Chem. Sci.* **2017**, *8*, 742-747.
18. Li, C. W.; Ciston, J.; Kanan, M. W. Electroreduction of Carbon Monoxide to Liquid Fuel on Oxide-Derived Nanocrystalline Copper. *Nature* **2014**, *508*, 504-507.
19. Gong, M.; Cao, Z.; Liu, W.; Nichols, E. M.; Smith, P. T.; Derrick, J. S.; Liu, Y.-S.; Liu, J.; Wen, X.; Chang, C. J. Supramolecular Porphyrin Cages Assembled at Molecular–Materials Interfaces for Electrocatalytic CO Reduction. *ACS Cent. Sci.* **2017**, *3*, 1032-1040.
20. Bertheussen, E.; Verdaguier-Casadevall, A.; Ravasio, D.; Montoya, J. H.; Trimarco, D. B.; Roy, C.; Meier, S.; Wendland, J.; Nørskov, J. K.; Stephens, I. E. L.; Chorkendorff, I. Acetaldehyde as an Intermediate in the Electroreduction of Carbon Monoxide to Ethanol on Oxide-Derived Copper. *Angew. Chem. Int. Ed.* **2016**, *55*, 1450-1454.
21. Zhu, D. D.; Liu, J. L.; Qiao, S. Z. Recent Advances in Inorganic Heterogeneous Electrocatalysts for Reduction of Carbon Dioxide. *Adv. Mater.* **2016**, *28*, 3423-3452.
22. Singh, M. R.; Clark, E. L.; Bell, A. T. Effects of Electrolyte, Catalyst, and Membrane Composition and Operating Conditions on the Performance of Solar-Driven Electrochemical Reduction of Carbon Dioxide. *Phys. Chem. Chem. Phys.* **2015**, *17*, 18924-18936.
23. Rosen, B. A.; Salehi-Khojin, A.; Thorson, M. R.; Zhu, W.; Whipple, D. T.; Kenis, P. J. A.; Masel, R. I. Ionic Liquid-Mediated Selective Conversion of CO₂ to CO at Low Overpotentials. *Science* **2011**, *334*, 643-644.
24. Lau, G. P. S.; Schreier, M.; Vasilyev, D.; Scopelliti, R.; Grätzel, M.; Dyson, P. J. New Insights into the Role of Imidazolium-Based Promoters for the Electroreduction of CO₂ on a Silver Electrode. *J. Am. Chem. Soc.* **2016**, *138*, 7820-7823.
25. Feaster, J. T.; Jongerius, A. L.; Liu, X.; Urushihara, M.; Nitopi, S. A.; Hahn, C.; Chan, K.; Nørskov, J. K.; Jaramillo, T. F. Understanding the Influence of [EMIM]Cl on the Suppression of the Hydrogen Evolution Reaction on Transition Metal Electrodes. *Langmuir* **2017**, *33*, 9464-9471.
26. Kim, C.; Jeon, H. S.; Eom, T.; Jee, M. S.; Kim, H.; Friend, C. M.; Min, B. K.; Hwang, Y. J. Achieving Selective and Efficient Electrocatalytic Activity for CO₂ Reduction using Immobilized Silver Nanoparticles. *J. Am. Chem. Soc.* **2015**, *137*, 13844-13850.
27. Esposito, D. V. Membrane-Coated Electrocatalysts—an Alternative Approach to Achieving Stable and Tunable Electrocatalysis. *ACS Catal.* **2018**, *8*, 457-465.
28. Roberts, F. S.; Kuhl, K. P.; Nilsson, A. High Selectivity for Ethylene from Carbon Dioxide Reduction over Copper Nanocube Electrocatalysts. *Angew. Chem. Int. Ed.* **2015**, *54*, 5179-5182.
29. Lobaccaro, P.; Singh, M. R.; Clark, E. L.; Kwon, Y.; Bell, A. T.; Ager, J. W. Effects of Temperature and Gas-Liquid Mass Transfer on the Operation of Small Electrochemical Cells for the Quantitative Evaluation of CO₂ Reduction Electrocatalysts. *Phys. Chem. Chem. Phys.* **2016**, *18*, 26777-26785.
30. Han, Z.; Kortlever, R.; Chen, H.-Y.; Peters, J. C.; Agapie, T. CO₂ Reduction Selective for C₂ Products on Polycrystalline Copper with N-Substituted Pyridinium Additives. *ACS Cent. Sci.* **2017**, *3*, 853-859.
31. Koczur, K. M.; Mourdikoudis, S.; Polavarapu, L.; Skrabalak, S. E. Polyvinylpyrrolidone (PVP) in Nanoparticle Synthesis. *Dalton Trans.* **2015**, *44*, 17883-17905.

32. Fang, Y.; Flake, J. C. Electrochemical Reduction of CO₂ at Functionalized Au Electrodes. *J. Am. Chem. Soc.* **2017**, *139*, 3399-3405.
33. Aeshala, L. M.; Uppaluri, R.; Verma, A. Electrochemical Conversion of CO₂ to Fuels: Tuning of the Reaction Zone Using Suitable Functional Groups in a Solid Polymer Electrolyte. *Phys. Chem. Chem. Phys.* **2014**, *16*, 17588-17594.
34. McCann, N.; Phan, D.; Wang, X.; Conway, W.; Burns, R.; Attalla, M.; Puxty, G.; Maeder, M. Kinetics and Mechanism of Carbamate Formation from CO₂(aq), Carbonate Species, and Monoethanolamine in Aqueous Solution. *J. Phys. Chem. A* **2009**, *113*, 5022-5029.
35. Bullock, R. M.; Appel, A. M.; Helm, M. L. Production of Hydrogen by Electrocatalysis: Making the H-H bond by Combining Protons and Hydrides. *Chem. Commun.* **2014**, *50*, 3125-3143.
36. Xu, G.-R.; Bai, J.; Yao, L.; Xue, Q.; Jiang, J.-X.; Zeng, J.-H.; Chen, Y.; Lee, J.-M. Polyallylamine-Functionalized Platinum Tripods: Enhancement of Hydrogen Evolution Reaction by Proton Carriers. *ACS Catal.* **2017**, *7*, 452-458.
37. Ahn, S.; Klyukin, K.; Wakeham, R. J.; Rudd, J. A.; Lewis, A. R.; Alexander, S.; Carla, F.; Alexandrov, V.; Andreoli, E. Poly-Amide Modified Copper Foam Electrodes for Enhanced Electrochemical Reduction of Carbon Dioxide. *ACS Catal.* **2018**, *8*, 4132-4142.
38. Cheng, T.; Xiao, H.; Goddard, W. A. III. Reaction Mechanisms for the Electrochemical Reduction of CO₂ to CO and Formate on the Cu(100) Surface at 298 K from Quantum Mechanics Free Energy Calculations with Explicit Water. *J. Am. Chem. Soc.* **2016**, *138*, 13802-13805.
39. Cheng, T.; Wang, L.; Merinov, B. V.; Goddard, W. A. III. Explanation of Dramatic pH-Dependence of Hydrogen Binding on Noble Metal Electrode: Greatly Weakened Water Adsorption at High pH. *J. Am. Chem. Soc.* **2018**, *140*, 7787-7790.
40. Hatsukade, T.; Kuhl, K. P.; Cave, E. R.; Abram, D. N.; Jaramillo, T. F. Insights into the Electrocatalytic Reduction of CO₂ on Metallic Silver Surfaces. *Phys. Chem. Chem. Phys.* **2014**, *16*, 13814-13819.

3.5 Supplementary Information

3.5.1 Experimental methods

Materials: All chemicals were obtained from commercial suppliers and used without further purification, unless otherwise noted. Copper foil (0.254 mm thick, 99.9%) was purchased from Alfa Aesar and cut with a bench shear into 2 cm x 3 cm electrodes before use. Carbon dioxide (99.995%) and nitrogen (99.999%) were obtained from Praxair. Polyvinylpyrrolidone (average MW 40,000), polyallylamine (average MW 17,000, 20 wt% in water), polyvinyl alcohol (MW 89,000-98,000, 99+% hydrolyzed), polyethylene glycol (average MW 20,000), polystyrene (average MW 192,000), didecyldimethylammonium bromide (98%), dihexadecyldimethylammonium bromide (97%), tetrahexadecylammonium bromide (98%), and trihexyltetradecylphosphonium bromide (95%) were purchased from Sigma-Aldrich. Cetyltrimethylammonium bromide (98%) was obtained from Spectrum Chemical. Selemion AMV anion-exchange membrane was purchased from AGC Engineering Co., LTD.

Instrumentation: Gas chromatography (GC) data was collected on a multiple gas analyzer #5 from SRI Instruments. High performance liquid chromatography (HPLC) was performed with an UltiMate 3000 HPLC from Thermo Fisher Scientific. ¹H NMR data was collected on an Ascend 500 MHz NMR from Bruker. Contact angle measurements were performed with a VCA Optima instrument from AST Products.

Electrochemical experiments: Electrochemical experiments were conducted in a two-compartment flow cell fabricated from PEEK following a reported design.¹ A Selemion AMV anion-exchange membrane separated the two chambers. A Pt foil was used as the counter electrode.

A Leak-Free Ag/AgCl electrode (LF-1, 1.0 mm outer diameter, Innovative Instruments, Inc.) was used as the reference electrode. The reference electrode was calibrated against a second reference electrode, which in turn was calibrated in a two-electrode system with H₂ bubbled over a Pt wire as the counter electrode and a 1M H₂SO₄ solution as the electrolyte.

The applied potentials were converted from Ag/AgCl scale to the RHE scale via the equation: $E_{\text{RHE}} = E_{\text{Ag/AgCl}} + 0.197 + 0.059 \cdot \text{pH}$, where the pH used is the bulk pH for the CO₂-saturated electrolyte (6.8).

Electrolyte preparation: Potassium carbonate solution (0.05M) was prepared from high purity potassium carbonate (99.995%, Sigma Aldrich) and water from a Milli-Q Water Purification System (resistivity of 18.2 MΩ-cm, Millipore). The solution was saturated with CO₂ for a minimum of 10 minutes within the experimental cell setup immediately prior to all electrochemical experiments.

Electrode preparation: Cu foil was mechanically polished (1200G Wetordry sandpaper, 3M) and then electropolished as described in a reported procedure.⁶ The two-compartment flow cell was assembled with the Cu foil, and cyclic voltammetry was run as described in previous reports in order to generate an oxide-derived Cu surface.^{28,29} Specifically, an electrolyte solution of 0.05 M K₂CO₃ and 4 mM KCl was prepared. After addition of this electrolyte, three cycles of cyclic

voltammetry were performed from 0.9 to -1.05V vs. RHE at a rate of 5 mV/s. This high surface area structure was chosen in order to generate greater amounts of product and facilitate product detection.

The cell was disassembled, the electrode was dried under N₂ flow and solutions of the organic modifier were dropcast onto the Cu surface as described below. Once dry, a solution of Nafion binder was dropcast onto the Cu surface. The electrode, once dry, was reassembled in the flow cell for electrochemical analyses.

Preparation of functionalized samples:

Polyvinylpyrrolidone (1) and polyallylamine (3): 10 mg of polymer was dissolved in iPrOH (1 mL), and 100 μ L of this solution was dropcast onto the Cu foil. Once dry, 100 μ L of Nafion solution (10 μ L of commercial Nafion solution in 1 mL iPrOH) was dropcast onto the Cu surface.

Tetrahexadecylammonium bromide (2): 5 mg of ammonium salt was suspended in iPrOH (5 mL) and heated briefly at 60°C to dissolve. 100 μ L of this solution was dropcast onto the Cu foil. Once dry, 100 μ L of Nafion solution (5 μ L of commercial Nafion solution in 5 mL iPrOH) was dropcast onto the Cu surface.

Polystyrene (4): 10 mg of polymer was dissolved in toluene (1 mL), and 100 μ L of this solution was dropcast onto the Cu foil. Once dry, 100 μ L of Nafion solution (10 μ L of commercial Nafion solution in 1 mL iPrOH) was dropcast onto the Cu surface.

Polyvinyl alcohol (5): 10 mg of polymer was suspended in water (400 μ L) and heated to 70°C to dissolve. An additional 600 μ L of MeOH was added to the solution. 100 μ L of this solution was dropcast onto the Cu foil. Once dry, 100 μ L of Nafion solution (10 μ L of commercial Nafion solution in 1 mL iPrOH) was dropcast onto the Cu surface.

Polyethylene glycol (6): 10 mg of polymer was suspended in MeOH (1 mL) and heated briefly at 60°C to dissolve. 100 μ L of this solution was dropcast onto the Cu foil. Once dry, 100 μ L of Nafion solution (10 μ L of commercial Nafion solution in 1 mL iPrOH) was dropcast onto the Cu surface.

Trihexyltetradecylphosphonium bromide (7), dihexadecyldimethylammonium bromide (8), didecyldimethylammonium bromide (9) and cetyltrimethylammonium bromide (10): 0.0274 mmol of the organic species was dissolved in iPrOH (1 mL), and 100 μ L of this solution was dropcast onto the Cu foil. Once dry, 100 μ L of Nafion solution (1 μ L of commercial Nafion solution per mg of organic species added to 1 mL iPrOH) was dropcast onto the Cu surface.

Chronoamperometry (CA) and product detection experiments: CA experiments were conducted in the cell with a CO₂ flow rate of 5 sccm using a Biologic potentiostat (SP-300). Prior to CA experiments, linear scan voltammetry was conducted from the open circuit potential to -1.05V vs. RHE at a scan rate of 20 mV/s in order to reduce any oxidized Cu. The impedance was then measured and correction for the ohmic resistance was applied to the CA experiment as described in a reported procedure.³⁰ Each trial was run at -0.7 V vs. RHE for 65 minutes. The outlet of the

electrochemical cell was connected to an in-line gas chromatograph (GC), and the gaseous products were injected into the chromatograph at 15, 30, 45 and 60 minutes after the beginning of the experiment. The average values from the four injections are reported. At the end of the experiment, the liquid from both the cathode and anode were analyzed via high performance liquid chromatography (HPLC) to quantify the amount of formic acid produced, including formate that had diffused through the membrane during the experiment. Product selectivities and activities in terms of Faradaic efficiencies (%) and partial current densities (mA/cm²) are reported with error calculated via standard error of the mean and standard deviations; standard error of the mean is used in the main text.

Measurement of the contact angle of water: Cu foil was electropolished, and the organic modifiers were dropcast onto the Cu foil at the same loadings as were used in the CA experiments. Once dry, the sample was placed on the goniometer, and 3 μ L droplets of water were dropped onto the sample. The right and left angles of the droplet with the Cu surface were measured, and the average of at least five droplets is reported.

ReaxFF MD simulation: All of the ReaxFF MD simulations were carried out using LAMMPS Molecular Dynamics Simulator. The force field parameters are supplied in the Supplementary Information. The simulation models consist of 1440 Cu atoms [4 \times 18 \times 20 Cu(111) surface], 2000 water molecules, 26 cations and 26 bromide anions, making the system neutral. The dimension of the simulation box is 4.60 nm \times 4.42 nm \times 5.00 nm. Energy optimizations were first carried out to relax the interface structure with a force converge criteria of 10⁻⁶ kcal/mol \cdot \AA . Constant temperature, constant volume (NVT) simulations were carried out at room temperature (298K) with Nose-Hoover thermostat for 5 ns with a time step of 0.25 fs. The binding energies of hydrogen were calculated at a coverage of 1M.

$$\Delta E_{H^*} = \frac{E_{1MLH^*} - E_{sur}}{n_{sites}} - 0.5E_{H_2}$$

Here, $n_{sites} = 360$ (18 \times 20) for 1ML H*.

The formation energy of HCOOH is calculated as follows:

$$\Delta E_{HCOOH} = E_{1MLH^*+HCOOH} - E_{1MLH^*} - (E_{H_2} + E_{CO_2} + 2\Delta E_{H^*})$$

3.5.2. Experiments with Nafion

Cu surfaces were tested with Nafion in the absence of other modifiers to evaluate whether Nafion on its own influenced the product selectivity. The data below, collected at the lowest and highest loadings of Nafion employed in the main manuscript, suggest that Nafion does not affect CO₂R selectivity of Cu.

Table S1. Faradaic efficiencies and total current of Ox Cu and Cu functionalized solely with Nafion at varying loadings. Reported values are averages from at least three trials.

	H ₂	CO	Formic Acid	Other	Total FE	Total Current (mA/cm ²)
Ox Cu	28%	28%	34%	6%	96%	0.73
1 μL Nafion per mL iPrOH ^a	27%	30%	31%	5%	93%	0.75
10 μL Nafion per mL iPrOH ^b	29%	31%	30%	4%	95%	0.80
15.8 μL Nafion per mL iPrOH ^c	27%	29%	30%	4%	90%	0.82

^a5 μL Nafion was dissolved in 5 mL iPrOH. 100 μL of this solution was dropcast onto oxide-derived Cu. This loading is the same as for experiments with **2**- the lowest loading of Nafion used for the figures in the main manuscript. ^b10 μL Nafion was dissolved in 1 mL iPrOH. 100 μL of this solution was dropcast onto oxide-derived Cu. ^c15.8 μL Nafion was dissolved in 1 mL iPrOH. 100 μL of this solution was dropcast onto oxide-derived Cu. This loading is the same as for experiments with **8**- the highest loading of Nafion used for the figures in the main manuscript.

In addition, experiments with modifiers **8** and **9** were conducted with and without Nafion to evaluate the role of the binder.

Chronoamperometry traces collected with Nafion were less noisy than traces without Nafion (**Fig. S1**). Furthermore, in the absence of Nafion, the electrolyte was observed to bubble more vigorously out of the cell, particularly in studies with more hydrophilic species. This observation suggests that in the absence of Nafion, the modifiers dissolve more readily in the electrolyte and yield a soapy solution. Therefore, Nafion was applied in all of the studies in the main manuscript at a loading of 1 μL Nafion per mg of modifier.

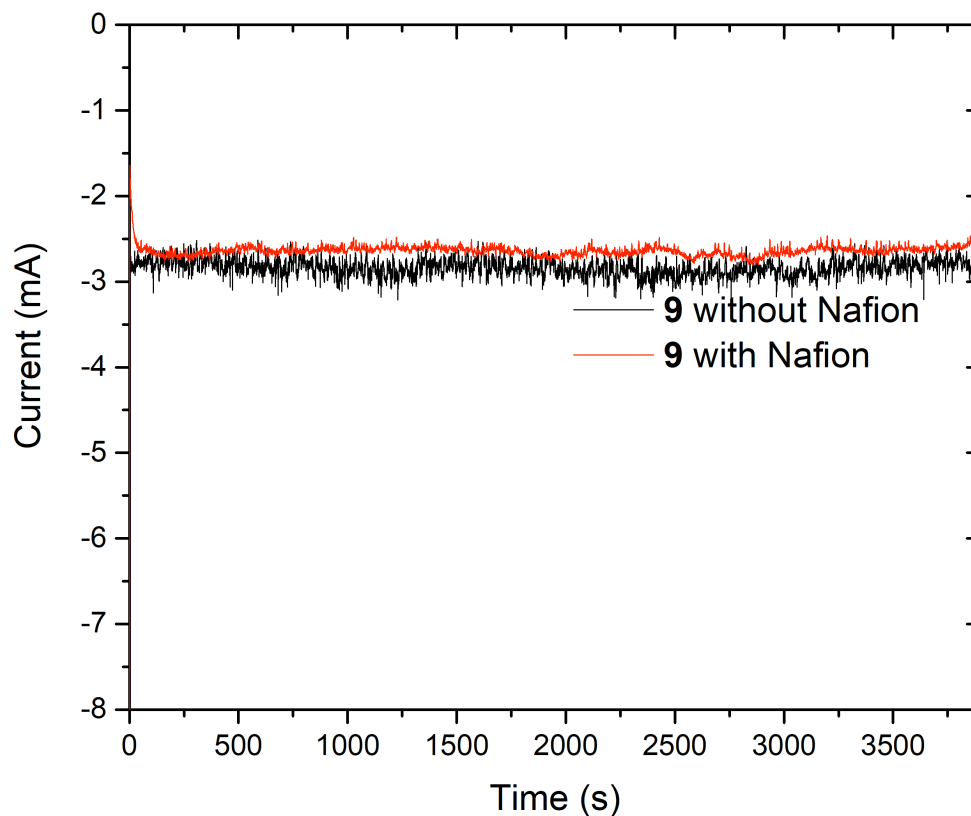


Figure S1. Chronoamperometry of Cu modified with 9, both with and without Nafion binder. In the presence of Nafion, the CA trace appears less noisy than in the absence of Nafion. Therefore, Nafion binder was employed as a binder for the experiments in the text. CA in the above figure was conducted at -0.7 V vs. RHE as described in the Experimental Methods.

The product distribution for these experiments without Nafion demonstrated the same trend as experiments with Nafion: **8** yielded more CO than the unfunctionalized surface, while **9** yielded more formic acid.

Table S2. Faradaic efficiency data with and without Nafion with 8

	H₂	CO	Formic Acid	Other	Total FE	Total Current (mA/cm²)
with Nafion	3%	76%	18%	0	97%	0.31
no Nafion	7%	63%	31%	0	101%	0.34

Table S3. Faradaic efficiency data with and without Nafion with 9

	H₂	CO	Formic Acid	other	Total FE	Total Current (mA/cm²)
with Nafion	21%	8%	62%	0	91%	2.45
no Nafion	21%	6%	73%	0	100%	2.84

3.5.3. Chronoamperometry traces

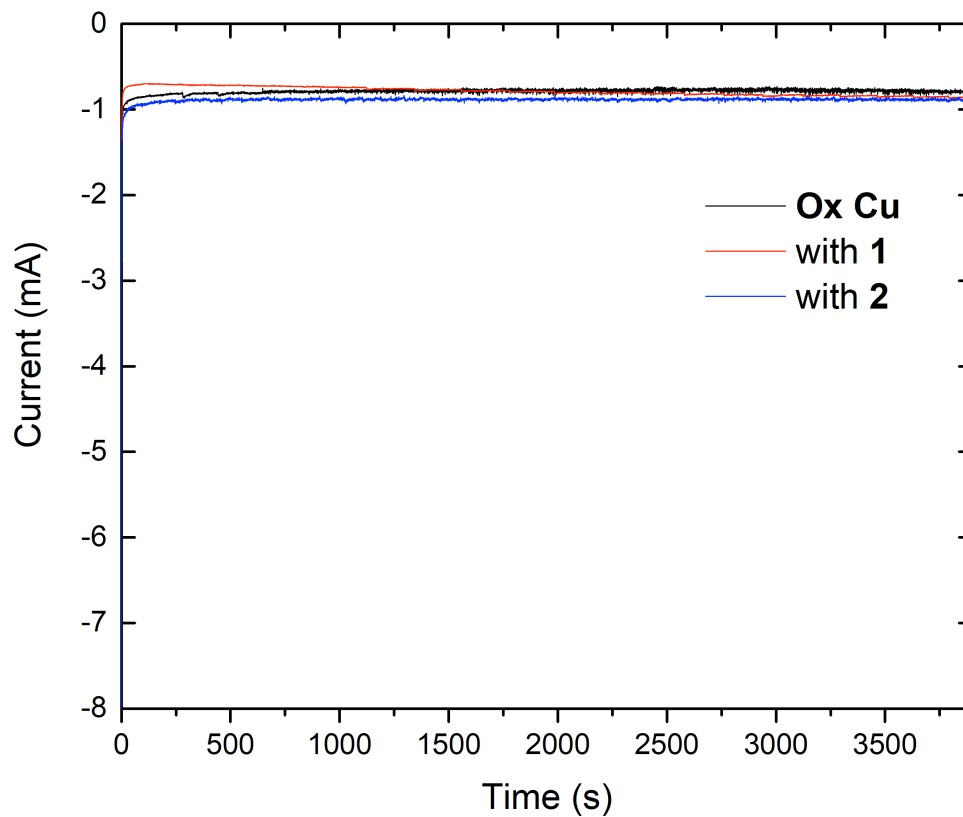


Figure S2. Chronoamperometry traces for Ox Cu and experiments with 1 and 2. Chronoamperometry traces indicate that for experiments with Ox Cu, 1 and 2, the currents remain stable over the course of the 65-minute experiment. The total current is also similar for the three traces, suggesting that mass transfer of CO₂ and protons is not substantially inhibited by the presence of the modifiers.

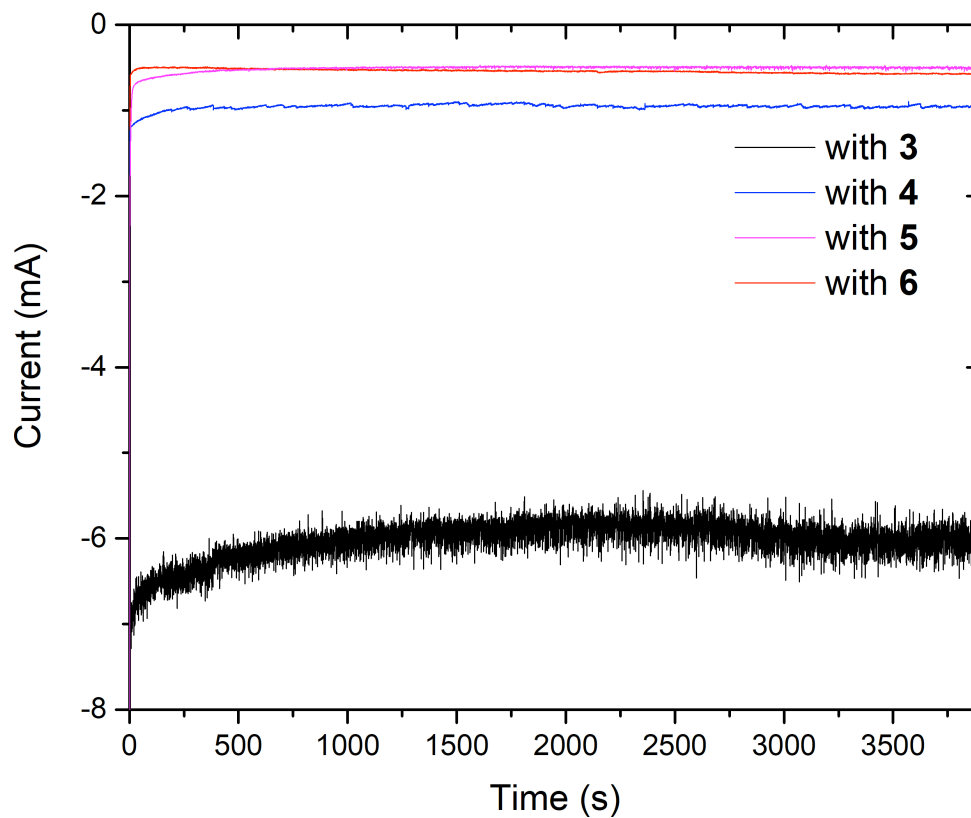


Figure S3. Chronoamperometry traces of neutral polymers as modifiers on Cu. CA traces indicate that the currents remain stable over the course of the 65-minute experiment.

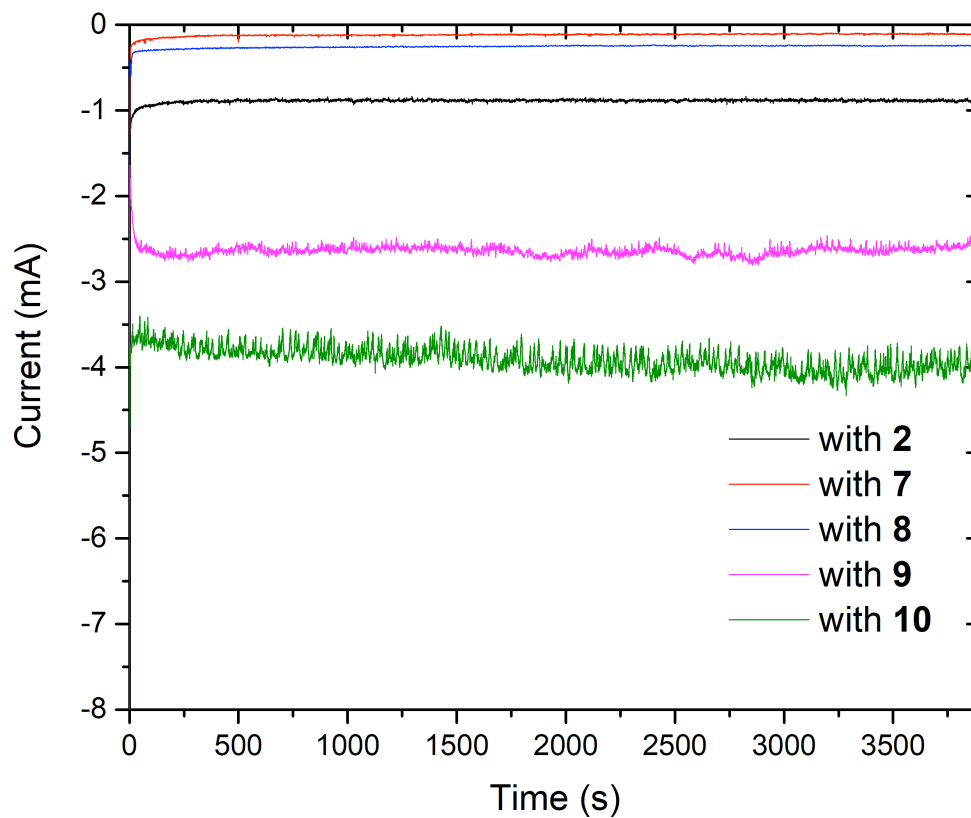


Figure S4. Chronoamperometry traces of cationic molecules as modifiers on Cu. CA traces indicate that the currents remain stable over the course of the 65-minute experiment.

3.5.4. Experiments with varying amounts of modifier

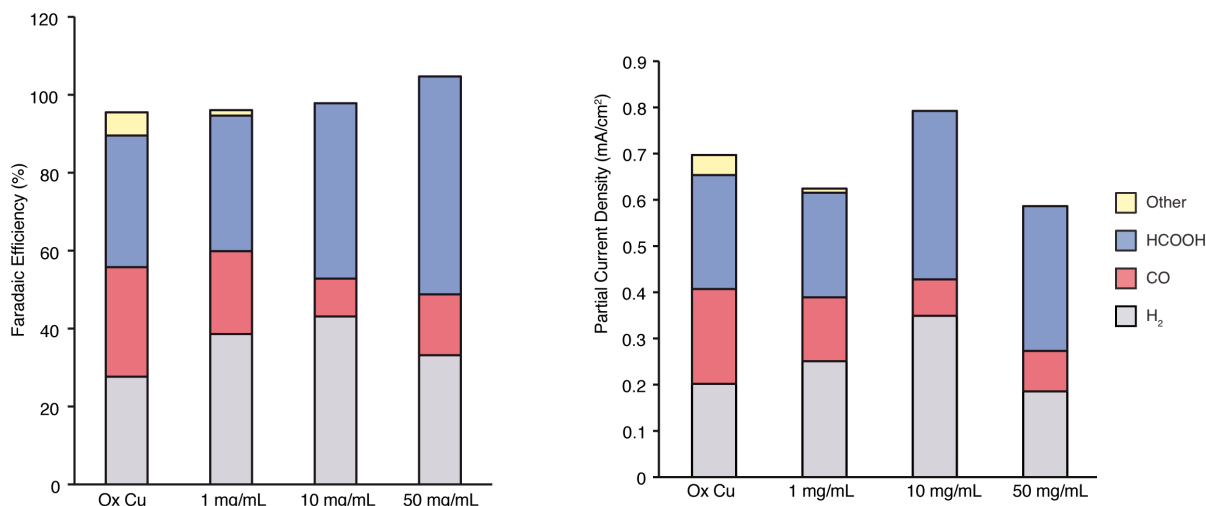


Figure S5. Experiments with varying loadings of polyvinylpyrrolidone (1). Solutions of 1, 10 and 50 mg of **1** in 1 mL iPrOH were prepared, and 100 μ L of this solution were dropcast onto oxide-derived copper surfaces as previously described. Once dry, 1, 10, and 50 μ L of Nafion, respectively, were then dissolved in iPrOH, and 100 μ L of this solution was dropcast onto the Cu surface. The product distribution was characterized as described in the Experimental Methods.

As compared to **Ox Cu**, which yields 34% formic acid, the selectivity increases to 35%, 45% and 56% formic acid with increasing loadings of **1**. We hypothesize that the lowest loading is too low to have a substantial effect on the product selectivity. In terms of partial current density, the amount of formic acid generated with **Ox Cu** (0.25 mA/cm²) changes to 0.23, 0.36 and 0.31 mA/cm² with the 1, 10 and 50 mg/mL solutions, respectively.

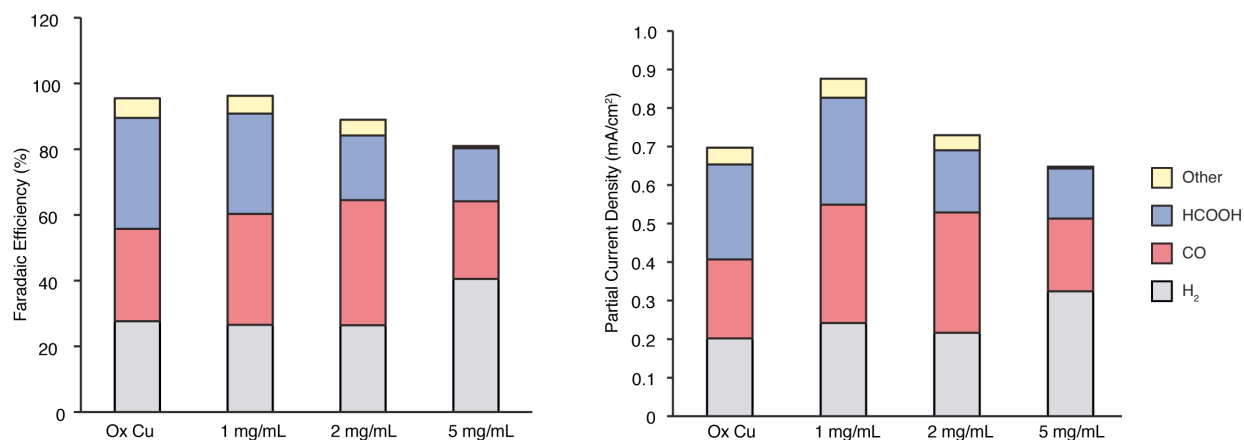


Figure S6. Experiments with varying loadings of tetrahexadecylammonium bromide (2). Solutions of 1, 2 and 5 mg of **2** per 1 mL iPrOH were prepared, and 100 μ L of this solution were dropcast onto oxide-derived copper surfaces as previously described. Once dry, 1, 2, and 5 μ L of Nafion, respectively, were then dissolved per mL of iPrOH, and 100 μ L of this solution was dropcast onto the Cu surface. The product distribution was characterized as described in the Experimental Methods.

As compared to **Ox Cu**, which yields 28% CO, the addition of **2** yields 34% and 38% CO with 1 and 2 mg/mL stock solutions, respectively. With a stock solution of 5 mg/mL, the selectivity for CO drops to 24%, and the total FE also drops to 81%. We observed in this experiment that the thick layer of modifier had partially peeled off of the electrode, and this mechanical instability may have affected the ability to close the FE gap. In terms of partial current density, the amount of CO generated with **Ox Cu** (0.21 mA/cm²) changes to 0.31, 0.31 and 0.19 mA/cm² with the addition of 1, 2 and 5 mg/mL stock solutions, respectively.

3.5.5. Product distribution at more negative potentials

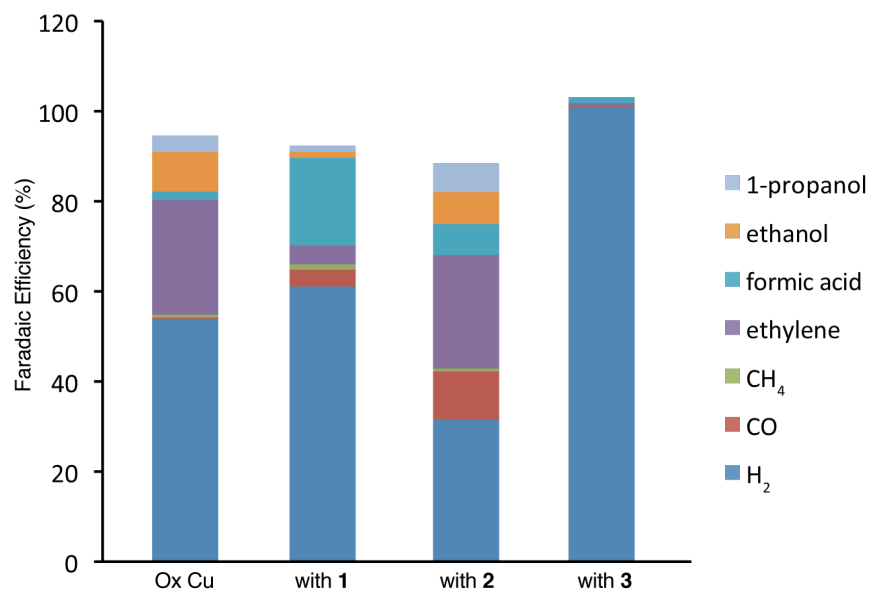


Figure S7. CO₂ reduction conducted at -1.0 V vs. RHE. The experiment was conducted as previously described, except at -1.0 V vs. RHE instead of -0.7 V vs. RHE, for **Ox Cu** and surfaces modified with **1**, **2**, and **3**.

3.5.6. Experiments under N₂

The substrates that demonstrated enhanced selectivity for CO₂R products were also examined under N₂. Experiments under N₂ were conducted with the same process, loadings and conditions as conducted for the data in **Fig. 1**, except with N₂ flow instead of CO₂. Faradaic efficiencies and total current for these trials are reported below. CO₂R activity disappears, indicating that the selectivities observed in **Fig. 1** originate from CO₂R, and not from decomposition of the modifier. The low FE for H₂ and low total FE observed with **8** is due to the low total current, which would yield an amount of H₂ that is close to the detection limit of our instrument.

Table S4. Functionalized Cu under N₂.

	H ₂	CO	Formic Acid	other	Total FE	Total Current (mA/cm ²)
Ox Cu-under N ₂	108.2%	0.2%	0%	0%	108.4%	0.41
With 1 under N ₂	115.0%	0.1%	0%	0%	115.0%	0.57
With 2 under N ₂	113.4%	0%	0%	0%	113.4%	0.31
With 6 under N ₂	113.9%	0.2%	0%	0%	114.1%	0.20
With 7 under N ₂	108.5%	0.1%	0%	0%	108.6%	0.12
With 8 under N ₂	31.6%	0.7%	0%	0%	32.3%	0.03
With 9 under N ₂	117.5%	0.2%	1.6%	0%	119.3%	0.35
With 10 under N ₂	109.6%	0%	0%	0%	109.6%	0.47

2.5.7. NMR characterization of modifiers and electrolyte

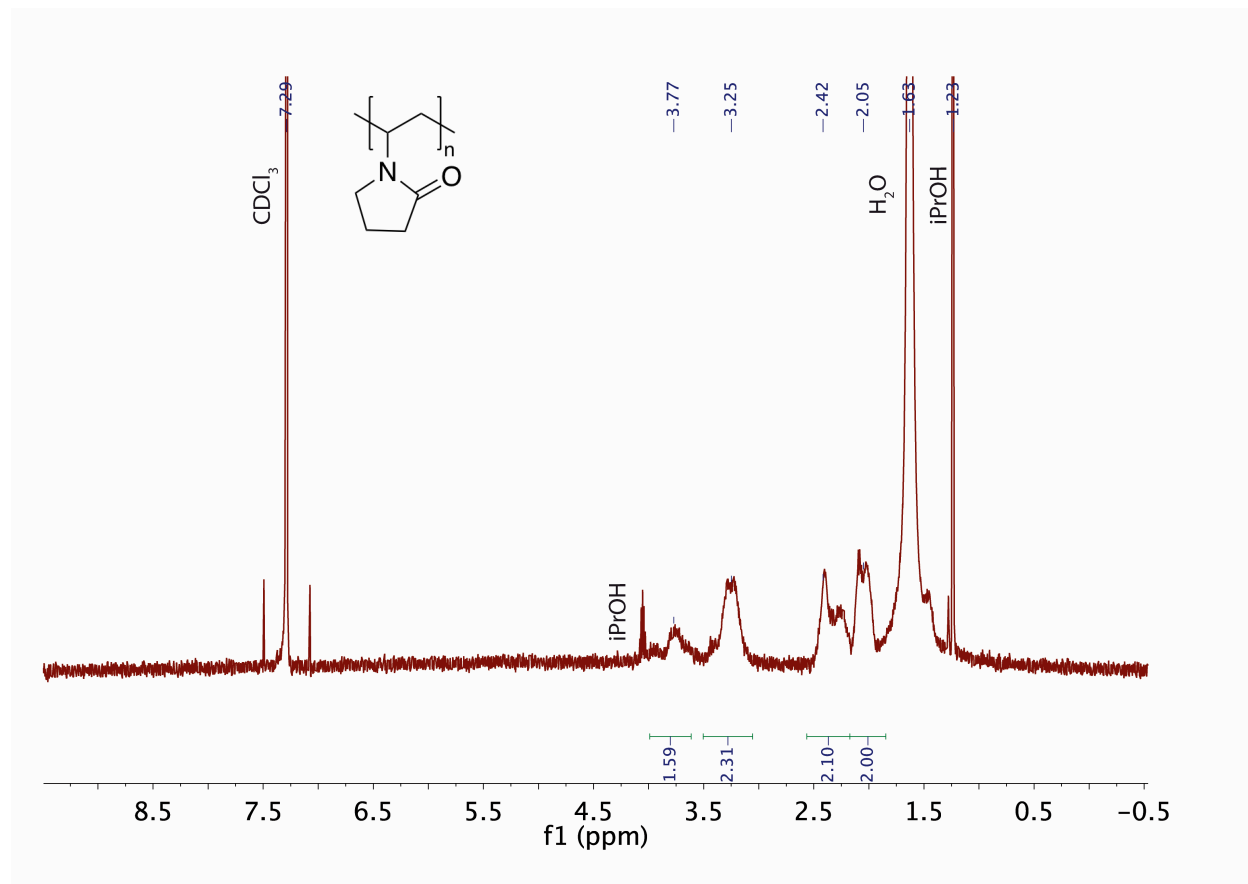


Figure S8. ^1H NMR of polyvinylpyrrolidone (**1**), rinsed from electrode after 65 minutes of chronoamperometry.

The CA experiment was conducted as described in the Experimental Methods, except with an increase in the loading. A 50 mg sample of polyvinylpyrrolidone (**1**) was dissolved in 1 mL iPrOH, and 100 μL of this solution was dropcast onto the oxide-derived Cu surface. 50 μL of Nafion solution was dissolved in 1 mL of iPrOH, and 100 μL of the Nafion solution was then dropcast onto the functionalized Cu surface.

^1H NMR (500 MHz, CDCl_3 , ppm): δ 3.77 (m, 1H), 3.25 (m, 2H), 2.42 (m, 2H), 2.05 (m, 2H), 1.63 (m, 2H).

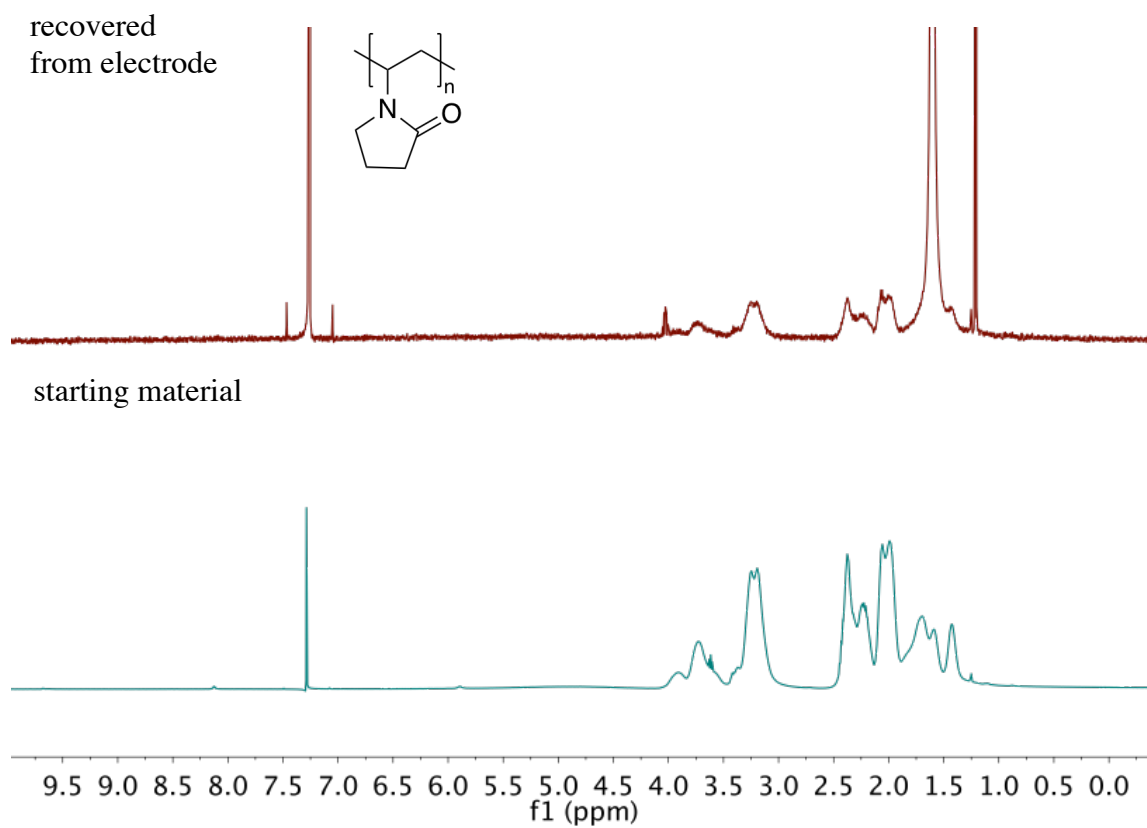


Figure S9. ^1H NMR of commercial polyvinylpyrrolidone (**1**) in CDCl_3 (bottom), compared with rinse of electrode after 65 minutes of chronoamperometry, also in CDCl_3 (top).

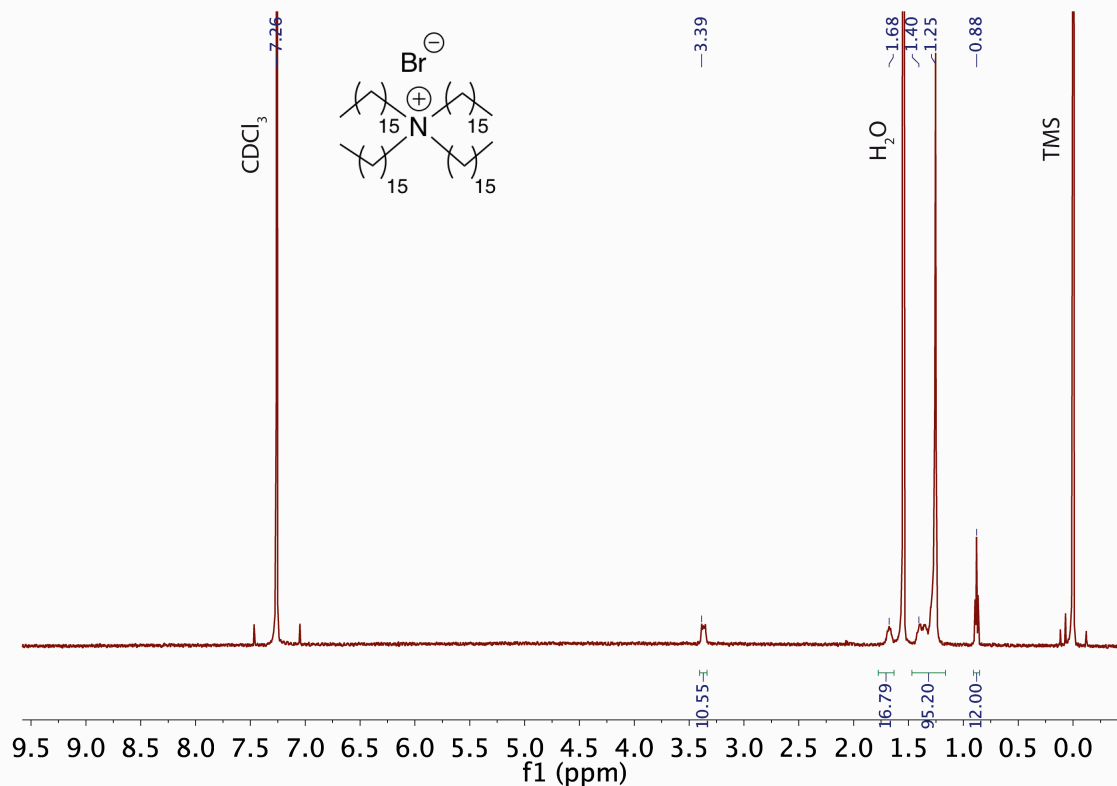


Figure S10. ^1H NMR of tetrahexadecylammonium bromide (**2**), rinsed from electrode after 65 minutes of chronoamperometry.

The CA experiment was conducted as described in the Experimental Methods, except with an increase in the loading. A 3 mg sample of (**2**) was dissolved in 1 mL iPrOH at 60 °C, and 100 μL of this solution was dropcast onto the oxide-derived Cu surface. 3 μL of Nafion solution was dissolved in 1 mL of iPrOH, and 100 μL of the Nafion solution was then dropcast onto the functionalized Cu surface.

^1H NMR (500 MHz, CDCl_3 , ppm): δ 3.39 (m, 8H), 1.68 (m, 16H), 1.25 (m, 96H), 0.88 (t, $J = 6.80$, 12H).

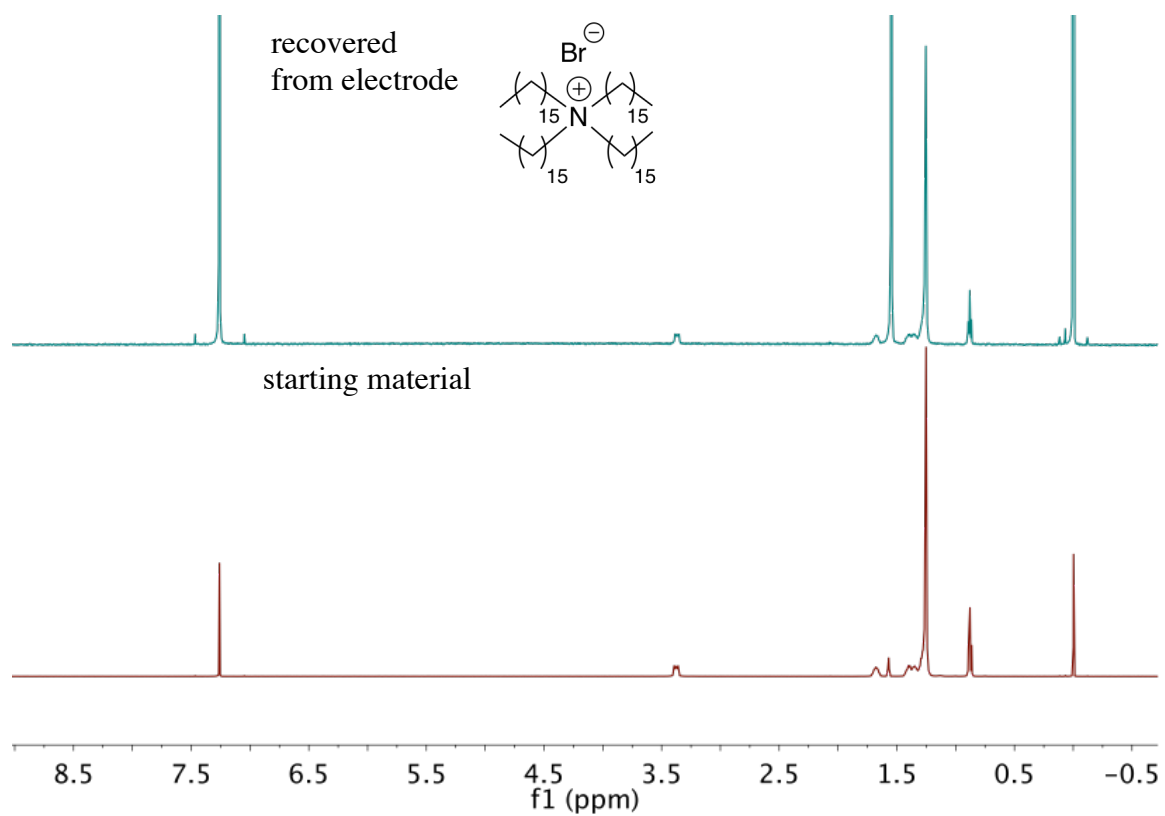


Figure S11. ^1H NMR of commercial tetrahexadecylammonium bromide (**2**) in CDCl_3 (bottom), compared with rinse of electrode after 65 minutes of chronoamperometry, also in CDCl_3 (top).

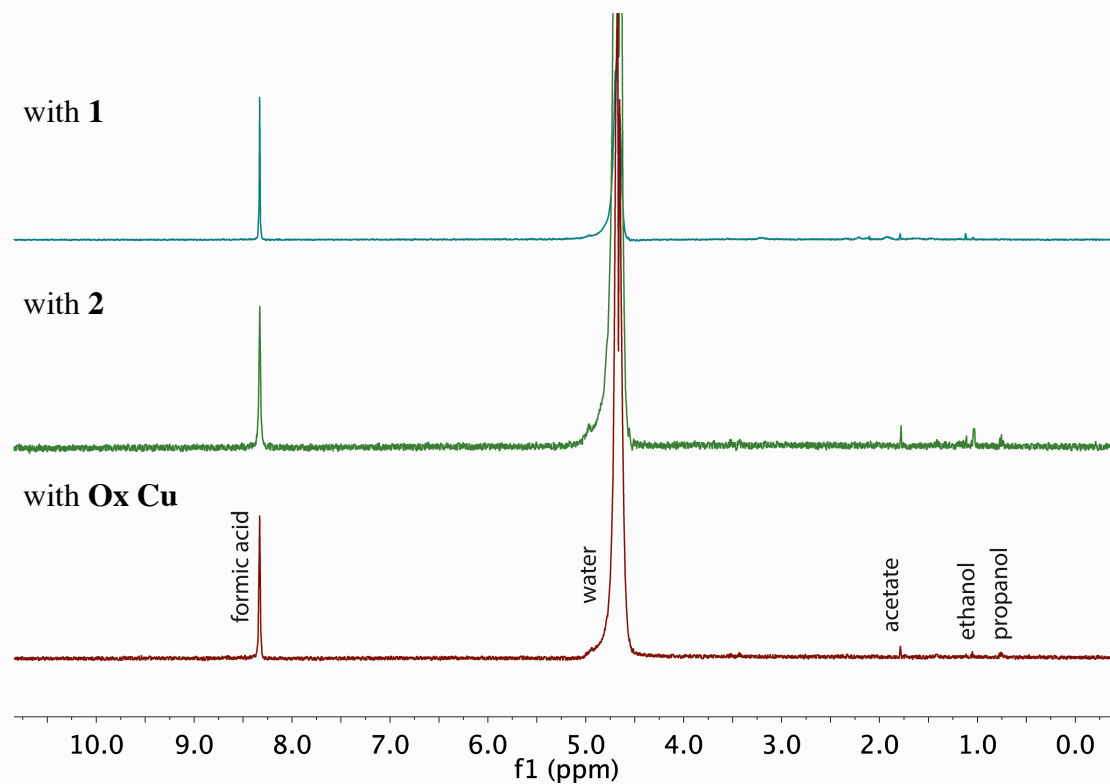


Figure S12. ^1H NMR of catholyte with suppression of the water peak, from bottom to top: a) reaction with Ox Cu, b) reaction with tetrahexadecylammonium bromide (**2**), c) reaction with polyvinylpyrrolidone (**1**). The spectra indicate the presence of formic acid and traces of other products; the absence of additional products, in conjunction with **Figures S8-11**, suggests that the modifiers remain intact throughout the experiment. The spectra were collected with 700 μL of catholyte and 35 μL of D_2O .

Catholyte samples were collected from the same experiments reported in **Fig 1**.

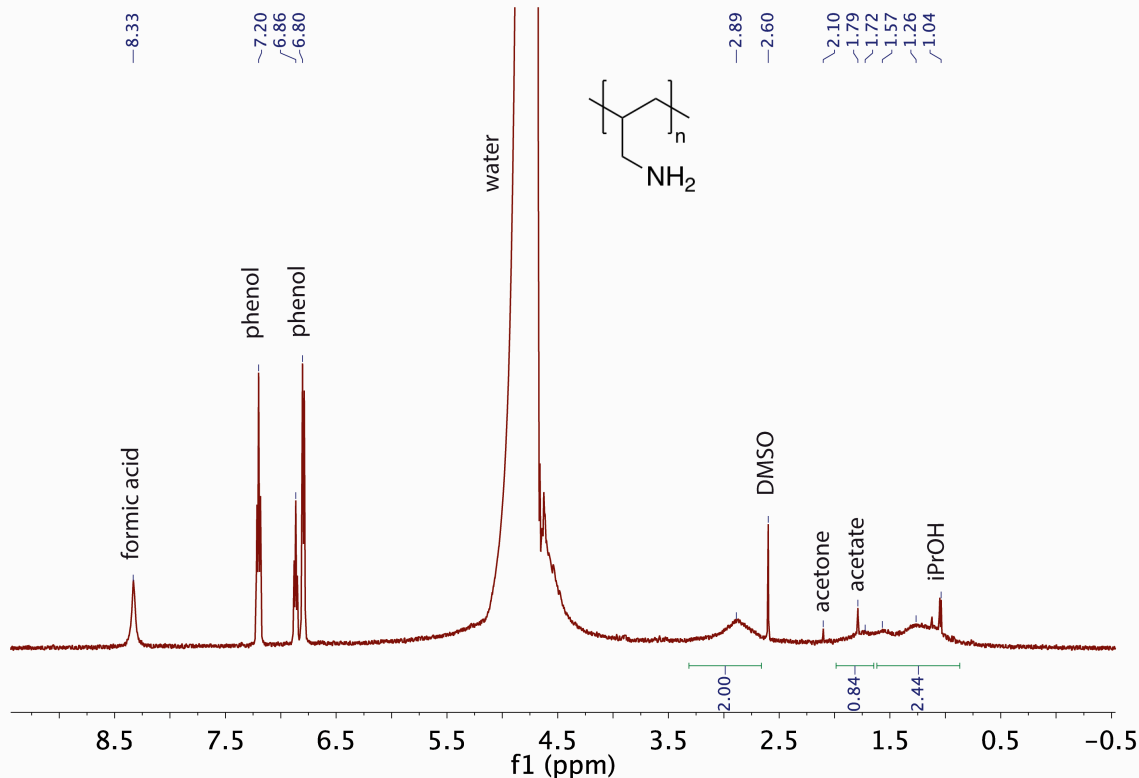


Figure S13. ^1H NMR of polyallylamine (**3**) from catholyte. Spectrum was collected using suppression of the water peak, and phenol and DMSO were added as internal standards.

The CA experiment was conducted as described in the Experimental Methods, except with an increase in the loading. A 50 mg sample of polyallylamine (**3**) was dissolved in 1 mL iPrOH, and 100 μL of this solution was dropcast onto the oxide-derived Cu surface. 50 μL of Nafion solution was dissolved in 1 mL of iPrOH, and 100 μL of the Nafion solution was then dropcast onto the functionalized Cu surface.

^1H NMR (500 MHz, H_2O and D_2O , ppm): δ 2.89 (m, 2H), 1.79 (m, 1H), 1.26 (m, 2H).

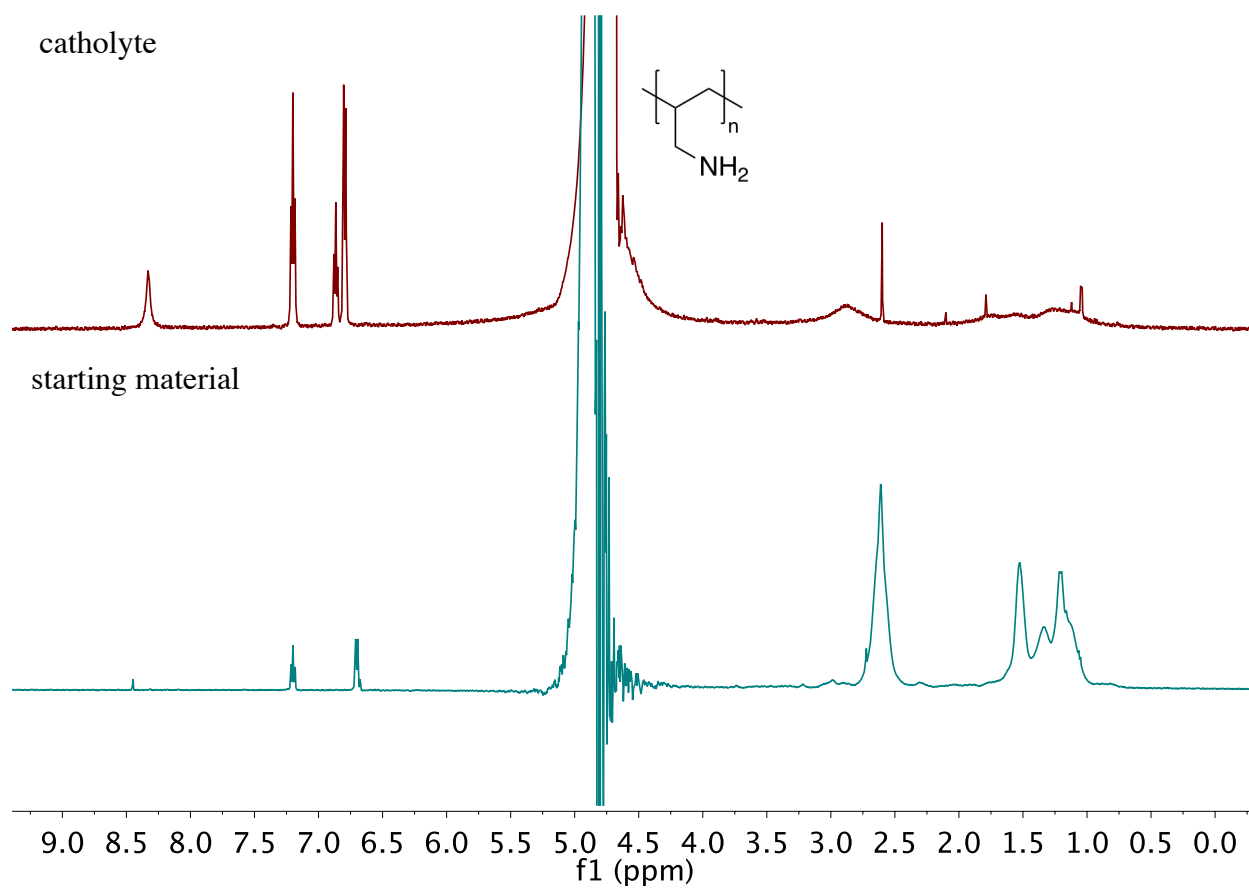


Figure S14. ¹H NMR of commercial polyallylamine (**3**) in H₂O and D₂O (bottom), compared with electrolyte after 65 minutes of chronoamperometry, also in H₂O and D₂O (top). Spectrum was collected using suppression of the water peak, and phenol and DMSO were added as internal standards.

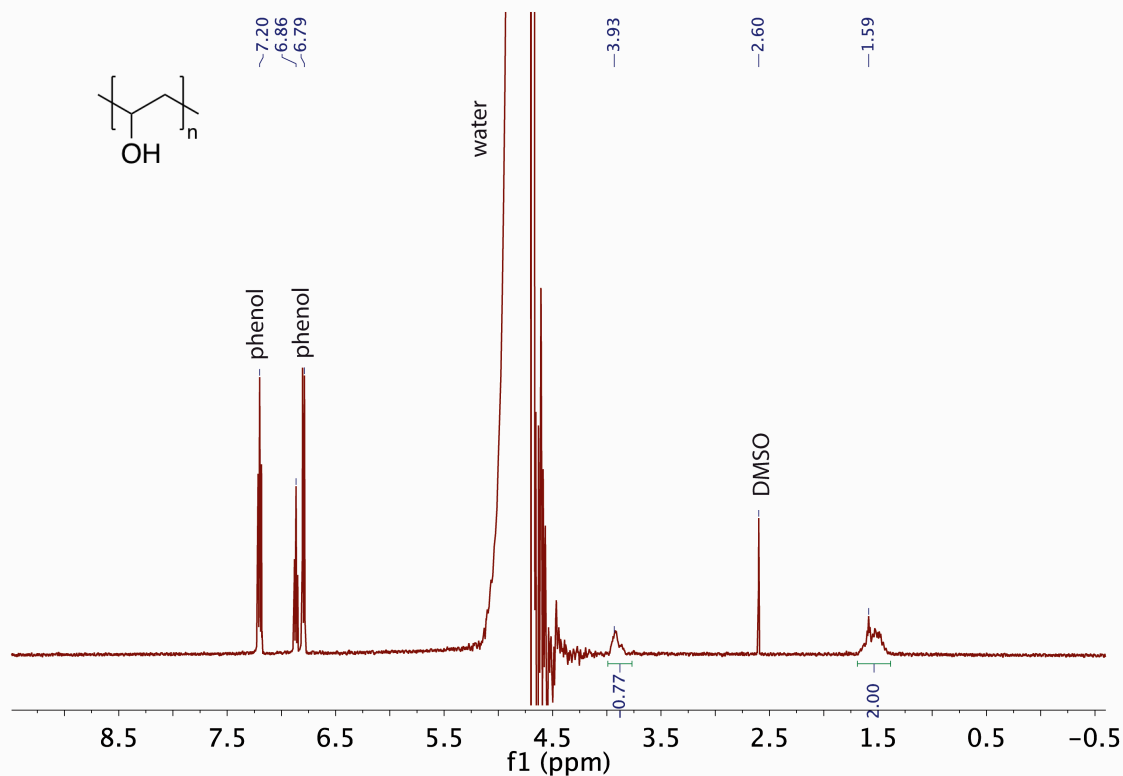


Figure S15. ^1H NMR of polyvinyl alcohol (**5**), rinsed from electrode after 65 minutes of chronoamperometry. Spectrum was collected using suppression of the water peak, and phenol and DMSO were added as internal standards.

The CA experiment was conducted as described in the Experimental Methods using the same loadings.

^1H NMR (500 MHz, H_2O and D_2O , ppm): δ 3.93 (m, 1H), 1.59 (m, 2H), (proton of $-\text{OH}$ cannot be seen because it overlapped with water peak).

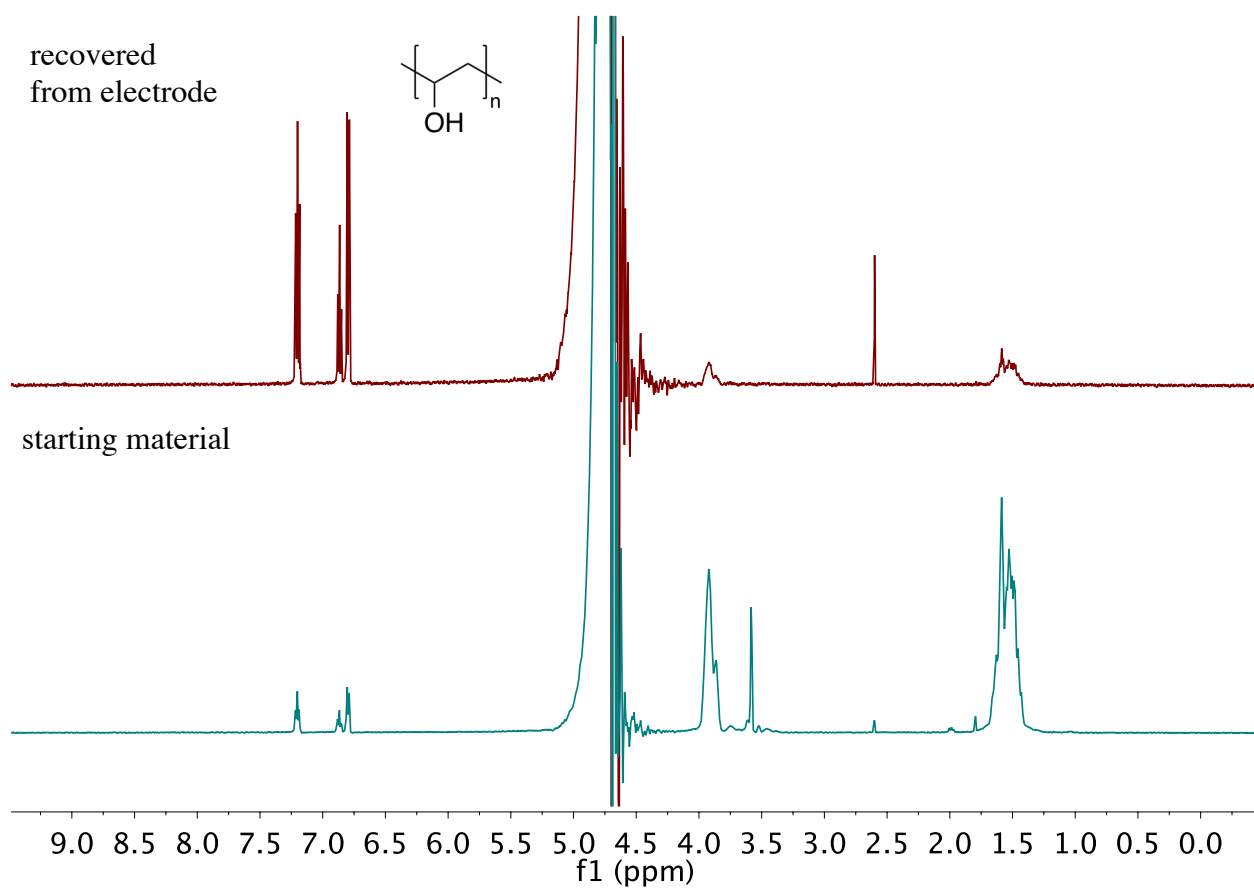


Figure S16. ^1H NMR of commercial polyvinyl alcohol in a mixture of H_2O and D_2O (**5**), compared with rinse of electrode after 65 minutes of chronoamperometry in the same solvent system. Spectra were collected using suppression of the water peak, and phenol and DMSO were added as internal standards.

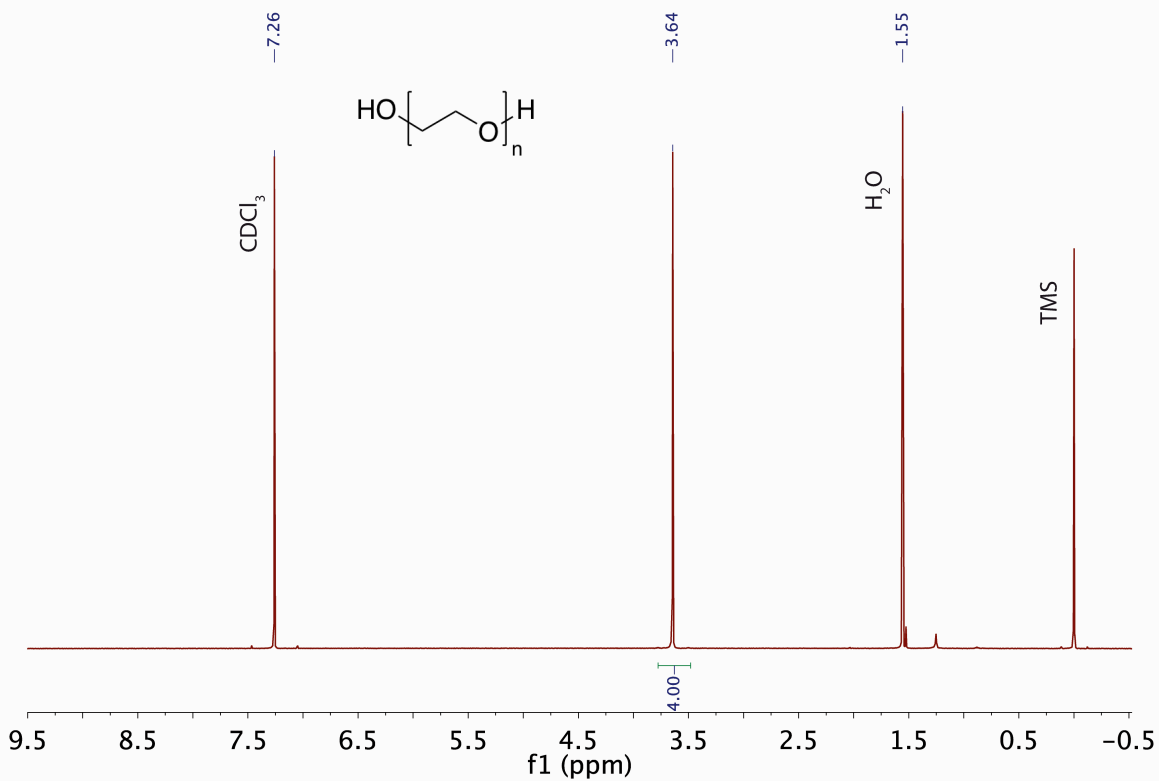


Figure S17. ^1H NMR of polyethylene glycol (**6**), rinsed from electrode after 65 minutes of chronoamperometry.

The CA experiment was conducted as described in the Experimental Methods, except with an increase in the loading. A 50 mg sample of polyethylene glycol (**6**) was dissolved in 1 mL MeOH at 60°C, and 100 μL of this solution was dropcast onto the oxide-derived Cu surface. 50 μL of Nafion solution was dissolved in 1 mL of iPrOH, and 100 μL of the Nafion solution was then dropcast onto the functionalized Cu surface.

^1H NMR (500 MHz, CDCl_3 , ppm): δ 3.64 (s, 4H).

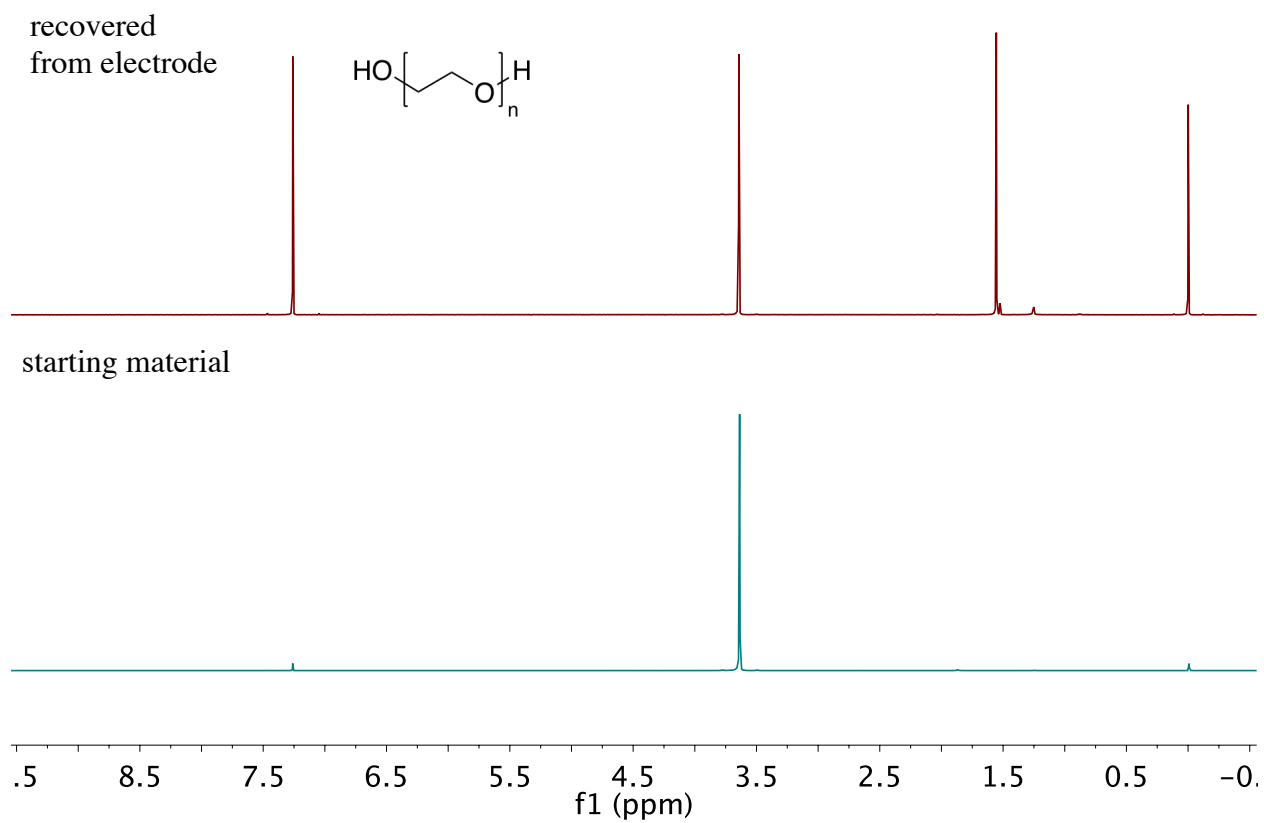


Figure S.18 ^1H NMR of commercial polyethylene glycol (**6**) in CDCl_3 (bottom), compared with rinse of electrode after 65 minutes of chronoamperometry, also in CDCl_3 (top).

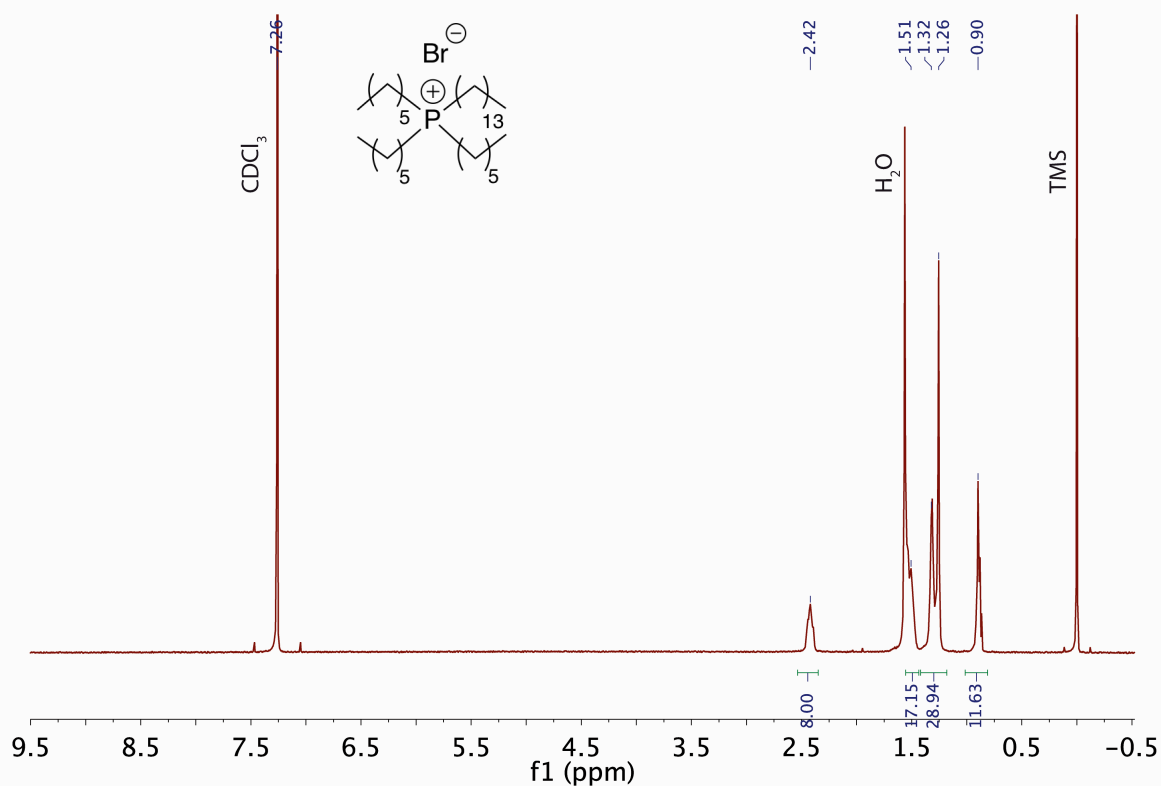


Figure S19. ¹H NMR of trihexyltetradecylphosphonium bromide (**7**), rinsed from electrode after 65 minutes of chronoamperometry.

The CA experiment was conducted as described in the Experimental Methods, except with an increase in the loading. A 50 mg sample of trihexyltetradecylphosphonium bromide (**7**) was dissolved in 1 mL iPrOH, and 100 μ L of this solution was dropcast onto the oxide-derived Cu surface. 50 μ L of Nafion solution was dissolved in 1 mL of iPrOH, and 100 μ L of the Nafion solution was then dropcast onto the functionalized Cu surface.

¹H NMR (500 MHz, CDCl₃, ppm): δ 2.42 (m, 8H), 1.51-1.26 (m, 48H), 0.90 (m, 12H).

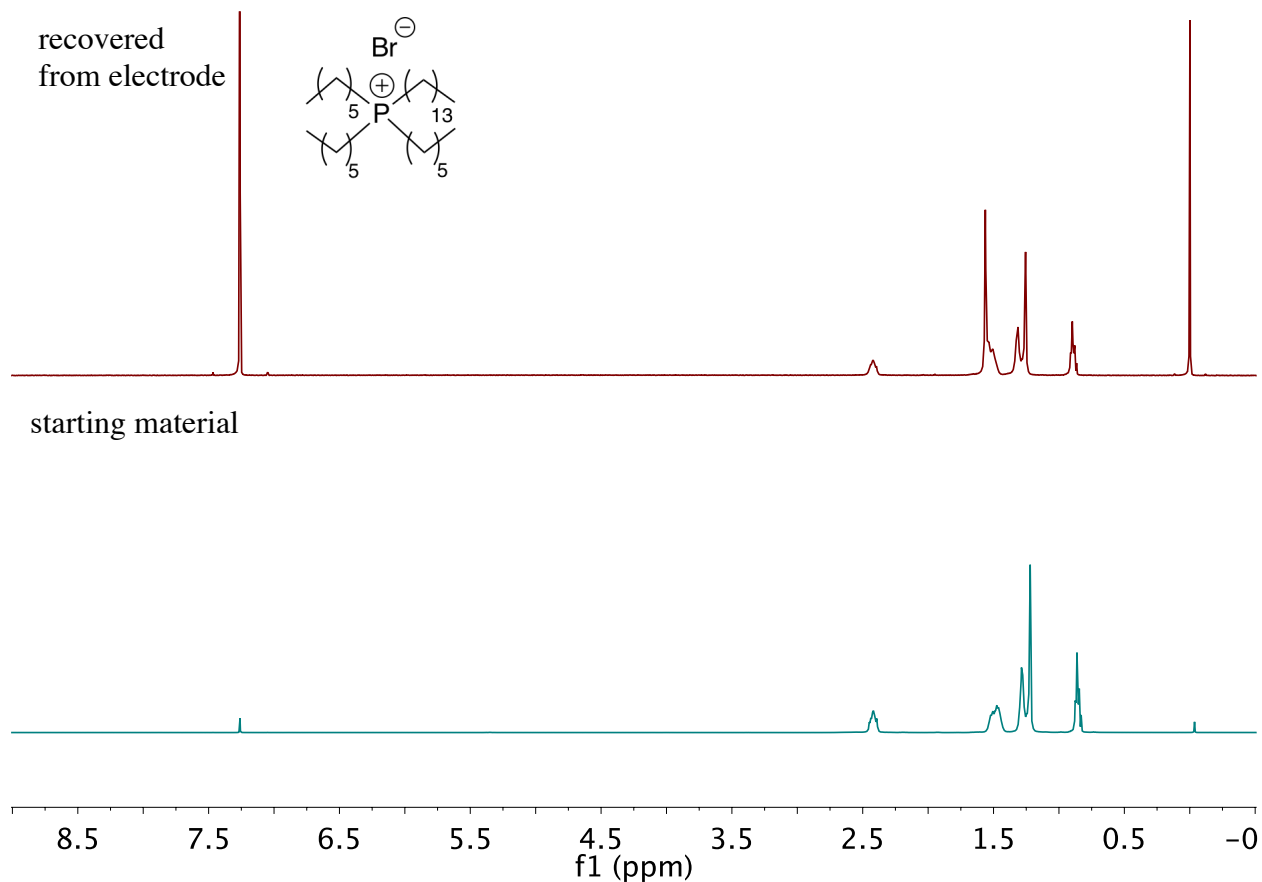


Figure S20. ^1H NMR of commercial trihexyltetradecylphosphonium bromide (**7**) in CDCl_3 (bottom), compared with rinse of electrode after 65 minutes of chronoamperometry, also in CDCl_3 (top).

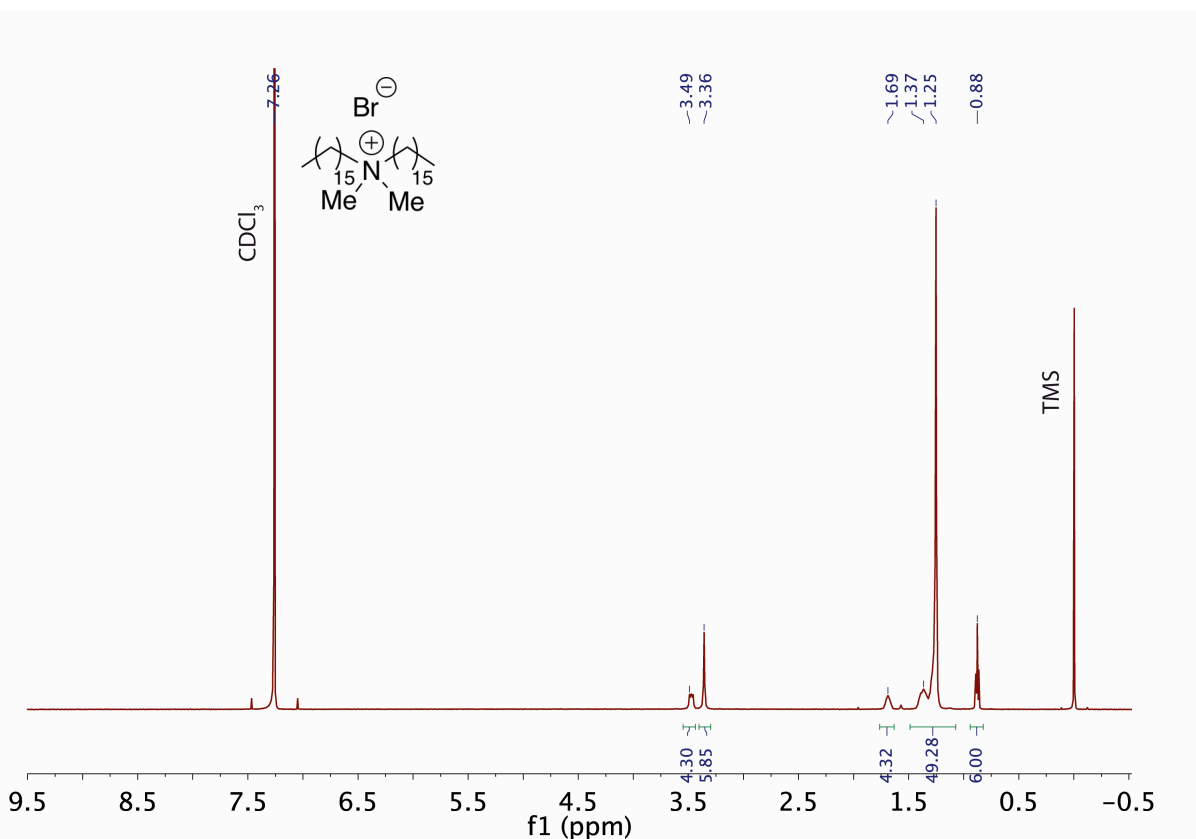


Figure S21. ^1H NMR of dihexadecyldimethylammonium bromide (**8**), rinsed from electrode after 65 minutes of chronoamperometry.

The CA experiment was conducted as described in the Experimental Methods, except with an increase in the loading. A 50 mg sample of dihexadecyldimethylammonium bromide (**8**) was dissolved in 1 mL iPrOH, and 100 μL of this solution was dropcast onto the oxide-derived Cu surface. 50 μL of Nafion solution was dissolved in 1 mL of iPrOH, and 100 μL of the Nafion solution was then dropcast onto the functionalized Cu surface.

^1H NMR (500 MHz, CDCl_3 , ppm): δ 3.49 (m, 4H), 3.36 (s, 6H), 1.69 (m, 4H), 1.37-1.25 (m, 52H), 0.88 (t, $J = 7.09$, 6H).

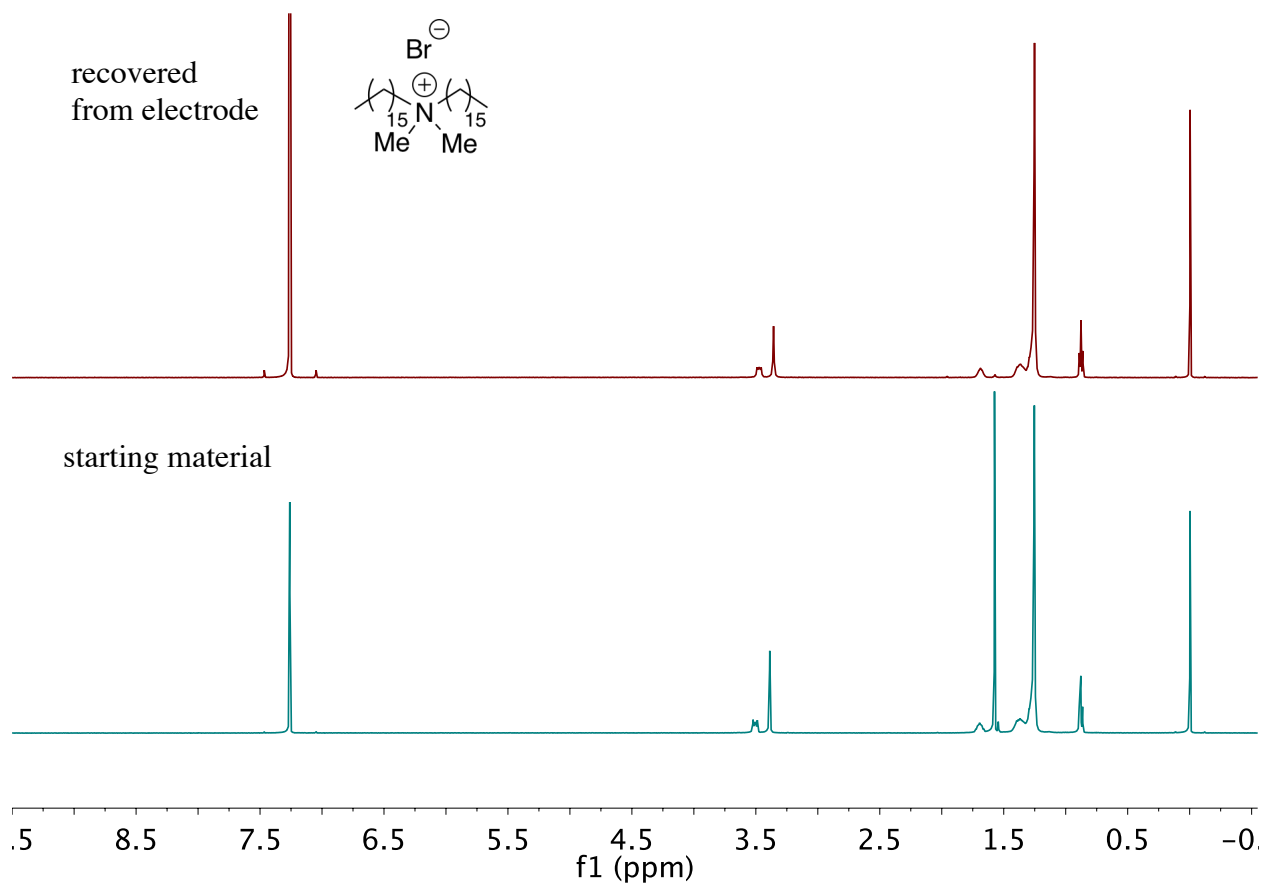


Figure S22. ¹H NMR of commercial dihexadecyldimethylammonium bromide (**8**) in CDCl₃ (bottom), compared with rinse of electrode after 65 minutes of chronoamperometry, also in CDCl₃ (top).

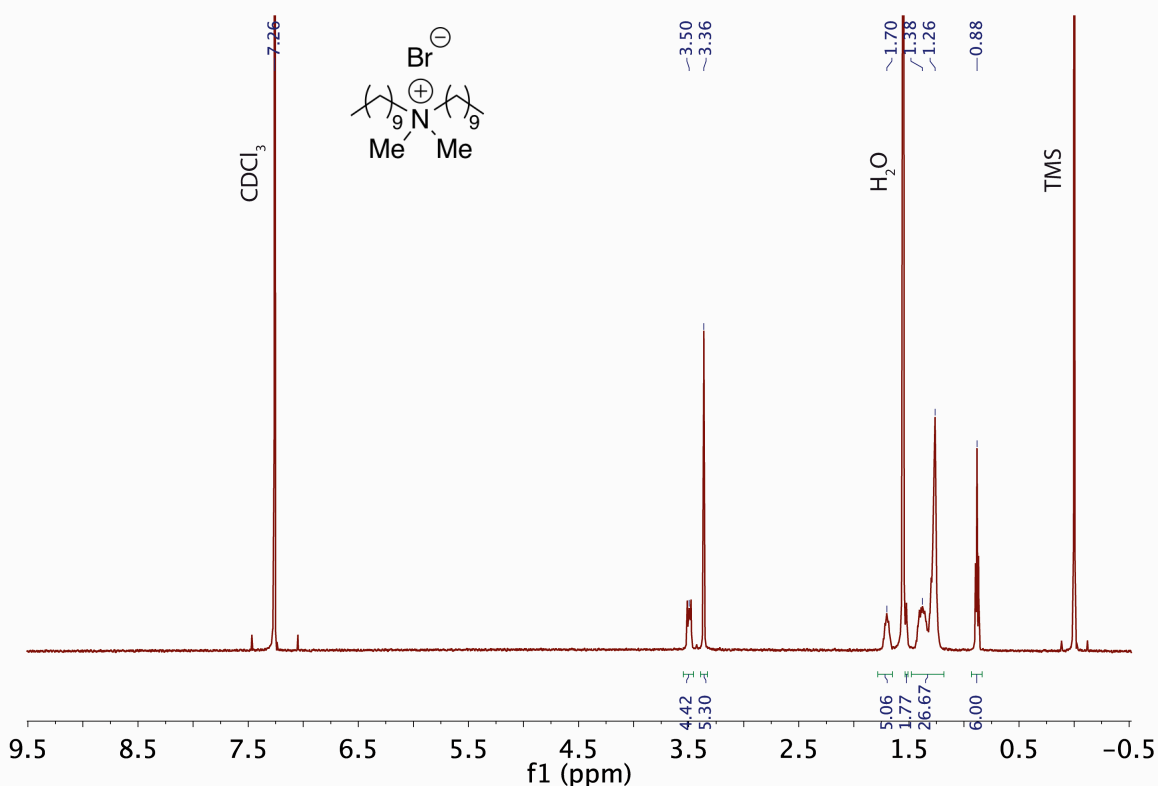


Figure S23. ^1H NMR of didecyldimethylammonium bromide (**9**), rinsed from electrode after 65 minutes of chronoamperometry.

The CA experiment was conducted as described in the Experimental Methods, except with an increase in the loading. A 20 mg sample of didecyldimethylammonium bromide (**9**) was dissolved in 1 mL iPrOH, and 100 μL of this solution was dropcast onto the oxide-derived Cu surface. 20 μL of Nafion solution was dissolved in 1 mL of iPrOH, and 100 μL of the Nafion solution was then dropcast onto the functionalized Cu surface.

^1H NMR (500 MHz, CDCl_3 , ppm): δ 3.50 (m, 4H), 3.36 (s, 6H), 1.70 (m, 4H), 1.38-1.26 (m, 28H), 0.88 (t, $J = 6.75$, 6H).

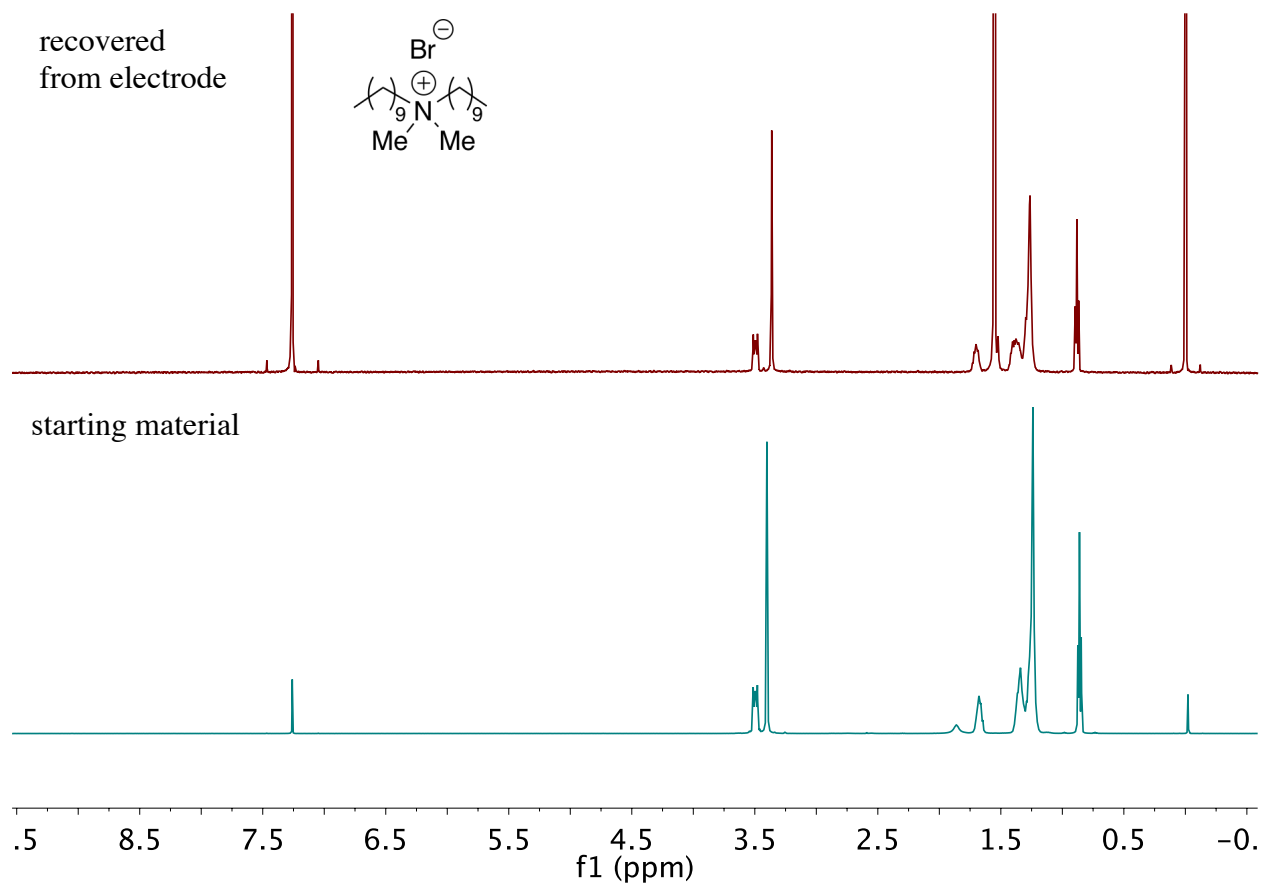


Figure S24. ¹H NMR of commercial didecyldimethylammonium bromide (**9**) in CDCl₃ (bottom), compared with rinse of electrode after 65 minutes of chronoamperometry, also in CDCl₃ (top).

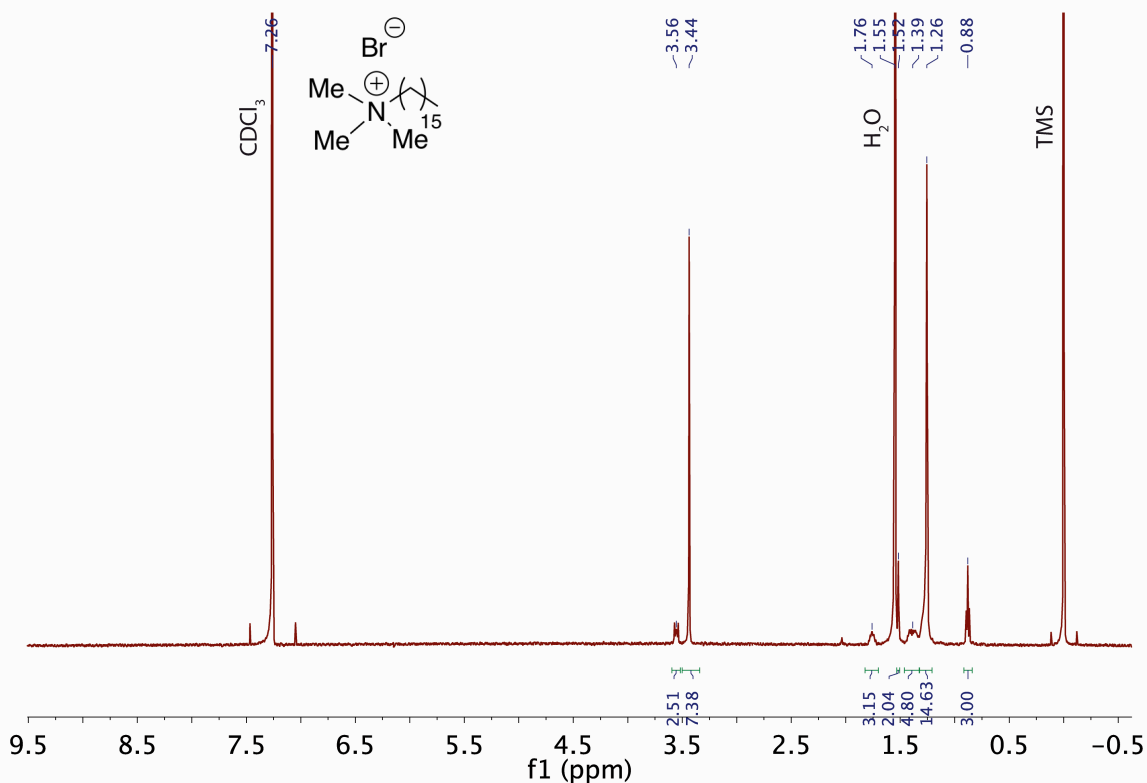


Figure S25. ¹H NMR of cetyltrimethylammonium bromide (**10**), rinsed from electrode after 65 minutes of chronoamperometry.

The CA experiment was conducted as described in the Experimental Methods, except with an increase in the loading. A 20 mg sample of cetyltrimethylammonium bromide (**10**) was dissolved in 1 mL iPrOH, and 100 μL of this solution was dropcast onto the oxide-derived Cu surface. 20 μL of Nafion solution was dissolved in 1 mL of iPrOH, and 100 μL of the Nafion solution was then dropcast onto the functionalized Cu surface.

¹H NMR (500 MHz, CDCl₃, ppm): δ 3.56 (m, 2H), 3.44 (s, 9H), 1.76-1.26 (m, 28H), 0.88 (t, *J* = 6.70, 3H).

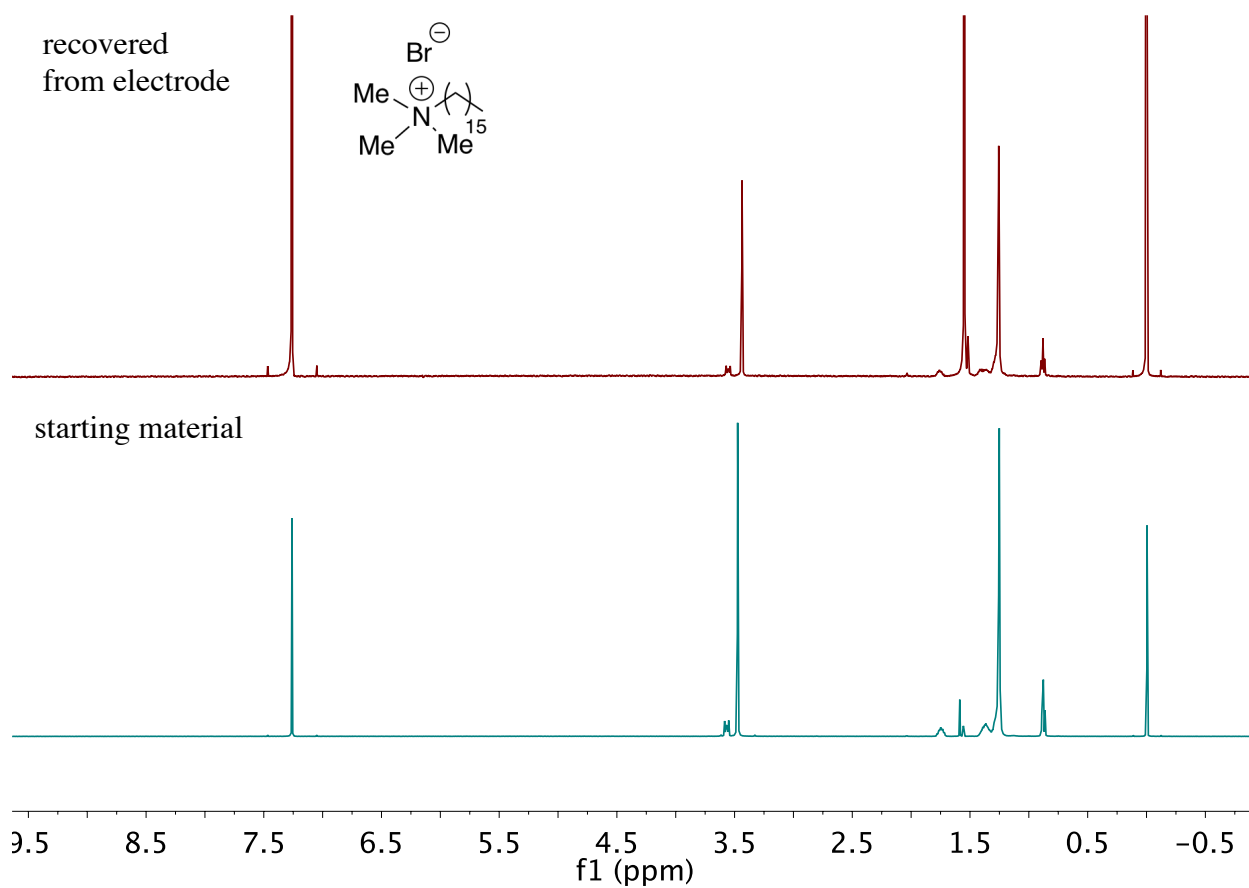


Figure S26. ^1H NMR of commercial cetyltrimethylammonium bromide (**10**) in CDCl_3 (bottom), compared with rinse of electrode after 65 minutes of chronoamperometry, also in CDCl_3 (top).

3.5.8. Partial current densities

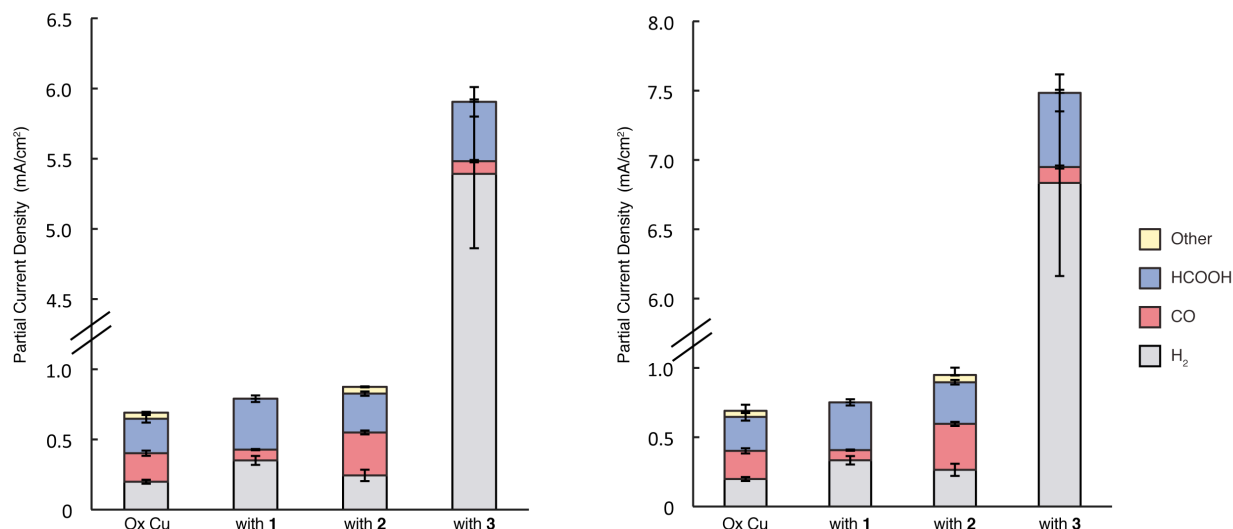


Figure S27. Partial current densities for H₂, CO and formic acid as determined by GC and HPLC (left) and normalized by double layer capacitance (right). The double layer capacitance of the modified surface after chronoamperometry was compared to that of unmodified oxide-derived copper, and the ratio of these values was used to normalize the partial current densities. Error bars illustrate the standard error of the mean.

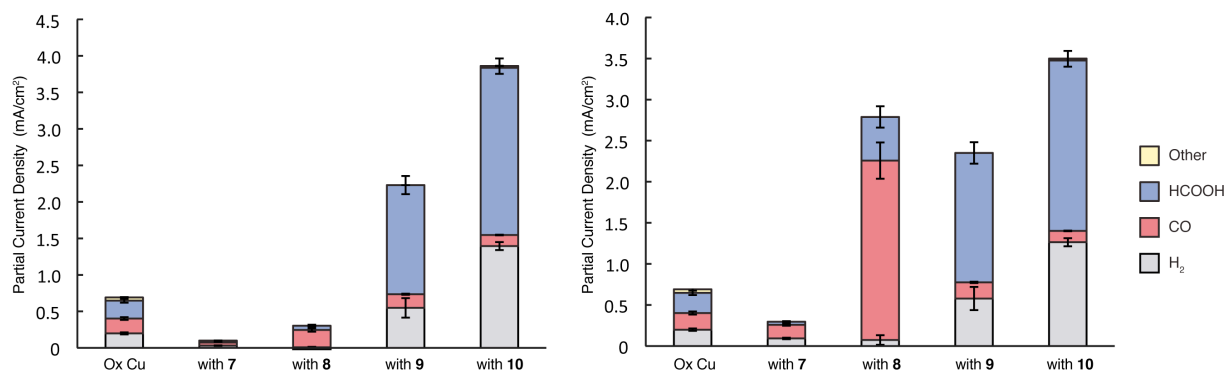


Figure S28. Partial current densities for H₂, CO and formic acid as determined by GC and HPLC (left) and normalized by double layer capacitance (right). The double layer capacitance of the modified surface after chronoamperometry was compared to that of unmodified oxide-derived copper, and the ratio of these values was used to normalize the partial current densities. Error bars illustrate the standard error of the mean.

3.5.9. Contact angle and summarized product distribution data

Table S5. Contact angle measurements, CO₂R selectivity and total current for modified Cu surfaces. Modifiers are listed in order of increasing hydrophobicity. Error values are derived from standard error of the mean.

Sample	Contact Angle (°)	H₂ (%)	CO (%)	Formic acid (%)	Other (%)	Total FE (%)	Total current (mA/cm²)
<i>Cetyltrimethyl ammonium bromide (10)</i>	5.4±0.9	34±1	3.64±0.05	56±2	0.08±0.05	93±1	4.17±0.15
<i>Polyvinyl pyrrolidone (1)</i>	11±2	43±1	10±1	45±2	0	98±1	0.81±0.05
<i>Didecyldimethyl ammonium bromide (9)</i>	13±4	21±3	8±1	62±3	0	91±2	2.45±0.29
<i>Polyethylene glycol (6)</i>	14±3	44±6	16±3	38±3	0	98±2	0.70±0.08
<i>Ox Cu</i>	27±4	28±2	28±2	34±3	6.0±0.6	96±2	0.73±0.05
<i>Polyvinyl alcohol (5)</i>	40±10	71±2	15.1±0.6	17±1	0	103±1	0.54±0.06
<i>Dihexadecyl dimethylammonium bromide (8)</i>	48±3	3±2	76±5	18±4	0	97±1	0.31±0.03
<i>Trihexyltetradecylphosphonium bromide (7)</i>	48±4	27±2	49±3	11±2	0	87±4	0.115±0.003
<i>Polyallylamine (3)</i>	54±4	97±2	1.63±0.04	8±1	0	106.4±0.4	5.6±0.6
<i>Tetrahexadecyl ammonium bromide (2)</i>	65±5	27±3	33.8±0.9	30.5±0.4	5.4±0.6	96±2	0.91±0.05
<i>Polystyrene (4)</i>	97±3	44.6±0.6	19±2	23.5±0.8	3.5±0.7	91±2	0.80±0.13

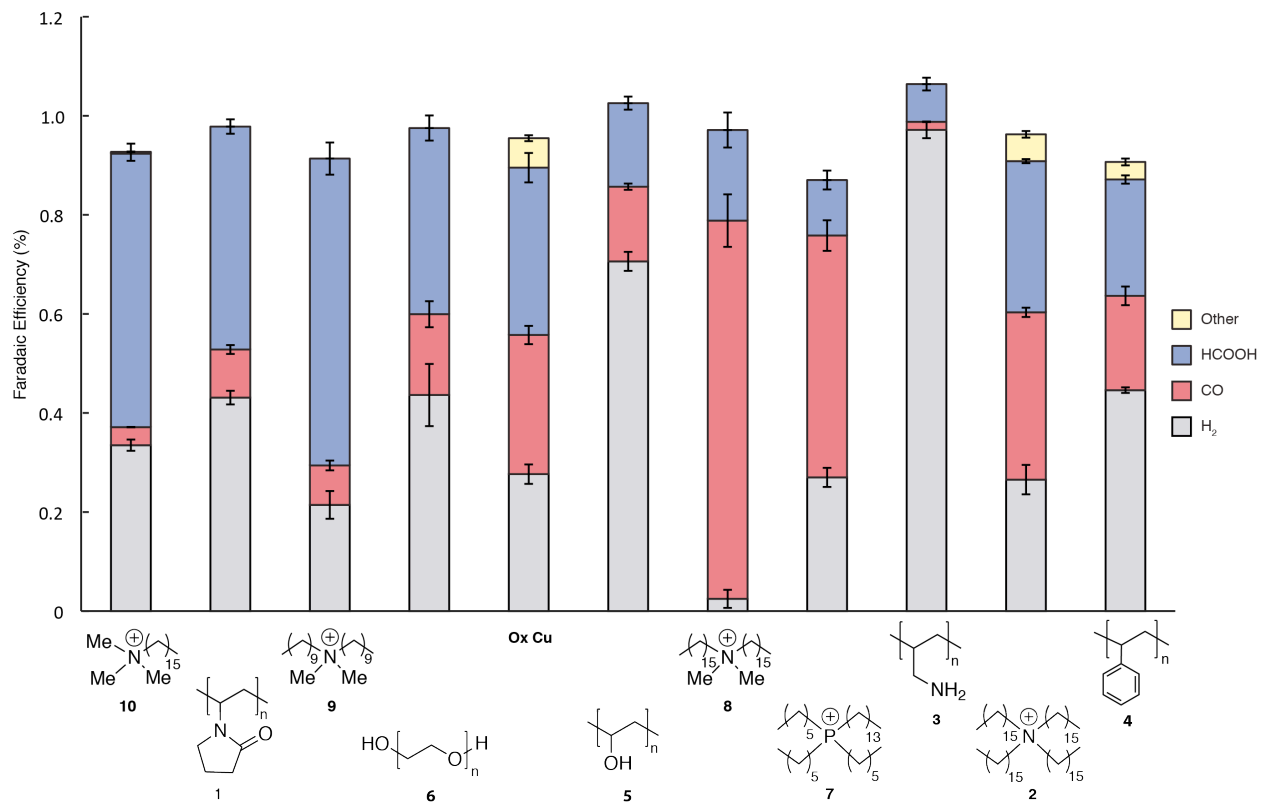


Figure S29. Faradaic efficiencies for modified Cu surfaces, from most hydrophilic (left) to hydrophobic (right). Graphical representation of the data presented in Table S5.

3.5.10. Contact angle measurements, CO₂R partial current densities and total current for modified Cu surfaces. Modifiers are listed in order of increasing hydrophobicity. Error values are derived from standard error of the mean.

Sample	Contact Angle (°)	H₂ (mA/cm²)	CO (mA/cm²)	formic acid (mA/cm²)	Other (mA/cm²)	Total current (mA/cm²)
<i>Cetyltrimethyl ammonium bromide (10)</i>	5.4±0.9	1.39±0.05	0.151±0.004	2.3±0.1	0.003±0.002	4.17±0.15
<i>Polyvinyl pyrrolidone (1)</i>	11±2	0.35±0.03	0.077±0.004	0.36±0.02	0	0.81±0.05
<i>Didecyldimethyl ammonium bromide (9)</i>	13±4	0.5±0.1	0.187±0.008	1.5±0.1	0	2.45±0.29
<i>Polyethylene glycol (6)</i>	14±3	0.32±0.08	0.108±0.005	0.26±0.02	0	0.70±0.08
<i>Ox Cu</i>	27±4	0.20±0.01	0.20±0.02	0.25±0.03	0.043±0.005	0.73±0.05
<i>Polyvinyl alcohol (5)</i>	40±10	0.38±0.03	0.080±0.006	0.09±0.01	0	0.54±0.06
<i>Dihexadecyldimethylammonium bromide (8)</i>	48±3	0.008±0.006	0.24±0.02	0.06±0.01	0	0.31±0.03
<i>Trihexyltetradecyl phosphonium bromide (7)</i>	48±4	0.031±0.003	0.056±0.003	0.013±0.002	0	0.115±0.003
<i>Polyallylamine (3)</i>	54±4	5.4±0.5	0.090±0.008	0.4±0.1	0	5.6±0.6
<i>Tetrahexadecyl ammonium bromide (2)</i>	65±5	0.24±0.04	0.31±0.01	0.28±0.02	0.048±0.004	0.91±0.05
<i>Polystyrene (4)</i>	97±3	0.36±0.05	0.15±0.01	0.19±0.03	0.029±0.009	0.80±0.13

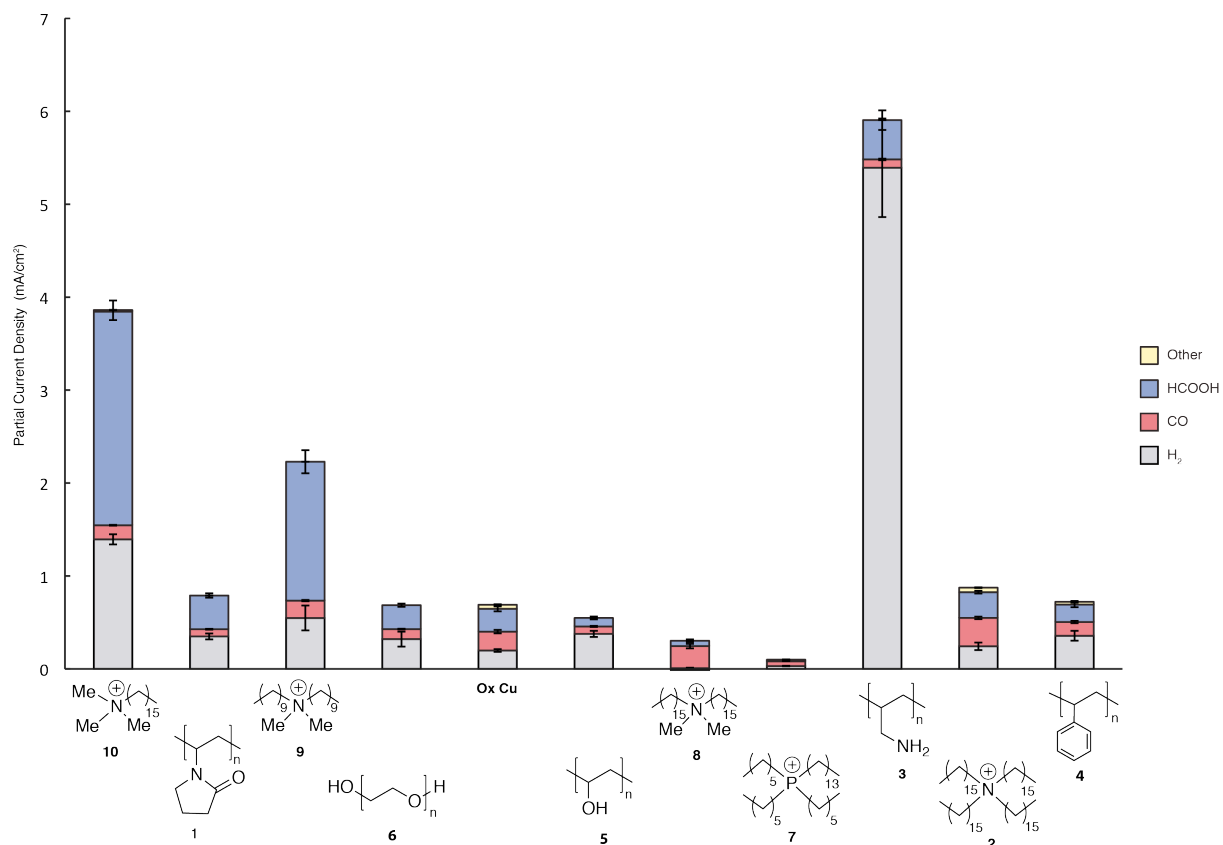


Figure S30. Partial current densities for modified Cu surfaces, from most hydrophilic (left) to hydrophobic (right). Graphical representation of the data presented in Table S6.

3.5.11. Relationship between Faradaic efficiency for CO, H₂ and the contact angle

Fig. 4b in the main text illustrates the relationship between the Faradaic efficiency for formic acid and the contact angle of the Cu surfaces in the text, including **Ox Cu** and with modifiers **1 – 10**. Fig. S31 and Fig. S32 below illustrate this relationship for CO and H₂.

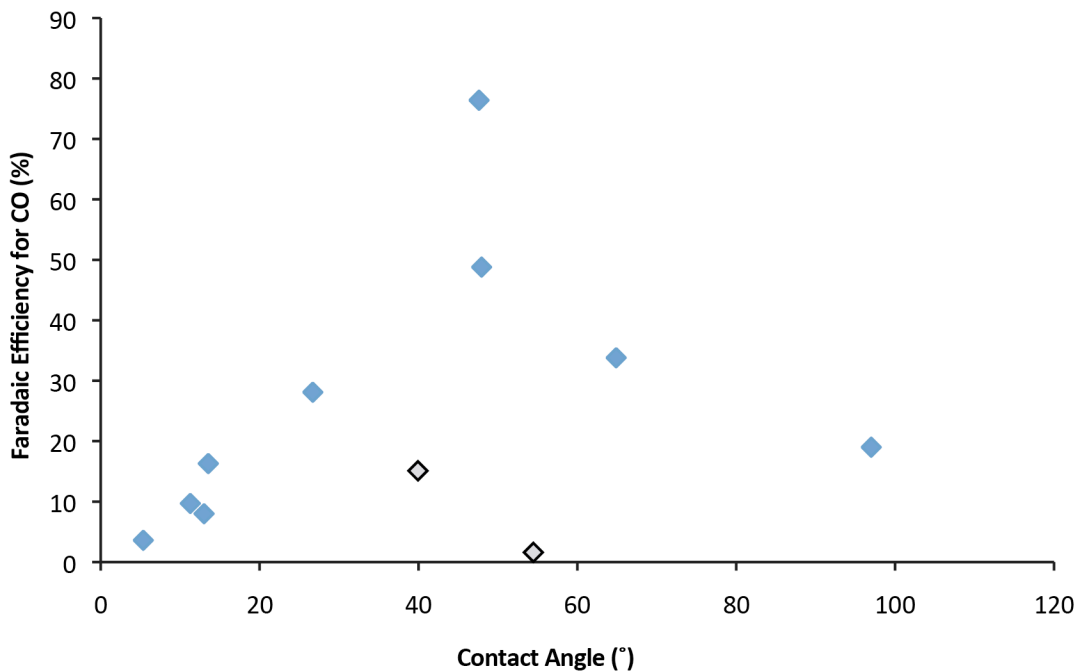


Figure S31. Relationship between Faradaic efficiency for CO and the contact angle of water on modified Cu surfaces. Data points in gray are protic species polyallylamine (**3**) and polyvinyl alcohol (**5**).

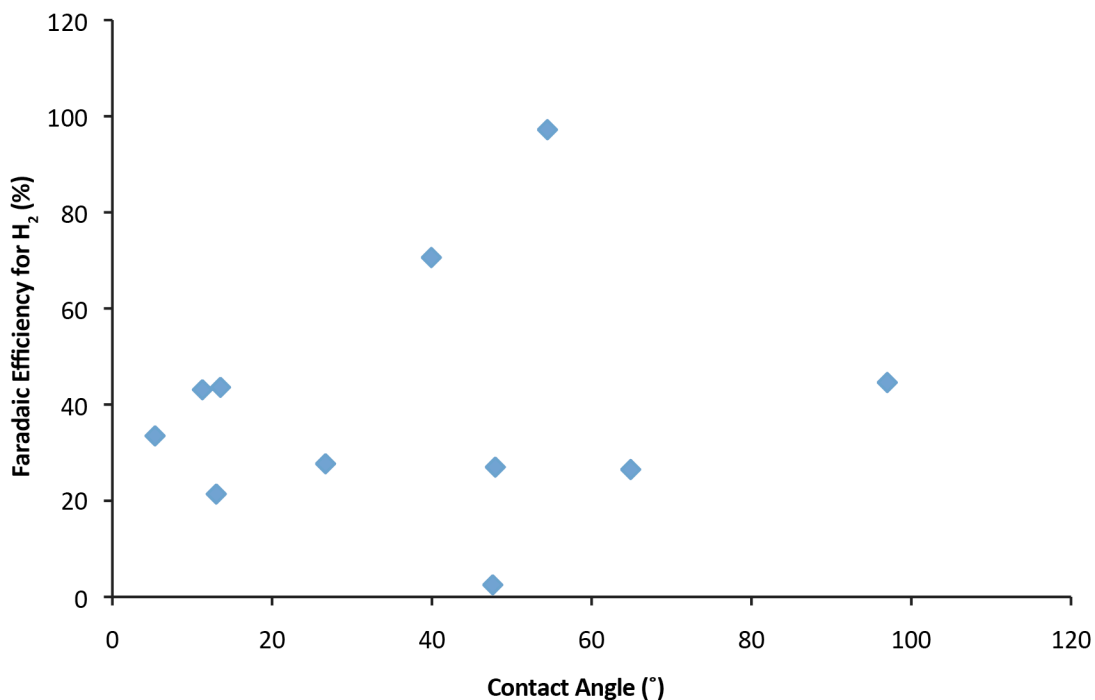


Figure S32. Relationship between Faradaic efficiency for H₂ and the contact angle of water on modified Cu surfaces. The selectivity for H₂ does not show a clear relationship with the contact angle of the modified surface. This may be due to the fact that the selectivity illustrates the amount of product formed relative to the amounts of the other products, which may convolute any trends. Examination of the amount of product formed (the partial current density), instead of the relative amount of product, indicates that the amount of H₂ formed decreases as the hydrophobicity increases, with **2** and **4** as outliers at 65° and 97°, respectively (see **Fig. S33** below).

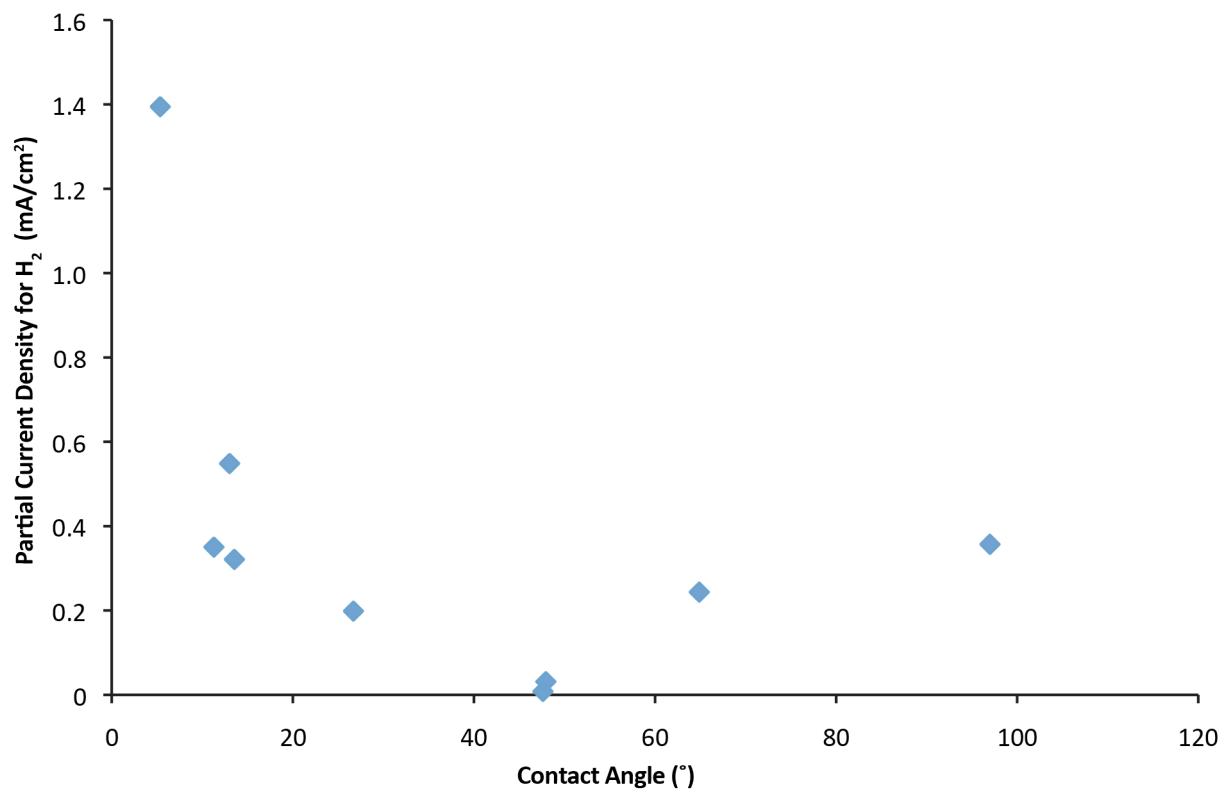


Figure S33. Relationship between partial current density for H₂ and the contact angle of water on modified Cu surfaces. Polyallylamine (**3**) and polyvinyl alcohol (**5**) are not included due to the enhanced activity for H₂ observed with these protic species.

3.5.12. Relationship between formation of H₂, CO and formic acid

In order to better understand the relationship between the formation of these three products, the partial current densities towards these products generated with Ox Cu and modified surfaces (excluding protic modifiers **3** and **5**) were plotted against each other. **Fig. S34** suggests that the formation of formic acid and H₂ may be related, while no such relationship emerges from **Fig. S35** and **Fig. S36**.

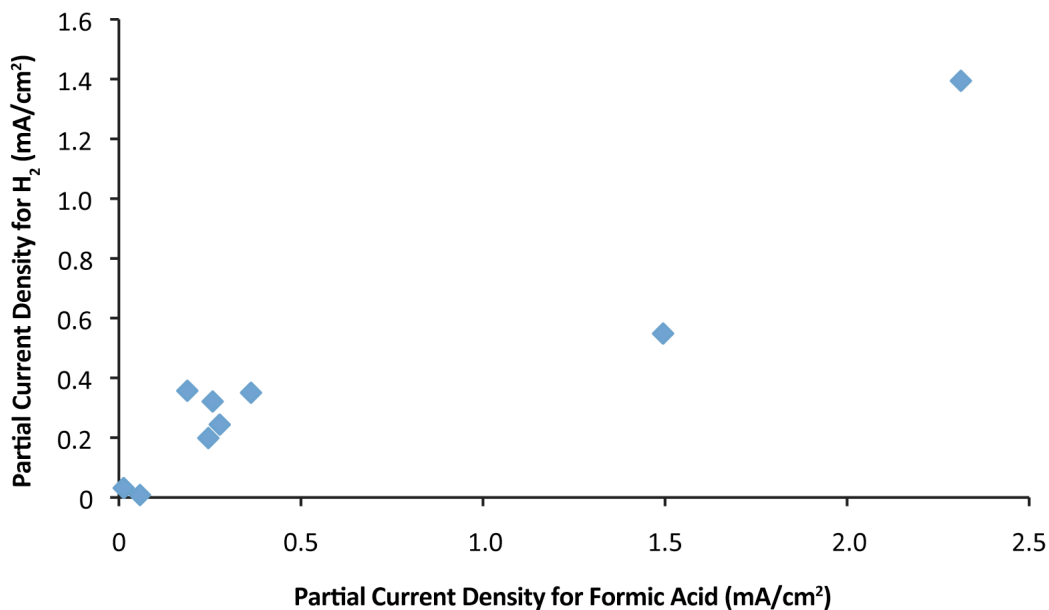


Figure S34. Plot of partial current of formic acid vs. partial current of H₂ from Ox Cu and modified surfaces.

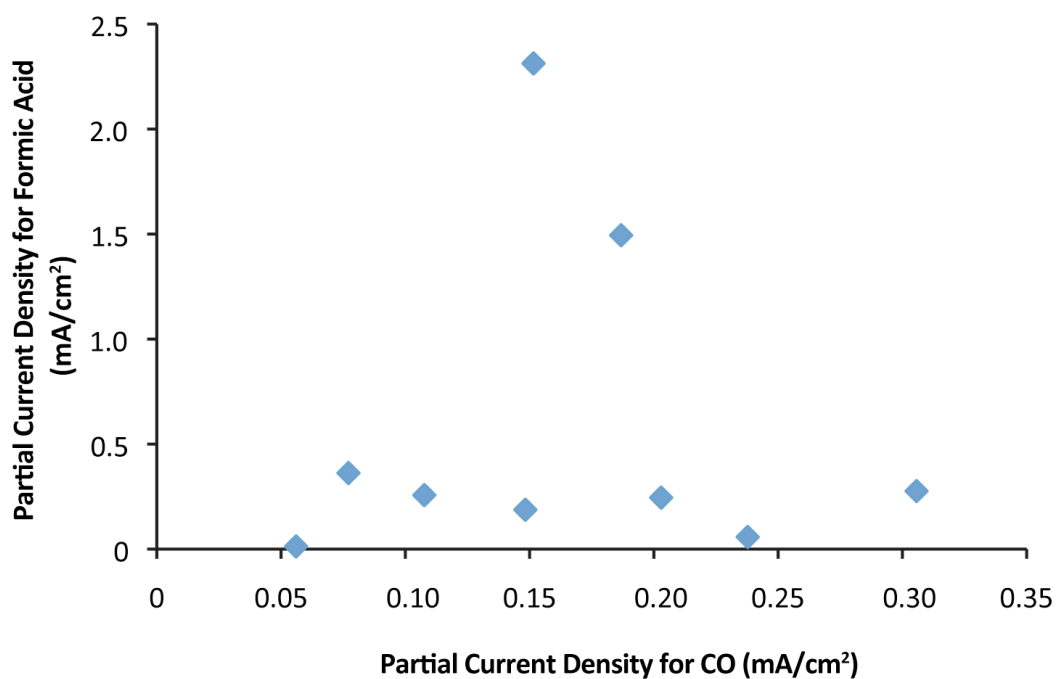


Figure S35. Plot of partial current of CO vs. partial current of formic acid from Ox Cu and modified surfaces.

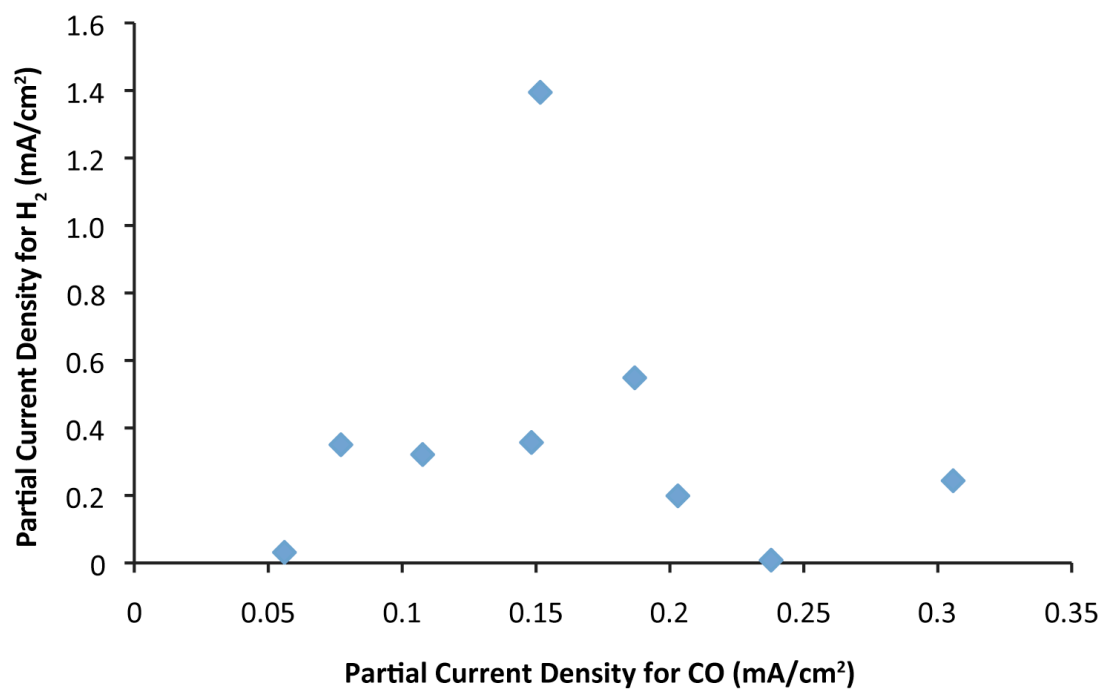


Figure S36. Plot of partial current of CO vs. partial current of H₂ from Ox Cu and modified surfaces.

3.5.13. Tables of Faradaic efficiency data

Tables include standard error of the mean (SEM) and standard deviation (STD). The STD illustrates the spread of the distribution of the data, while the SEM provides a measure of how the sample mean relates to the population mean, or the typical uncertainty for a measurement. The discussion of the main manuscript focuses upon the trends observed between various modifiers, rather than the observed quantities, and so SEM is employed in the text and figures of the main manuscript, while both values are reported below.

Table S7. Data for Figure 1

A	Ox Cu	H ₂	CO	Formic Acid	Other	Total FE	Total Current (mA/cm ²)
	Average	28%	28%	34%	6.0%	96%	0.73
	SEM	2%	2%	3%	0.6%	2%	0.05
	STD	4%	4%	7%	1%	5%	0.12
	<i>Trial 1</i>	27%	24%	36%	6.9%	95%	0.86
	<i>Trial 2</i>	23%	29%	44%	7.6%	103%	0.66
	<i>Trial 3</i>	24%	34%	27%	5.3%	91%	0.79
	<i>Trial 4</i>	29%	24%	33%	5.6%	92%	0.77
	<i>Trial 5</i>	34%	29%	29%	4.4%	97%	0.55
B	Polyvinylpyrrolidone (1)	H ₂	CO	Formic Acid	Other	Total FE	Total Current (mA/cm ²)
	Average	43%	10%	45%	0%	98%	0.81
	SEM	1%	1%	2%	0%	1%	0.05
	STD	3%	2%	3%	0%	2%	0.12
	<i>Trial 1</i>	46%	9%	42%	0%	97%	0.79
	<i>Trial 2</i>	38%	13%	51%	0%	102%	0.71
	<i>Trial 3</i>	45%	8%	45%	0%	98%	1.01
	<i>Trial 4</i>	44%	9%	44%	0%	96%	0.82
	<i>Trial 5</i>	42%	10%	44%	0%	96%	0.71
C	Tetrahexadecylammonium bromide (2)	H ₂	CO	Formic Acid	Other	Total FE	Total Current (mA/cm ²)
	Average	27%	33.8%	30.5%	5.4%	96%	0.91
	SEM	3%	0.9%	0.4%	0.6%	2%	0.05
	STD	5%	2%	0.7%	1%	3%	0.08
	<i>Trial 1</i>	26%	32.5%	29.7%	6.0%	94%	0.88
	<i>Trial 2</i>	32%	33.2%	30.7%	4.1%	100%	1.00
	<i>Trial 3</i>	22%	35.6%	31.1%	6.1%	95%	0.84
D	Polyallylamine (3)	H ₂	CO	Formic Acid	Other	Total FE	Total Current (mA/cm ²)
	Average	97%	1.63%	8%	0%	106.4%	5.6
	SEM	2%	0.04%	1%	0%	0.4%	0.6
	STD	3%	0.1%	2%	0%	0.7%	1.0

<i>Trial 1</i>	100%	1.68%	5%	0%	107.0%	4.4
<i>Trial 2</i>	97%	1.54%	8%	0%	106.5%	6.3
<i>Trial 3</i>	94%	1.66%	10%	0%	105.6%	6.0

Table S8. Data for Table 1

Ox Cu, polyvinylpyrrolidone (1) and polyallylamine (3) may be found in Table S6.

A	<i>Polystyrene (4)</i>	H₂	CO	Formic Acid	Other	Total FE	Total Current (mA/cm²)
	Average	44.6%	19%	23.5%	3.5%	91%	0.80
	SEM	0.6%	2%	0.8%	0.7%	2%	0.13
	STD	1%	3%	1%	1.2%	4%	0.2
	<i>Trial 1</i>	43.8%	18%	24.2%	3.0%	89%	0.95
	<i>Trial 2</i>	44.3%	17%	21.8%	4.9%	88%	0.91
	<i>Trial 3</i>	45.7%	23%	24.5%	2.7%	96%	0.55

B	<i>Polyvinyl alcohol (5)</i>	H₂	CO	Formic Acid	Other	Total FE	Total Current (mA/cm²)
	Average	71%	15.1%	17%	0%	103%	0.54
	SEM	2%	0.6%	1%	0%	1%	0.06
	STD	3%	1%	2%	0%	2%	0.1
	<i>Trial 1</i>	69%	14.7%	19%	0%	103%	0.51
	<i>Trial 2</i>	68%	14.2%	18%	0%	100%	0.65
	<i>Trial 3</i>	74%	16.3%	14%	0%	105%	0.45

C	<i>Polyethylene glycol (6)</i>	H₂	CO	Formic Acid	Other	Total FE	Total Current (mA/cm²)
	Average	44%	16%	38%	0%	98%	0.70
	SEM	6%	3%	3%	0%	2%	0.08
	STD	13%	5%	5%	0%	3%	0.17
	<i>Trial 1</i>	36%	19%	38%	0%	93%	0.57
	<i>Trial 2</i>	30%	22%	45%	0%	97%	0.54
	<i>Trial 3</i>	57%	11%	33%	0%	101%	0.86
	<i>Trial 4</i>	52%	13%	35%	0%	99%	0.83

Table S9. Data for Figure 2

Ox Cu and tetrahexadecylammonium bromide (2) may be found in Table S6.

A	Trihexyltetradecyl-phosphonium bromide (7)	H₂	CO	Formic Acid	Other	Total FE	Total Current (mA/cm²)
	Average	27%	49%	11%	0%	87%	0.115

SEM	2%	3%	2%	0%	4%	0.003
STD	4%	6%	4%	0%	8%	0.006
<i>Trial 1</i>	22%	52%	9%	0%	84%	0.11
<i>Trial 2</i>	26%	50%	7%	0%	83%	0.11
<i>Trial 3</i>	31%	40%	12%	0%	83%	0.12
<i>Trial 4</i>	29%	53%	16%	0%	98%	0.12

B	Dihexadecyldimethylammonium bromide (8)	H ₂	CO	Formic Acid	Other	Total FE	Total Current (A/cm ²)
	Average	3%	76%	18%	0%	97%	0.31
	SEM	2%	5%	4%	0%	1%	0.03
	STD	3%	9%	6%	0%	2%	0.06
	<i>Trial 1</i>	0%	81%	14%	0%	95%	0.35
	<i>Trial 2</i>	1%	82%	16%	0%	99%	0.25
	<i>Trial 3</i>	6%	66%	25%	0%	97%	0.34

C	Didecyldimethylammonium bromide (9)	H ₂	CO	Formic Acid	Other	Total FE	Total Current (mA/cm ²)
	Average	21%	8%	62%	0%	91%	2.45
	SEM	3%	1%	3%	0%	2%	0.29
	STD	6%	2%	7%	0%	5%	0.57
	<i>Trial 1</i>	19%	8%	61%	0%	89%	2.15
	<i>Trial 2</i>	16%	10%	71%	0%	97%	1.85
	<i>Trial 3</i>	29%	6%	59%	0%	93%	3.15
	<i>Trial 4</i>	22%	8%	57%	0%	87%	2.64

D	Cetyltrimethylammonium bromide (10)	H ₂	CO	Formic Acid	Other	Total FE	Total Current (mA/cm ²)
	Average	34%	3.64%	56%	0.08%	93%	4.17
	SEM	1%	0.05%	2%	0.05%	1%	0.15
	STD	2%	0.1%	3%	0.09%	2%	0.26
	<i>Trial 1</i>	35%	3.65%	54%	0.18%	93%	3.91
	<i>Trial 2</i>	34%	3.55%	54%	0%	91%	4.42
	<i>Trial 3</i>	31%	3.72%	59%	0.07%	94%	4.17

3.5.14. References

1. Lobaccaro, P.; Singh, M. R.; Clark, E. L.; Kwon, Y.; Bell, A. T.; Ager, J. W. Effects of Temperature and Gas-Liquid Mass Transfer on the Operation of Small Electrochemical Cells for the Quantitative Evaluation of CO₂ Reduction Electrocatalysts. *Phys. Chem. Chem. Phys.* **2016**, *18*, 26777-26785.

Chapter 4:

Effect of Quaternary Ammonium Salts on the Behavior of Ag
in the CO₂ Reduction Reaction

4.1 Introduction

The complexity of electrochemical interfaces clouds the effort to rationally design catalysts to promote electrocatalytic processes. Efforts to tune a single parameter, such as the electrolyte, can have a wide-ranging influence on such related features as the local pH, electric field, or binding of surface species.¹ As a result, efforts to tune the selectivity of such reactions as the reduction of CO₂ by varying a single parameter often raise more questions than are answered regarding the mechanism for the change in catalytic behavior.

For example, organic species have been employed to tune the CO₂ reduction selectivity of metallic catalysts, but the mechanism for the change in selectivity remains a subject of study. In 2011, Masel *et al.* reported that the ionic liquid 1-ethyl-3-methylimidazolium tetrafluoroborate lowers the overpotential for the formation of CO from CO₂ on Ag surfaces.² Since this finding, a number of mechanistic proposals for this and other organic modifiers have been examined in the literature, probed via variations to the organic structure,³ spectroscopic methods^{4,5} or theoretical studies⁶. These hypotheses include the suppression of the competing hydrogen evolution reaction (HER)⁷, interaction with CO₂⁻ radical or other proposed intermediates in solution⁸ or at the metal surface⁹, and tuning of the reaction microenvironment¹⁰. The number of suggested mechanisms indicates that multiple parameters may have an influence on the catalytic system, and that a consensus has not emerged as to which have the most substantial impact.

In a recent study, our group considered these challenges in the context of CO₂ reduction on Cu and decided to approach these questions by working to identify the most sensitive and influential selectivity-determining factors, rather than choosing a single parameter and varying it.¹¹ By examining the effect of a diverse but structurally simple set of organic species on the product selectivity, the characteristics that played the most influential role in dictating the observed selectivity were identified. Unexpectedly, the hydrophilicity/phobicity of the organic modifiers emerged as a key parameter that dictated whether formic acid or CO was favored. Within the hydrophobic species that were examined, a cationic functionality was also important in obtaining improved selectivity for CO, an observation that remains open to further mechanistic investigation.

In order to more specifically examine the role of the cation in CO formation, we herein apply the cationic modifiers from our previous work and measure their impact on CO formation on Ag. The observed trends point to a new parameter that is important to obtaining improved CO selectivities. We anticipate that the trends observed here will aid in the more targeted design of modifiers for the CO formation process.

4.2 Results and Discussion

We characterized the CO₂ reduction selectivity of Ag foil, and then Ag in the presence of a series of quaternary alkylammonium salts, in order to understand which features of the ammonium salts were key to influencing CO formation.

Polycrystalline Ag foil was placed in a cell of previously reported design¹² to evaluate the CO₂ reduction behavior. Additional experimental details may be found in the Supporting Information (4.5.1). The resulting product distribution for Ag foil closely resembles previous reports for polycrystalline Ag.¹³

We then dropcast solutions of quaternary ammonium salts of varying substitution patterns onto Ag foil and characterized the influence of these salts (**Fig. 1**). We examined the CO₂ reduction behavior at -0.8 V vs. RHE, a relatively low potential, in order to focus on the catalytic behavior at the onset of CO formation. On Cu, we had observed that the relatively hydrophilic

cetyltrimethylammonium bromide (**1**) and dimethyldidecylammonium bromide (**3**) promoted H₂ and formic acid formation via weakening of the metal-hydride interaction in the hydrophilic environment, while the hydrophobic dimethyldihexadecylammonium bromide (**2**) promoted CO formation. We therefore hypothesized that we may observe more H₂ with **1** and **3**, and more CO with **2**.

Unexpectedly, we found that surfaces modified with **1** and **2** demonstrated substantially higher selectivities for CO, while Ag with modifier **3** was only slightly more selective for CO relative to the unfunctionalized surface. Intrigued by this behavior, we decided to also characterize the effect of trimethyldecylammonium bromide (**4**). We identified a trend in which the marked enhancement in CO selectivity is specific to ammonium salts with long, 16-carbon chains, with similar behavior between trimethyl and dimethylammonium salts.

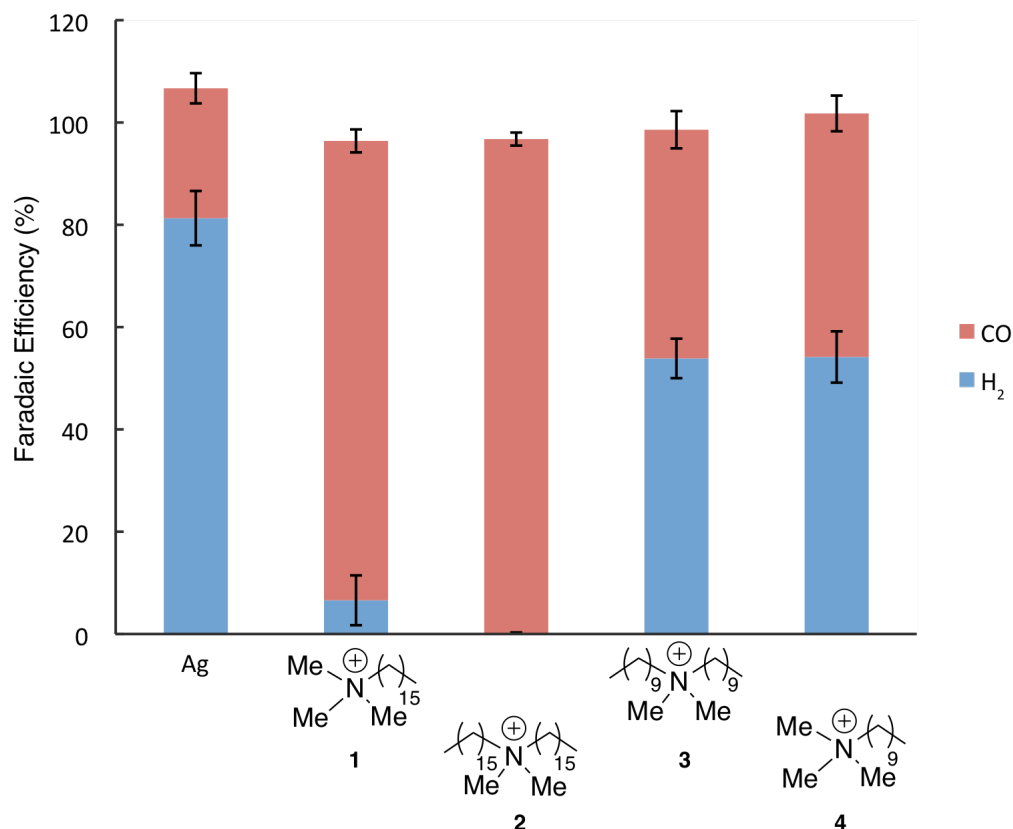


Figure 1. CO₂ reduction selectivity of Ag foil, as well as with ammonium salts **1-4**, at -0.8 V vs. RHE. Increased selectivity for CO is observed with modifiers **1** and **2**, with less pronounced increases in CO formation with **3** and **4**. Values and error bars are calculated from three trials, with error bars reported as standard error of the mean.

An examination of the partial current densities indicates that, in terms of the activity, the amount of CO formed is substantially increased, and the amount of H₂ substantially decreased, in the presence of **1** and **2** (4.5.2).

This trend related to hydrocarbon chain length provides interesting clues into what the selectivity-determining factor may or may not be. In our previous work, we had found that

whether the ammonium salt was di- or trimethyl substituted and the length of the longest hydrocarbon chains both had an effect on the hydrophilicity of the molecule. We measured the contact angle of Ag and functionalized Ag surfaces and found that **1**, **3**, and **4** have similar hydrophilicities; however, **1** and **2** demonstrated similar selectivities, while **3** and **4** substantially enhanced in CO selectivity (**4.5.3**). While the surrounding water has been implicated in mechanisms for CO formation on Ag,^{14,15} we surmise that this lack of correlation indicates that the selectivity-determining change is not related to the interaction of these organic species with the surrounding water.

Moreover, the series in **Fig. 1a** indicates that the presence of a cationic functionality or bromide anion is not sufficient for an change in selectivity to be observed. We sought to understand how a change from a C10 to C16 chain could have such a pronounced impact on the behavior of these organic species.

Previous work in the literature suggests that the length of these alkyl chains plays an important role in the ordering of these molecules. One study by Osman reports that a self-assembled layer of these ammonium salts undergoes a change in conformation upon heating, with a more pronounced reliance on chain length than on such factors as the number of long hydrocarbon chains.¹⁶ We therefore hypothesize that the difference in catalytic behavior between the C16 and C10 substituted salts is due to the differences in their conformation at the interface.

In examining the conformation of imidazolium salts on Ag using sum frequency generation spectroscopy, the Dlott group found that the salts undergo a structural transition at potentials similar to the onset of CO formation. They suggested that the conformation of the salts on the surface may be related to the formation of CO.⁴

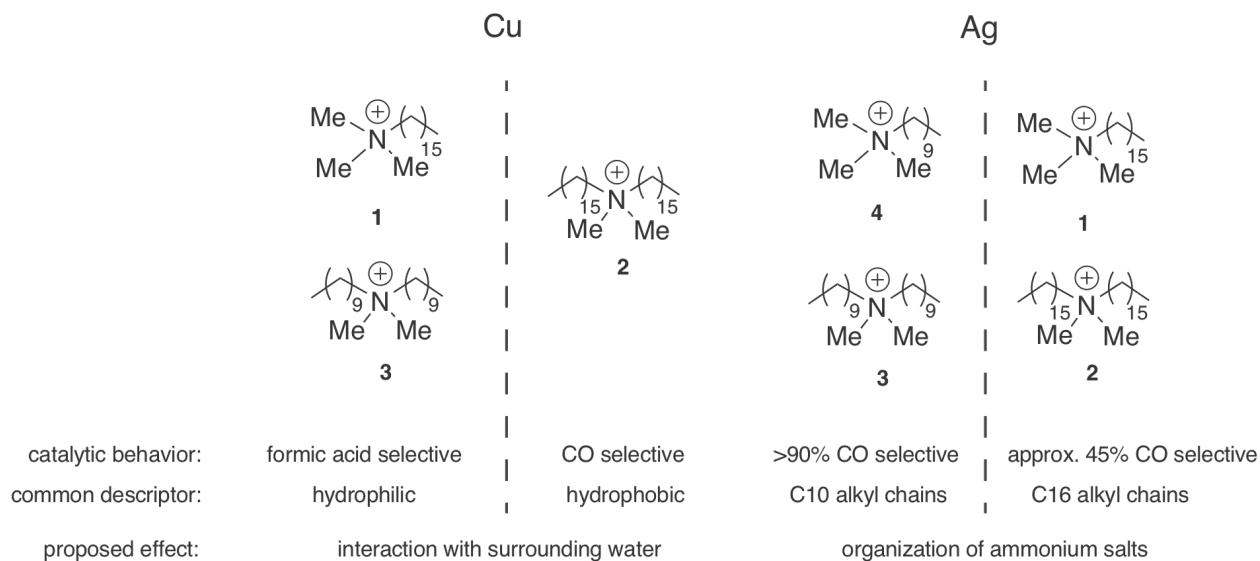


Figure 2. Summary of how ammonium salts influence CO₂ reduction on Cu and Ag surfaces.

The trend we observe in **Fig. 1** may be a manifestation of this phenomenon, in which the conformation of the cationic species at the surface is implicated in the CO formation (**Fig. 2**). This generality in cationic species on Ag surfaces raises the possibility of a new strategy in

developing catalysts for CO formation; while several studies have discussed possible interactions of these organic modifiers with surface species, and our previous work highlighted the interaction of these organic species with the surrounding water, the selectivity-determining interaction in this case may be the interaction of these organic modifiers with themselves.

With this insight into the selectivity-determining parameter, the ordering of the ammonium salt at the interface, we considered how this ordering may influence CO formation at the Ag surface. One possibility is that the ordering of these ammonium salts influences the local environment, such as the local concentration and availability of CO₂.¹⁷ A second possibility is that these cationic functionalities directly influence the energy of polar surface intermediates, including *COO⁻ or *COOH.⁶ This stabilization may be facilitated with the ordering of these ammonium salts at the interface. Our group is currently probing these potential mechanistic pathways.

4.3 Conclusions

In examining how cationic ammonium salts influence CO formation, we find that the defining parameter, unexpectedly, is the length of the longest hydrocarbon chain, rather than the number of these chains. This provides a strong indication that the way in which these ammonium salts interact with each other, rather than with the surrounding aqueous environment, is key to the observed change in selectivity. This methodology allows access to up to 97% CO formation at -0.8 V vs. RHE, with an 8-fold increase in activity relative to the bare Ag surface. In our future work, we hope to understand how organic species may be designed to optimize these interactions between the surrounding organic species, the aqueous environment and the catalyst surface to further improve CO₂ reduction activity and selectivity.

4.4 References

1. Waegele, M. M.; Gunathunge, C. M.; Li, J.; Li, X. How Cations Affect the Electric Double Layer and the Rates and Selectivity of Electrocatalytic Processes. *J. Chem. Phys.* **2019** *151*, 160902.
2. Rosen, B. A.; Salehi-Khojin, A.; Thorson, M. R.; Zhu, W.; Whipple, D. T.; Kenis, P. J. A.; Masel, R. I. Ionic Liquid-Mediated Selective Conversion of CO₂ to CO at Low Overpotentials. *Science* **2011** *334*, 643-644.
3. Lau, G. P. S.; Schreier, M.; Vasilyev, D.; Scopelliti, R.; Grätzel, M.; Dyson, P. J. New Insights into the Role of Imidazolium-Based Promoters for the Electroreduction of CO₂ on a Silver Electrode. *J. Am. Chem. Soc.* **2016** *138*, 7820-7823.
4. Rey, N. G.; Dlott, D. D. Structural Transition in an Ionic Liquid Controls CO₂ Electrochemical Reduction. *J. Phys. Chem. C* **2015** *119*, 20892-20899.
5. Cuesta, A.; Papisizza, M. In Situ Monitoring Using ATR-SEIRAS of the Electrocatalytic Reduction of CO₂ on Au in an Ionic Liquid/Water Mixture. *ACS Catal.* **2018** *8*, 6345-6352.
6. Ringe, S.; Clark, E. L.; Resasco, J.; Walton, A.; Seger, B.; Bell, A. T.; Chan, K. Understanding Cation Effects in Electrochemical CO₂ Reduction. *Energy Environ. Sci.* **2019** *12*, 3001-3014.
7. Quan, F.; Xiong, M.; Jia, F.; Zhang, L. Efficient Electroreduction of CO₂ on Bulk Silver Electrode in Aqueous Solution via the Inhibition of Hydrogen Evolution. *Applied Surface Sci.* **2017**, *399*, 31, 48-54.
8. Rosen, B. A.; Haan, J. L.; Mukherjee, P.; Braunschweig, B.; Zhu, W.; Salehi-Khojin, A.; Dlott, D. D.; Masel, R. I. In Situ Spectroscopic Examination of a Low Overpotential Pathway for Carbon Dioxide Conversion to Carbon Monoxide. *J. Phys. Chem. C* **2012** *116*, 29, 15307-15312.
9. Tanner, E. E. L.; Batchelor-McAuley, C.; Compton, R. G. Carbon Dioxide Reduction in Room-Temperature Ionic Liquids: The Effect of the Choice of Electrode Material, Cation, and Anion. *J. Phys. Chem. C* **2016** *120*, 46, 26442-26447.
10. Lim, H.-K.; Kwon, Y.; Kim, H. S.; Jeon, J.; Kim, Y.-H.; Lim, J.-A.; Kim, B.-S.; Choi, J.; Kim, H. Insight into the Microenvironments of the Metal-Ionic Liquid Interface during Electrochemical CO₂ Reduction. *ACS Catal.* **2018** *8*, 2420-2427.
11. Buckley, A. K.; Lee, M.; Cheng, T.; Kazantsev, R. V.; Larson, D. M.; Goddard III, W. A.; Toste, F. D.; Toma, F. M. Electrocatalysis at Organic-Metal Interfaces: Identification of Structure-Reactivity Relationships for CO₂ Reduction at Modified Cu Surfaces. *J. Am. Chem. Soc.* **2019** *141*, 18, 7355-7364.
12. Lobaccaro, P.; Singh, M. R.; Clark, E. L.; Kwon, Y.; Bell, A. T.; Ager, J. W. Effects of Temperature and Gas-Liquid Mass Transfer on the Operation of Small Electrochemical Cells for the Quantitative Evaluation of CO₂ Reduction Electrocatalysts. *Phys. Chem. Chem. Phys.* **2016** *18*, 26777-26785.
13. Hatsukade, T.; Kuhl, K. P.; Cave, E. R.; Abram, D. N.; Jaramillo, T. F. Insights into the Electrocatalytic Reduction of CO₂ on Metallic Silver Surfaces. *Phys. Chem. Chem. Phys.* **2014** *16*, 13814-13819.
14. Seifitokaldani, A.; Gabardo, C. M.; Burdyny, T.; Dinh, C.-T.; Edwards, J. P.; Kibria, M. G.; Bushuyev, O. S.; Kelley, S. O.; Sinton, D.; Sargent, E. H. Hydronium-Induced Switching between CO₂ Electroreduction Pathways. *J. Am. Chem. Soc.* **2018** *140*, 3833-3837.

15. Wang, Z.; Wu, L.; Sun, K.; Chen, T.; Jiang, Z.; Cheng, T.; Goddard, W. A. Surface Ligand Promotion of Carbon Dioxide Reduction through Stabilizing Chemisorbed Reactive Intermediates. *J. Phys. Chem. Lett.* **2018**, *9*, 11, 3057-3061.
16. Osman, M. A. Organo-vermiculites: Synthesis, Structure and Properties. Platelike Nanoparticles with High Aspect Ratio. *J. Mat. Chem.* **2006**, *16*, 3007-3013.
17. Sakamoto, N.; Arai, T. Enhanced Electrochemical CO₂ Reduction Selectivity by Application of Self-Assembled Polymer Microparticles to a Silver Electrode. *Chem. Commun.* **2019** *55*, 11623-11625.

4.5 Supplementary Information

4.5.1 Experimental methods

Materials: All chemicals were obtained from commercial suppliers and used without further purification, unless otherwise noted. Silver foil (1.0mm thick, 99.9985%) was purchased from Alfa Aesar. Carbon dioxide (99.995%) was obtained from Praxair. Cetyltrimethylammonium bromide (**1**, 98%) was obtained from Spectrum Chemical. Dihexadecyldimethylammonium bromide (**2**, 97%), didecyldimethylammonium bromide (**3**, 98%), and trimethyldecylammonium bromide (**4**, 98%) were purchased from Sigma-Aldrich. Selemion AMV anion-exchange membrane was purchased from AGC Engineering Co., LTD.

Instrumentation: Gas chromatography (GC) data was collected on a multiple gas analyzer #5 from SRI Instruments.

Electrode preparation: Ag foil was mechanically polished (1200G Wetordry sandpaper, 3M) and rinsed with water before use. To prepare modified Ag surfaces, 0.027 mmol of the organic species was dissolved in iPrOH (1 mL), and 100 μ L of this solution was dropcast onto the Cu foil. Once dry, 100 μ L of Nafion solution (1 μ L of commercial Nafion solution per mg of organic species added to 1 mL iPrOH) was dropcast onto the Ag surface.

Electrochemical studies: The prepared electrodes were placed in a two-compartment flow cell, fabricated from a reported design,¹ and electrochemical experiments were conducted as previously described.² Product distribution data was determined via chronoamperometry experiments conducted for 35 minutes, and the average of data from three independently prepared electrodes are reported.

4.5.2 Partial current densities

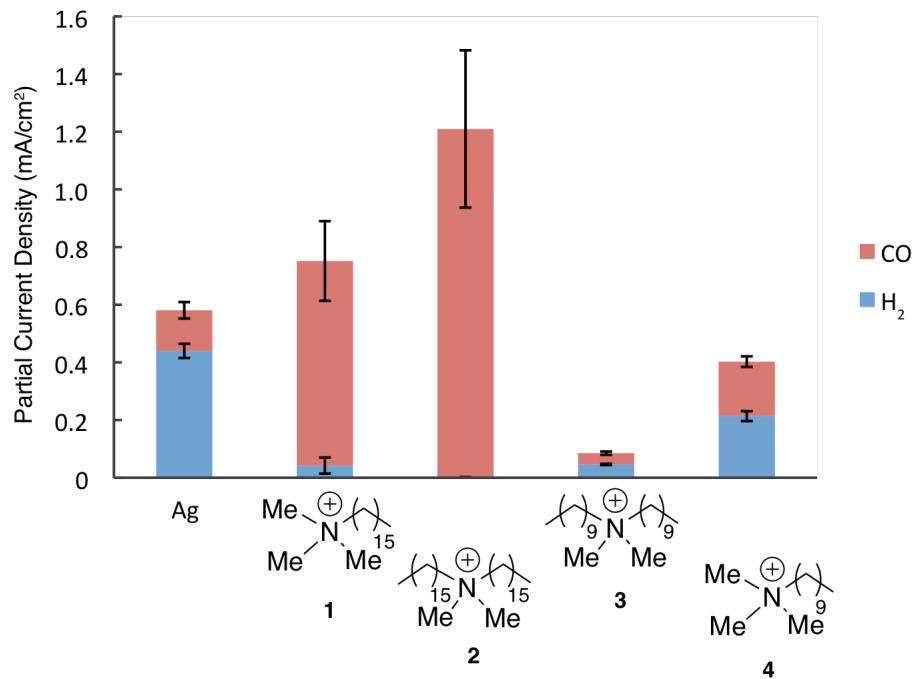
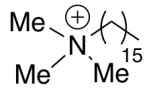
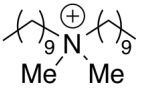
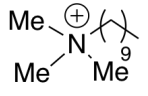
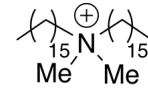


Figure S1. Partial current densities of Ag and functionalized Ag surfaces at -0.8 V vs. RHE. Substantial increases in activity towards CO are observed with **1** and **2**, with decreased activity towards H₂. Values are expressed as geometric current densities. Values are averages of three trials, with error bars reported as standard error of the mean.

4.5.3 Contact angle of functionalized Ag surfaces

Table S1: Ag surfaces in order of increasing hydrophobicity, compared to the selectivity of these surfaces for CO. Modified Ag surfaces were prepared by dropcasting at the same loading as for the chronoamperometry measurements. Contact angle measurements were obtained with 1 μ L droplets of water, and the average of at least four measurements is reported.

We find that surfaces with **1** and **2** have similar CO selectivities but very different hydrophilicities, suggesting that the interaction of the modifiers with the surrounding water is not the selectivity-determining factor.

Surface:	 1	 3	 4	 2	Ag foil
Contact angle:	4° \pm 1	11° \pm 1	15° \pm 2	54° \pm 3	69° \pm 1
CO selectivity:	90%	45%	48%	97%	25%

4.5.4 References for supplementary information

1. Lobaccaro, P.; Singh, M. R.; Clark, E. L.; Kwon, Y.; Bell, A. T.; Ager, J. W. Effects of Temperature and Gas-Liquid Mass Transfer on the Operation of Small Electrochemical Cells for the Quantitative Evaluation of CO₂ Reduction Electrocatalysts. *Phys. Chem. Chem. Phys.* **2016**, *18*, 26777-26785.
2. Buckley, A. K.; Lee, M.; Cheng, T.; Kazantsev, R. V.; Larson, D. M.; Goddard III, W. A.; Toste, F. D.; Toma, F. M. Electrocatalysis at Organic-Metal Interfaces: Identification of Structure-Reactivity Relationships for CO₂ Reduction at Modified Cu Surfaces. *J. Am. Chem. Soc.* **2019** *141*, 18, 7355-7364.